

Junctions of three quantum wires

Masaki Oshikawa

*Department of Physics, Tokyo Institute of Technology,
Oh-okayama, Meguro-ku, Tokyo 152-8551 JAPAN*

Claudio Chamon

Department of Physics, Boston University, Boston, MA 02215, U.S.A.

Ian Affleck

Dept. of Physics and Astronomy, University of British Columbia, Vancouver, BC, Canada V6T 1Z1

(Dated: February 2, 2008)

We study a junction of three quantum wires enclosing a magnetic flux. The wires are modeled as single-channel spinless Tomonaga-Luttinger liquids. This is the simplest problem of a quantum junction between Tomonaga-Luttinger liquids in which Fermi statistics enter in a non-trivial way. We study the problem using a mapping onto the dissipative Hofstadter model, describing a single particle moving on a plane in a magnetic field and a periodic potential coupled to a harmonic oscillator bath. Alternatively we study the problem by identifying boundary conditions corresponding to the low energy fixed points. We obtain a rich phase diagram including a chiral fixed point in which the asymmetric current flow is highly sensitive to the sign of the flux and a phase in which electron pair tunneling dominates. We also study the effects on the conductance tensor of the junction of contacting the three quantum wires to Fermi liquid reservoirs.

PACS numbers:

I. INTRODUCTION

While electron-electron interactions can, in many cases, be adequately described by Fermi liquid theory in two- or three-dimensional systems, they lead to more exotic effects in one-dimensional Tomonaga-Luttinger liquids (TLL). One context in which striking TLL behavior occurs is in the response of a quantum wire [1] or a spin chain [2] to a single constriction or weak link. The conductance through the constriction scales to zero at low temperatures in the case of repulsive interactions, corresponding to a TLL parameter $g < 1$ or to the ideal value of ge^2/h for attractive interactions, $g > 1$. TLL behavior has recently been studied experimentally in carbon nano-tubes. [3, 4]

In order to construct a useful circuit out of quantum wires it will be necessary to incorporate junctions of three or more wires. These and other closely related problems exhibit rather rich TLL effects which have been the subject of a number of recent papers. [5, 6, 7, 8, 9, 10, 11, 12, 13, 14, 15, 17, 18, 19, 20, 21, 22] Much of the work in this field has used bosonization. As emphasized by Nayak et al. [5], when the number of wires meeting at a junction exceeds two, the Klein factors which give bosonized operators Fermi statistics play a crucial role. We recently introduced [22] a new method to study this problem, mapping it into the dissipative Hofstadter model (DHM), which describes a single particle moving in a uniform magnetic field and a periodic potential in two dimensions and coupled to a bath of harmonic oscillators. This mapping is useful because it allows us to take advantage of earlier results of Callan and Freed on the DHM [23]. When the three quantum wires enclose a

magnetic flux, the mapping to the DHM also allows us to identify a new low energy chiral fixed point with an asymmetric flow of current that is highly sensitive to the sign of the flux.

The purpose of this paper is to present a comprehensive study of the three-wire junction (or Y-junction) problem. We describe the mapping to the DHM and its implications in more detail, and we further study the problem using a complimentary method which involves identifying boundary conditions on the boson fields which correspond to low energy fixed points. In combination, these methods provide a coherent picture of the possible stable fixed point conductances of the three-wire junction, and this picture shows a regime with chiral current flow and a regime in which electron pair tunneling dominates. This paper also addresses the problem of how the fixed point conductance tensor of the three-wire junction is modified if the TLL wires are connected to Fermi liquid leads far from the junction.

The paper is organized as follows. In Sec. II we provide a brief summary of the results for the conductance tensor of the Y-junction and for the Renormalization Group (RG) flow diagrams for different ranges of the Luttinger parameter g . In Sec. III we present our effective model for the three-wire junction. In particular, we show explicitly how the magnetic flux dependence comes into the problem in which the three wires are connected to a circular ring by taking into account the discrete energy levels on the ring. In Sec. IV we review the bosonization of the Y-junction model. In Sec. V we discuss the strong coupling limit of the junction that is obtained by simply taking the hopping between the three wires to infinity. We show that such a simple argument does not provide informa-

tion on the nature of the fixed points for a range of the parameter g , and that different methods that we describe in the paper are needed to shed light onto the nature of the strong coupling fixed points. In Sec. VI we establish the mapping of the Y-junction model onto the DHM and deduce its consequences for the phase diagram of the Y-junction model. In Sec. VII we introduce the study of the system by looking at the boundary conditions satisfied by the bosonic fields at the junction. In Sec. VIII we discuss the twisted structure of the Hilbert space that is manifest in the compactification of the bosons so as to take proper care of the fermionic statistics of the electrons in the wires. In Sec. IX we introduce what we refer to as the method of delayed evaluation of boundary conditions (DEBC), which is less reliant on the apparatus of BCFT. In Sec. X we apply all the results from the previous sections to analyze the RG fixed points in the junction problem. We also show in this section that asymmetries in the couplings between the three wires are irrelevant at low energies and temperatures, so the simple Z_3 symmetric model of the system may indeed be a good description of realistic junctions. In Sec. XI we use simple arguments based on energy conservation to obtain constraints on the conductance tensor. We show that all the fixed points that we are able to understand in this paper correspond to physical situations where no energy is transferred to neutral (non-charge carrying) modes in the quantum wires. In Sec. XII we discuss how the conductance tensors are modified if the Luttinger liquid wires are connected to Fermi liquid leads far from the junction. Depending on details of the potential experiment, this may be a better model. In Sec. XIII we present and discuss open problems. In Appendix A we give results on the non-interacting version of our model. In Appendix B we review boundary conformal field theory. In Appendix C we review the boundary conformal field theory of standard free bosons. In Appendix D we review the boundary conformal field theory approach to calculating the conductance. In Appendix E we discuss the related problem of a Y-junction of quantum Hall edge states.

II. SUMMARY OF RESULTS

We summarize in this section our results for the conductance tensor for the three wire junction, as well as our conjectured RG flow diagrams for several different ranges of the interaction parameter g . These results are based on our findings from three different methods discussed in the paper: mapping to the dissipative Hofstadter model, boundary conformal field theory, and delayed evaluation of boundary conditions. Our results rely on various assumptions and arguments which we believe to be reasonable in the light of several supporting evidences. The details of our analysis and assumptions are given in later sections.

The device we consider is shown in Fig. 1, where the

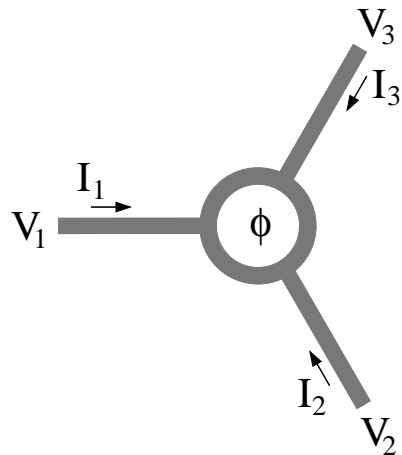


FIG. 1: Junction of three quantum wires with a magnetic flux threading the ring. The $V_{1,2,3}$ are the voltages applied on each wire, and the $I_{1,2,3}$ the currents arriving at the junction from each of the three wires.

three quantum wires are connected to a ring which can be threaded by a magnetic flux. The electron transfer processes between the three wires meeting at the Y-junction is modeled by the effective Hamiltonian

$$H_B = - \sum_{j=1}^3 [\Gamma e^{i\phi/3} \psi_j^\dagger(0) \psi_{j-1}(0) + \text{h.c.}], \quad (2.1)$$

where $\psi_j(x=0)$ is the electron operator at the endpoint of the j -th ($j = 1, 2, 3$, and we identify $j \equiv j + 3$) quantum wire that connects to the junction ($x = 0$). Γ is the tunneling amplitude between the leads, and ϕ is a phase that depends on the flux that threads the ring. In addition to the boundary term Eq. (2.1), there is a bulk Hamiltonian H_{bulk} that models the Luttinger liquid wires characterized by the interaction parameter g . The derivation of this effective Hamiltonian at the junction, and the effective Hamiltonian for the wire part, is given in section III.

The presence of a magnetic flux breaks generically time-reversal invariance, with the exception of $\phi = 0, \pi$, in which case time-reversal symmetry exists. In this paper, we assume the three wires to be identical. Nevertheless, the junction can be asymmetric if the wires are attached to the ring in different ways. If all three wires are attached identically to the ring, the junction is symmetric under cyclic permutations of the wires; this is the Z_3 symmetric case.

The important physical quantity for the three-wire junction problem is the conductance tensor. Within the linear response theory, the total current I_j flowing into the junction from wire j is related to the voltage V_k applied to wire k by

$$I_j = \sum_k G_{jk} V_k, \quad (2.2)$$

where $j, k = 1, 2, 3$ and G_{jk} is the 3×3 conductance

tensor. Note that current conservation implies that:

$$\sum_j I_j = 0. \quad (2.3)$$

Furthermore, a common voltage applied to all three wires results in zero current. Thus:

$$\sum_j G_{jk} = \sum_k G_{jk} = 0. \quad (2.4)$$

For a Z_3 symmetric junction, the conductance tensor takes the form

$$G_{jk} = \frac{G_S}{2} (3\delta_{jk} - 1) + \frac{G_A}{2} \epsilon_{jk}, \quad (2.5)$$

where we separate the symmetric and anti-symmetric components of the tensor, and G_S and G_A are scalar conductances. (The ϵ_{ij} are defined as follows: $\epsilon_{12} = \epsilon_{23} = \epsilon_{31} = 1$, $\epsilon_{21} = \epsilon_{32} = \epsilon_{13} = -1$ and $\epsilon_{jj} = 0$.) The anti-symmetric component, controlled by G_A , is present only when time-reversal symmetry is broken by a magnetic flux. Namely, G_A should vanish in the time-reversal symmetric case $\phi = 0, \pi$. Even when time-reversal symmetry is broken in the microscopic model, G_A might vanish in the low-energy fixed point if the RG flow restores the time-reversal symmetry.

From the tensor conductance Eq. (2.5), one reads

$$G_S = G_{11} = G_{22} = G_{33}. \quad (2.6)$$

This represents the conductance of each wire when zero voltage is applied to the other two wires. For this reason, we shall sometimes refer to G_S in the text as the single terminal conductance.

We also consider the same three-wire junction device when connected to Fermi liquid reservoirs, as depicted in Fig. 2 (the wide regions at the ends of the wires represent the Fermi liquid contacts). It is known that the contact to the reservoirs affect the two-terminal conductance of single quantum wires [30, 31, 32]. This renormalization of the conductance also takes place in the three-wire junctions, and we calculate these renormalization effects in this paper. In the presence of the Fermi liquid leads, we obtain that the ‘‘dressed’’ 3×3 conductance tensor $\bar{\mathbf{G}} \equiv \mathbf{G}_{\text{w/leads}}$ of the system is related to the ‘‘bare’’ conductance tensor $\mathbf{G} \equiv \mathbf{G}_{\text{w/o leads}}$ by

$$\mathbf{G}_{\text{w/leads}}^{-1} = \mathbf{G}_{\text{w/o leads}}^{-1} + G_c^{-1} \mathbf{1}, \quad (2.7)$$

where $G_c = 2g/(g-1) e^2/h$ is effectively a contact conductance between the leads and the quantum wires. This relationship in Eq. (2.7) can be interpreted physically as the addition in series of the lead/wire interface resistances to the Y-junction resistance tensor. (Notice that, because of the $\sum_k G_{jk} = 0$ condition, the inverse \mathbf{G}^{-1} does not exist. Hence one must work directly with the conductance instead of the resistance tensor as discussed in section XII.)

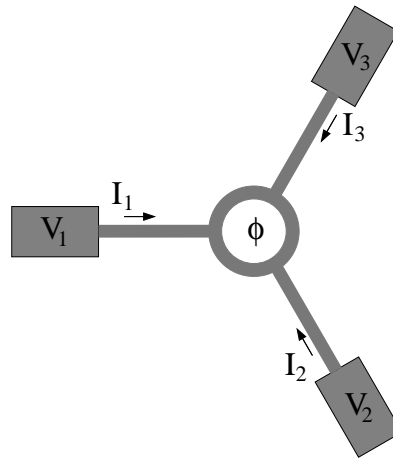


FIG. 2: The same three-wire junction as in Fig. 1, but now with the Fermi liquid reservoirs attached at the ends of the three wires. The $V_{1,2,3}$ are now the voltages as measured at the three reservoirs.

We are mostly interested in the stable RG fixed points of the problem. They would govern the physics in the low-energy limit – namely in the limit of low bias voltages and low temperature. Below we list our results for the low-energy fixed point conductances for the Y-junction devices. Which fixed point is the stable one is determined by the Luttinger parameter g that depends on the strength of local electron-electron interactions. We find that the stable fixed point has the Z_3 symmetry in most cases. Namely, even if the Z_3 symmetry is broken at the junction, the Z_3 symmetry would be restored in the low-energy limit, except for a few special cases. Thus we primarily focus on the RG flow in the presence of the Z_3 symmetry. The most important parameters of the junction are then the hopping strength Γ and the enclosed magnetic flux ϕ . If we understand the RG flow most simply by the effective values of Γ and ϕ varying as functions of the energy scale, the RG flow diagram could be drawn on the Γ - ϕ plane as shown in the following.

As in the case of junctions of two wires, the interaction parameter g controls the RG flow and dictates the phase diagram. Now we present our results for several different ranges of g .

A. $g < 1$

When the interaction in the quantum wires is repulsive ($g < 1$), the hopping amplitude Γ decreases along the RG flow. The stable fixed point corresponds to $\Gamma = 0$, namely to completely decoupled wires, as pictorially illustrated in Fig. 3. We will call this fixed point the N fixed point, where N stands for Neumann boundary condition. We note that the value of the effective flux ϕ does not matter in the decoupled limit, so in the N fixed point there is no breaking of time reversal. Moreover, even if the junction is Z_3 asymmetric, the system is generically renormalized

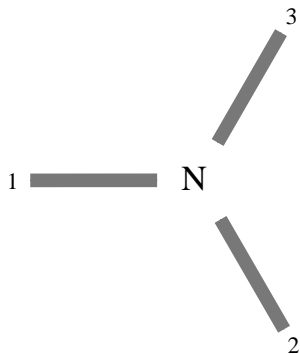


FIG. 3: Pictorial representation of the N fixed point. It just corresponds to three decoupled wires.

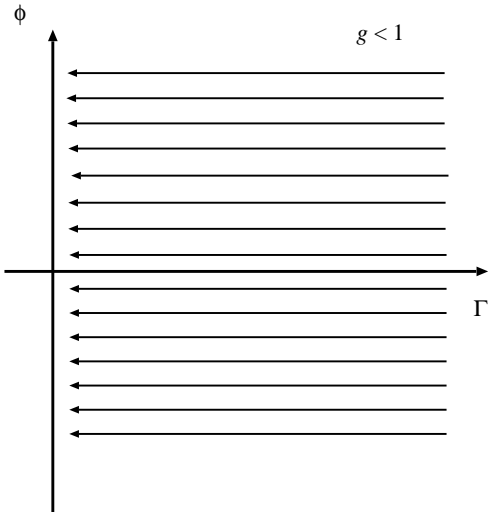


FIG. 4: RG flow diagram for $g < 1$. The junction is renormalized toward the decoupled N fixed point.

into the N fixed point; the Z_3 asymmetry turns out to be irrelevant. The leading irrelevant perturbation to the N fixed point is the electron hopping between two wires, which has scaling dimension $(1/g) > 1$.

The conductance tensor at the N fixed point is obviously

$$G_{jk} = \bar{G}_{jk} = 0. \quad (2.8)$$

Of course there is no difference between the “bare” conductance \mathbf{G} and the “dressed” (by the reservoirs) conductance $\bar{\mathbf{G}}$ at the N fixed point.

The corresponding flow diagram in the Γ - ϕ plane is shown in Fig. 4.

B. $g = 1$

For the noninteracting case $g = 1$, one can solve the original electron model as a single particle problem. The junction is then characterized by the 3×3 scattering matrix of a single free electron. Thus there is a continuous

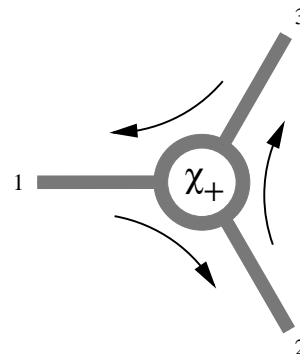


FIG. 5: Pictorial representation of the chiral fixed point. The incoming electrons from one wire is diverted to one of the other wires.

manifold of RG fixed points. In other words, electron hopping is exactly marginal.

Several special cases on the “free electron” manifold are worth mentioning. Let us consider the Z_3 symmetric case first. The N fixed point, as introduced above for $g < 1$, corresponds to a complete reflection for each wire and thus is a special point on the RG fixed manifold. If we further impose the time reversal symmetry, we always have $G_A = 0$ while the maximal single-terminal conductance on the “free electron” manifold is $G_S = 8/9 e^2/h$. The constraint on the maximum of G_S in the time reversal symmetric case is due to the unitarity of the single electron scattering matrix as discussed in Ref. [5]. On the other hand, if the time reversal symmetry is broken by the flux ϕ , the maximal single-terminal conductance $G_S = e^2/h$ can be realized by a complete transmission of electrons from wire j to wire $j + 1$ (or $j - 1$), where again we identify $j \equiv j + 3$. We call them chiral fixed points χ_{\pm} ; they are pictorially represented in Fig. 5, and they are also on the RG fixed manifold. At the χ_{\pm} points $G_A = \pm G_S$. The conductance tensor at χ_{\pm} reads

$$G_{jk} = \frac{e^2}{2h} [(3\delta_{jk} - 1) \pm \epsilon_{jk}] = \frac{e^2}{h} (\delta_{jk} - \delta_{j,k\pm 1}). \quad (2.9)$$

If we allow breaking of the Z_3 symmetry, a simple fixed point is given by connecting perfectly two of the wires, while the other is left decoupled completely, as depicted in Fig. 6. This fixed point, which we call D_A , is also described by a single electron scattering matrix and thus a special point on the “free electron” manifold. It is clear that there are other fixed points on the manifold with varying degrees of Z_3 asymmetry.

In fact, even for noninteracting wires or $g = 1$, other RG fixed points, which cannot be characterized by the single electron scattering matrix, exist in the presence of the interaction at the junction. However, these fixed points are more unstable, and the RG flows (shown in Fig. 7) are towards the “free electron” manifold.

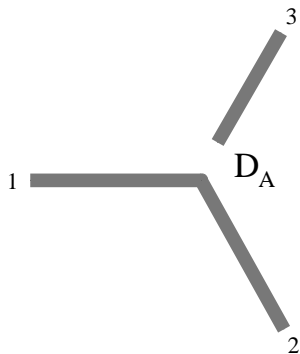


FIG. 6: Pictorial representation of the asymmetric fixed point D_A , in which two of the wires (for example wires 1 and 2 in the figure) are perfectly connected while the other (wire 3) is left decoupled. This fixed point is unstable for all values of g with the exception of $g = 1, 3$, in which case D_A may belong to the continuous manifold of fixed points.

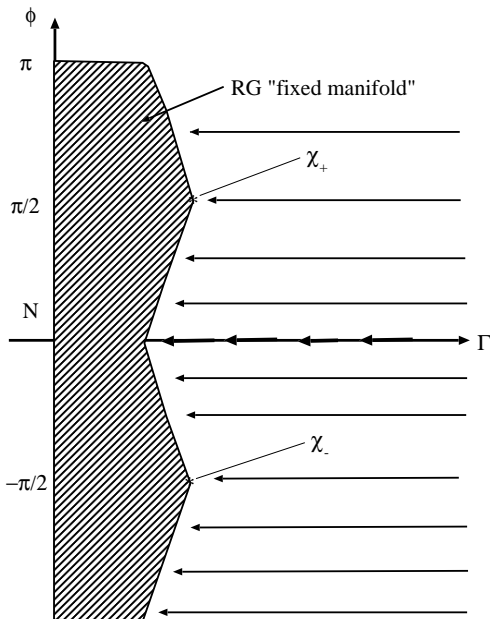


FIG. 7: RG flow diagram for $g = 1$. There is a stable RG fixed manifold which includes N and χ_{\pm} as special points.

C. $1 < g < 3$

The N fixed point is now unstable against the inclusion of electron hoppings, which have scaling dimension $1/g < 1$. For the time-reversal symmetric case $\phi = 0, \pi$, the system is renormalized into the M fixed point. The M fixed point should have the single-terminal conductance G_S in the range $0 < G_S < (4g/3) (e^2/h)$, as shown in Section XI. The M fixed point is unstable against turning on the flux ϕ . Unfortunately, we do not have an exact solution corresponding to the M fixed point, and other properties are not known.

For $0 < \phi < \pi$ and $-\pi < \phi < 0$, the RG flows are towards the stable, chiral fixed points χ_+ and χ_- , respec-

tively. The chiral fixed points exhibit the asymmetric conductance tensor

$$G_{jk}^{\pm} = \frac{G_{\chi}}{2} [(3\delta_{jk} - 1) \pm g \epsilon_{jk}] \quad (2.10)$$

with the single terminal conductance or symmetric component

$$G_S = G_{\chi} = \frac{4g}{3+g^2} \frac{e^2}{h}, \quad (2.11)$$

and anti-symmetric component $G_A = \pm g G_S$. We note that, in the limit $g \rightarrow 1$, the chiral χ_{\pm} fixed points reduce to the complete transmission of single electron from wire j to wire $j \pm 1$ discussed previously.

An intriguing aspect of the conductance (2.10) is that, when a voltage is applied to one of the wires while the other two are kept at zero voltage (as illustrated in Fig. 8a), the current is rather ‘‘sucked in’’ from one of the wires with the zero voltage. However, if we include the non-interacting leads to the system (as shown now in Fig. 8b), the effective conductance tensor for χ_{\pm} are given by the conductance tensor Eq. (2.9) obtained for χ_{\pm} at $g = 1$ (in which $\bar{G}_A = \pm \bar{G}_S$ with $\bar{G}_S = e^2/h$). Namely, the ‘‘sucking’’ effect disappears in the presence of non-interacting leads, while the asymmetry holds.

The RG flow diagram (shown in Fig. 9) implies that even a tiny flux ϕ brings the junction to the completely asymmetric conductance in the low-energy limit. The leading irrelevant perturbation to the χ_{\pm} fixed points has scaling dimension $4g/(3+g^2) > 1$. A remarkable aspect of the fixed points χ_{\pm} is that the conductance, as well as the scaling dimension, exhibit *non-monotonic* dependence on the interaction parameter g , unlike in other known applications of TLL. Making the electron interaction more attractive can decrease the conductance!

We note that the D_A fixed point, which breaks the Z_3 symmetry, is unstable for this range of g . Hence, small asymmetries in the physical device do not affect the conductance of the χ_{\pm} fixed points at low voltages and temperatures for this range of the g parameter.

D. $g = 3$

The N fixed point is again unstable. On the other hand, there is an RG fixed manifold (shown in Fig. 10), as we have seen for $g = 1$. For $g = 3$, the manifold is again characterized by the scattering matrix of a free fermion, which is *not* the original electron. The chiral fixed points χ_{\pm} become the special points on the manifold as $g \rightarrow 3$. The largest single-terminal conductance is realized on another special point D_P on the manifold, which is explained in the next subsection for $3 < g < 9$.

The system with $\phi \neq 0, \pi$ is renormalized into the fixed manifold. On the other hand, for the time-reversal symmetric case $\phi = 0, \pi$, the infrared M fixed point is *not* on the manifold, and it is unstable against the inclusion of the flux ϕ .

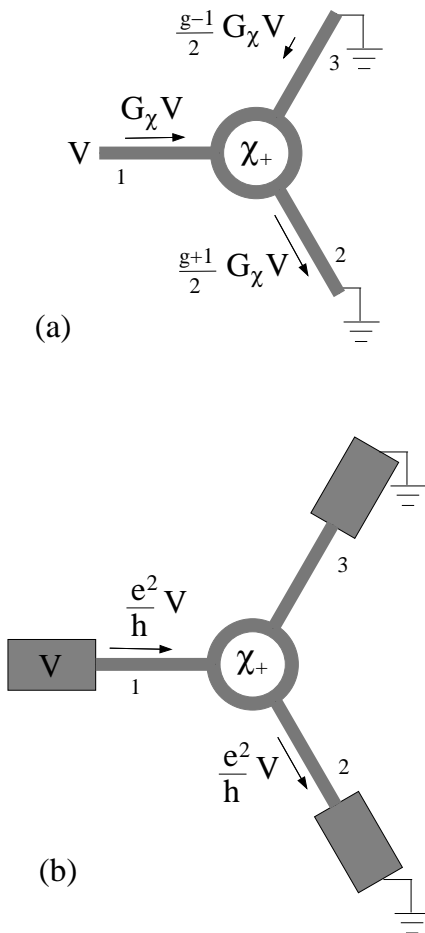


FIG. 8: Response of the Y-junction system at the χ_+ fixed point when a voltage V is applied to wire 1, while wires 2 and 3 are grounded. Case (a) is when wire 1 is directly at a voltage V , and case (b) is when wire 1 is in contact with a reservoir at voltage V . Notice that in case (a) some current is sucked into the junction region from lead 3, while in case (b) this effect goes away and the junction behaves as a perfect “circulator”, transmitting all incoming current from lead 1 to lead 2. The response for the χ_- fixed point is similar, with the current flowing from 1 to 3 instead.

E. $3 < g < 9$

There is a stable fixed point D_P , which becomes a special point on the fixed manifold in the limit $g \rightarrow 3$ as discussed above. The conductance tensor at D_P takes the symmetric form ($G_A = 0$) with $G_S = (4g/3) (e^2/h)$. Including the non-interacting leads, the effective conductance tensor is again symmetric ($\bar{G}_A = 0$), but the effective single-terminal conductance is $\bar{G}_S = (4/3) (e^2/h)$.

Notice that the maximum values $G_S = (4g/3) (e^2/h)$ or $\bar{G}_S = (4/3) (e^2/h)$ is larger than the maximum conductance $G_S = (8/9) e^2/h$ for unitary scattering of single particle states; this shows that multiparticle scattering at the junction takes place for interacting quantum wires. Indeed, the enhanced conductance at D_P may be un-

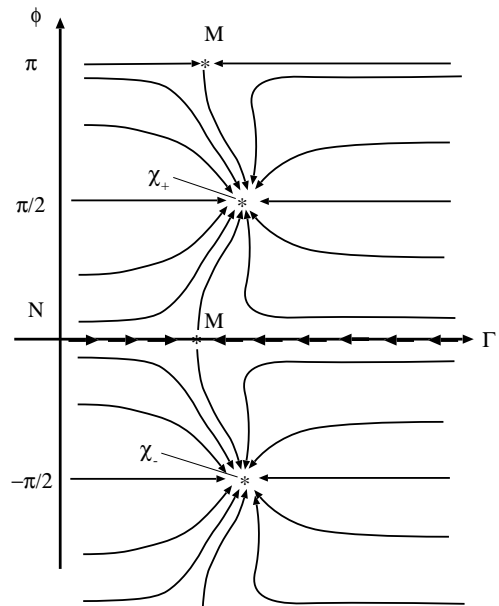


FIG. 9: RG flow diagram for $1 < g < 3$. For $\phi \neq 0, \pi$ the system is renormalized toward the chiral fixed point χ_\pm . For the time-reversal symmetric case $\phi = 0, \pi$, the infrared fixed point is the nontrivial M fixed point. It is unstable against the addition of flux ϕ .

derstood as a consequence of pair tunneling, and this is pictorially illustrated in Fig. 11.

The RG flow diagram for this range of g 's is shown in Fig. 12. For $\phi \neq 0, \pi$, the system is generically renormalized into the D_P fixed point. Although the D_P fixed point itself does not break the time-reversal symmetry, the system does not reach there with $\phi = 0, \pi$. In the time-reversal symmetric case $\phi = 0, \pi$, the property of the infrared M fixed point is not known precisely. It should be unstable against inclusion of the flux.

F. $9 < g$

The time-reversal invariant system with $\phi = 0, \pi$ is now renormalized into the stable D_N fixed point. For $\phi \neq 0, \pi$, the infrared stable fixed point is still the D_P fixed point as in the case $3 < g < 9$. The flow diagram for $g > 9$ is shown in Fig. 13.

As far as the conductance is concerned, the D_N fixed point is identical to the D_P fixed point. The difference is in the scaling dimension of the leading irrelevant operator; it is $g/3$ for D_P but is $g/9$ for D_N . As both D_N and D_P are stable, there must be another critical fixed point between these two; its properties however are not known.

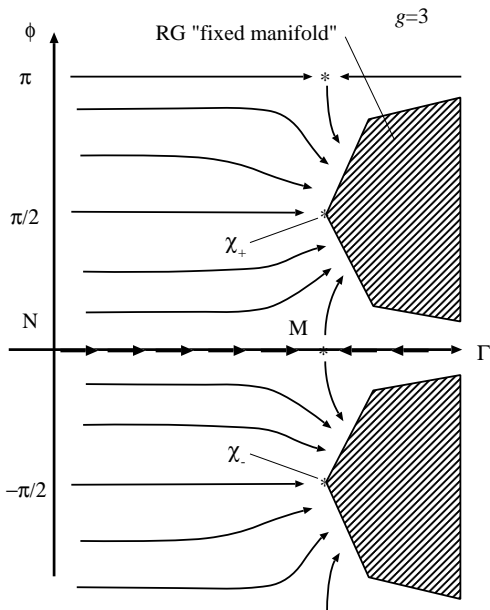


FIG. 10: RG flow diagram for $g = 3$. For $\phi \neq 0, \pi$ the system is renormalized toward the RG fixed manifold, which includes χ_{\pm} as special points. For the time-reversal symmetric case $\phi = 0, \pi$, the infrared fixed point is the nontrivial M fixed point. It is unstable against the addition of flux ϕ .

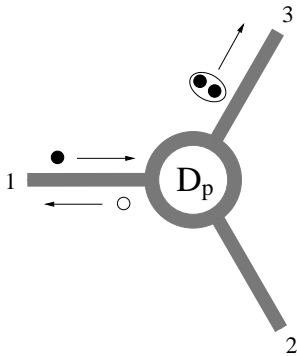


FIG. 11: Pictorial representation of the D_P fixed point. The conductance is enhanced by the Andreev reflection process. We only illustrate the process where the electron pair exits through lead 3; but notice that, since the D_P fixed point is time-reversal symmetric, the pair has exactly the same amplitude for exiting through lead 2.

III. MODEL

In this Section, we define the model Hamiltonian precisely, for the junction introduced in Fig. 1.

We study only the simplest model of a Y-junction which includes TLL effects. Thus we consider only a single channel of electrons in each wire, ignore electron spin, assume that the interactions are short-ranged, and ignore phonons and impurities. We also assume that all three wires are equivalent in the bulk, and consider the Z_3 symmetric junction. (The generalization to the Z_3

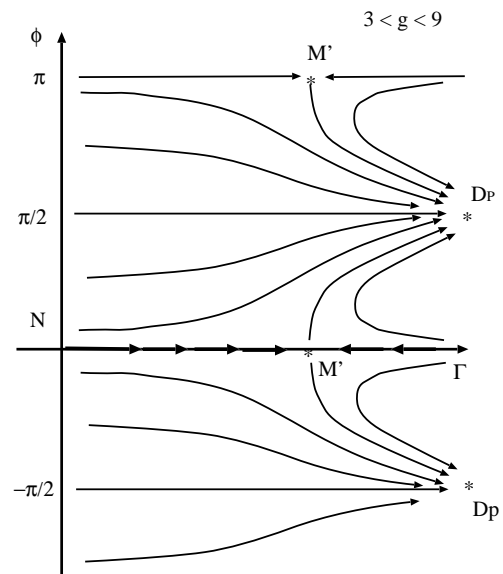


FIG. 12: RG flow diagram for $3 < g < 9$. For $\phi \neq 0, \pi$ the system is renormalized to the D_P fixed point exhibiting Andreev reflection. For the time-reversal symmetric case $\phi = 0, \pi$, the infrared fixed point is the nontrivial M fixed point. It is unstable against the addition of flux ϕ .

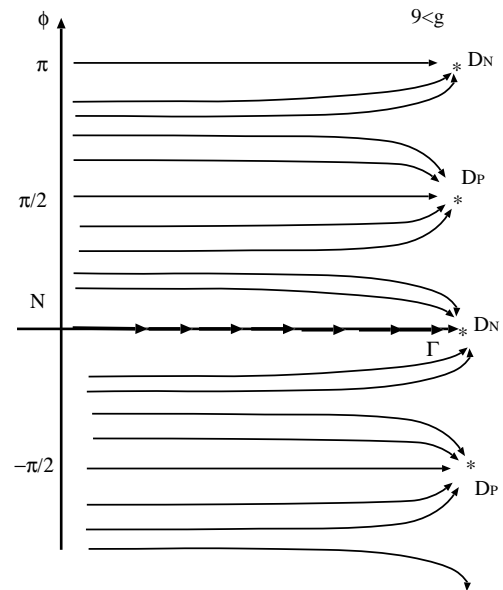


FIG. 13: RG flow diagram for $9 < g$. For $\phi \neq 0, \pi$ and $\phi = 0, \pi$, the system is renormalized to D_P and D_N fixed points respectively. Both exhibits the enhanced conductance due to the Andreev reflection.

asymmetric junctions is straightforward, and we find in Sec. XD that the Z_3 asymmetry turns out to be irrelevant.)

It is convenient to start by defining a tight-binding version of our model. Let $\psi_{n,i}$ annihilate an electron on site n on wire i . Here $n = 0, 1, 2, 3, \dots, \infty$ and $j = 1, 2$ or

3. The Hamiltonian is:

$$H = H_0 + H_B + H_{\text{int}}, \quad (3.1)$$

where:

$$H_0 = -t \sum_{n=0}^{\infty} \sum_{j=1}^3 (\psi_{n,j}^\dagger \psi_{n+1,j} + h.c.), \quad (3.2)$$

$$H_B = - \sum_{j=1}^3 \left[(\tilde{\Gamma}/2) e^{i\phi/3} \psi_{0,j}^\dagger \psi_{0,j-1} + h.c. \right] \quad (3.3)$$

and

$$H_{\text{int}} = \tilde{V} \sum_{n=0}^{\infty} \sum_{j=1}^3 \hat{n}_{n,j} \hat{n}_{n+1,j}. \quad (3.4)$$

Here $\hat{n}_{n,j} = \psi_{n,j}^\dagger \psi_{n,j}$ is the number density and the wire index $j = 0$ is identified with $j = 3$. Note that we have allowed for a non-zero phase ϕ in the tunneling matrix element $\Gamma e^{i\phi/3}$. By making redefinitions of the phases of the fields $\psi_{n,i}$, independently on the different wires, we can make the phase of each tunneling matrix element equal. However, we cannot transform away a uniform phase, $\phi/3$. We may think of the phase ϕ as being the flux through the junction. It must vanish if the system is time-reversal invariant but will generally be non-zero otherwise, for example if a magnetic field is applied to the junction.

While it seems intuitively reasonable that ϕ should become non-zero in the presence of a magnetic field, it is not so obvious how ϕ actually depends on the field. To study this issue it is convenient to consider a slightly more realistic model in which each lead is connected to a circular conducting ring, which may contain a flux. In particular, if the ring is very small and the Fermi energy of the leads is in resonance with a single unoccupied energy level in the ring, so that we may ignore all other energy levels of the ring, then ϕ actually vanishes. This follows since the tunneling Hamiltonian then takes the form:

$$H_B = \sum_{j=1}^3 [a_j \psi_{0,j}^\dagger d + h.c.], \quad (3.5)$$

where d annihilates an electron at the single level in the ring. We are now free to redefine the phases of $\psi_{n,j}$ independently on each lead, making all the a_j 's real. This is nothing but the junction constructed with a "quantum dot" as introduced in Ref. [5].

On the other hand, if two or more energy levels in the ring are considered, ϕ will generally be non-zero. More generally, if the operators d_l annihilate electrons in the ring in eigenstates with energies E_l , then we may write the tunneling Hamiltonian as:

$$H_B = \sum_{j=1}^3 \sum_l [a_{j,l} \psi_{0,j}^\dagger d_l + h.c.]. \quad (3.6)$$

The tunneling amplitudes, $a_{j,l}$ from the j^{th} lead to the l^{th} ring state may be assumed to be j -independent constants multiplied by the wave-functions of the ring at the locations of the j^{th} wire, at angle $\theta = 2\pi j/3$. We may take the ring wave-functions to be $f_l(\theta) = e^{il\theta}$ for integer l , with energies $E_l = Il^2/2$. A non-zero dimensionless flux, $\tilde{\phi}$, changes the energies to $I(l - \tilde{\phi}/2\pi)^2/2$ so that the states with angular quantum numbers $\pm l$ do not have the same energy. We may assume that the phases of the tunneling amplitudes $a_{j,l}$ are given by the phases of the ring states at the locations $\theta = 2\pi j/3$ where the j^{th} wire joins the ring:

$$a_{j,l} = a_l e^{i2\pi j l/3}. \quad (3.7)$$

To get a tunneling Hamiltonian of the form of Eq. (3.3) we assume that $|a_l| \ll \Delta E$, the level spacing in the ring. Then we consider processes of second order in the a_l 's: 1) in which an electron tunnels from a lead to an unoccupied ring state l and then tunnels off to a different lead, and 2) in which an electron in an occupied ring state l first tunnels off to a lead and then an electron from a different lead tunnels into the ring to fill the hole. This gives a low-energy effective tunneling Hamiltonian of the form of Eq. (3.3) with:

$$\Gamma e^{i\phi/3} = \sum_l \frac{|a_l|^2 e^{i2\pi l/3}}{E_F - E_l} \quad (3.8)$$

We see that if only one (occupied or unoccupied) level l dominates the sum, then: $\phi = 2\pi l$, equivalent to zero. If 2 levels dominate the sum, say l_1 and l_2 , with the contribution from the l_1^{th} level much bigger than the contribution from the l_2^{th} , then

$$\phi \approx 3 \frac{|a_{l_2}|^2}{|a_{l_1}|^2} \frac{E_{l_1} - E_F}{E_{l_2} - E_F} \sin[2\pi(l_2 - l_1)/3], \quad (3.9)$$

with $|\phi| \ll 1$. So, ϕ becomes small near a resonance. Of course, when there is zero flux ($\tilde{\phi} = 0$) in the ring, ϕ also vanishes due to the cancellation of the ring levels with quantum numbers $\pm l$. In general, ϕ will be some periodic odd function of the flux $\tilde{\phi}$ in the ring.

We now consider the continuum limit of the tight-binding model of Eq. (3.1). We introduce left and right movers as usual, keeping only narrow bands of wave-vectors near the Fermi "surface" at $\pm k_F$:

$$\psi_{n,j} \approx e^{ik_F n a} \psi_{Rj}(na) + e^{-ik_F n a} \psi_{Lj}(na). \quad (3.10)$$

(a is the lattice spacing.) Linearizing the dispersion relation, H_0 then becomes:

$$H_0 \approx iv_F \sum_j \int_0^\infty dx \left[\psi_{Lj}^\dagger \frac{d}{dx} \psi_{Lj} - \psi_{Rj}^\dagger \frac{d}{dx} \psi_{Rj} \right], \quad (3.11)$$

where $v_F = 2t \sin k_F$. The interaction Hamiltonian H_{int}

takes the form

$$H_{\text{int}} = \tilde{V} \sum_j \int_0^\infty dx [J_{L,j}^2(x) + J_{R,j}^2(x)] \\ + \tilde{V}_{RL} \sum_j \int_0^\infty dx J_{L,j}(x) J_{R,j}(x), \quad (3.12)$$

where

$$J_{L,j}(x) = \psi_{L,j}^\dagger \psi_{L,j} \quad \text{and} \quad J_{R,j}(x) = \psi_{R,j}^\dagger \psi_{R,j} \quad (3.13)$$

and $\tilde{V}_{RL} = 2\tilde{V}[1 - \cos(2k_F a)]$. The first term in Eq. (3.12) can be absorbed into a renormalization of the Fermi velocity. It is the second term, the one proportional to \tilde{V}_{RL} , that controls the Luttinger parameter g . For repulsive interactions ($\tilde{V}_{RL} > 0$), $g < 1$, while for attractive interactions ($\tilde{V}_{RL} < 0$), $g > 1$.

The open boundary conditions in the tight binding model are equivalent to a vanishing boundary condition at $x = -a$, i.e.

$$e^{-ik_F a} \psi_R(-a) + e^{ik_F a} \psi_L(-a) = 0. \quad (3.14)$$

Since ψ_{Rj} is a function only of $(x - v_F t)$ and ψ_{Lj} of $(x + v_F t)$, Eq. (3.14) implies that we may regard the right-movers as the analytic continuation of the left-movers to the negative x -axis:

$$\psi_{Rj}(x) \approx -e^{2ik_F a} \psi_{Lj}(-x), \quad (x > 0). \quad (3.15)$$

Thus we can apparently write H_0 entirely in terms of left-movers:

$$H_0 \approx iv_F \sum_j \int_{-\infty}^\infty dx \psi_{Lj}^\dagger \frac{d}{dx} \psi_{Lj}. \quad (3.16)$$

However, treating the boundary condition of Eq. (3.14) more carefully, we see that H actually contains an extra term when $k_F \neq \pi/2a$. To obtain this boundary

condition on the left-movers we must add a term to the Hamiltonian:

$$\delta H_B = -r \sum_j \psi_{Lj}^\dagger(0) \psi_{Lj}(0). \quad (3.17)$$

The corresponding Schrödinger equation (which does not mix the leads at this point) is:

$$iv_F \frac{d}{dx} \Psi_j - r \delta(x) \Psi_j = E \Psi_j. \quad (3.18)$$

The energy eigenvalues are $E = v_F k$, and the wavefunctions are:

$$\Psi_j(x) = A_{\text{in},j} e^{-ikx}, \quad (x > 0) \quad (3.19)$$

$$= A_{\text{out},j} e^{-ikx}, \quad (x < 0). \quad (3.20)$$

Interpreting $\Psi_j(0)$ in the second term of Eq. (3.18) as $[\Psi_j(0^+) + \Psi_j(0^-)]/2$, this implies:

$$A_{\text{out},j} = \frac{iv_F - r/2}{iv_F + r/2} A_{\text{in},j}. \quad (3.21)$$

From Eq. (3.14) we see that the phase of the wavefunction advances by $e^{-2ik_F a}$ upon scattering so that:

$$-e^{2ik_F a} = \frac{iv_F - r/2}{iv_F + r/2}, \quad (3.22)$$

and hence:

$$r = -2v_F \cot(k_F a). \quad (3.23)$$

In the continuum limit, the total boundary term in H is:

$$H_B \approx \sum_{j=1}^3 \left\{ [\Gamma e^{i\phi/3} \psi_{L,j}^\dagger(0) \psi_{L,j-1}(0) + h.c.] + r \psi_{L,j}^\dagger(0) \psi_{L,j}(0) \right\}, \quad (3.24)$$

where the relation between the coupling Γ in the continuum limit and the $\tilde{\Gamma}$ in the tight-binding model is obtained in Appendix A by matching the scattering matrices for non-interacting electrons calculated in both cases:

$$\Gamma = |r - 2iv_F| \tilde{\Gamma}/2, \quad (3.25)$$

with r given by Eq. (3.23). For interacting systems, r has no effect on the conductance (in the zero frequency,

zero temperature limit), so we henceforth ignore it. It is important to note that the continuum form of H_0 and H_B in Eqs. (3.16) and (3.24) is very general and not restricted to the underlying tight-binding model.

IV. BOSONIZATION

The effects of electron-electron interactions on the three 1D quantum wires is treated using bosonization methods. (For a review, see e.g. [34]). Here we shall focus on the simpler case of spinless electrons. In the low-energy limit, the effective theory for each quantum wire is given by the free boson field theory, which is nothing but the Tomonaga-Luttinger liquid. In formulating the junction of three wires, we can generalize the “folding” trick used in Ref. [36] and define the three wires on the half-line $x > 0$, so that the boundary at $x = 0$ represents the junction. The (imaginary-time) low-energy effective action of the wires is thus given as

$$S = \int_{-\infty}^{\infty} d\tau \int_0^{\infty} dx \sum_{j=1}^3 \frac{g}{4\pi} (\partial_{\mu}\varphi_j)^2, \quad (4.1)$$

where $j = 1, 2, 3$ labels each wire. The electron-electron interaction strength is essentially contained in a single parameter g , which determines various physical quantities and exponents, as we will see later. The cases $g < 1$ and $g > 1$ correspond, respectively, to repulsive and attractive interactions, while $g = 1$ is the Fermi liquid.

The same theory can be also described in terms of the dual field θ_j for each wire, with the similar action

$$S = \int d\tau dx \sum_{j=1}^3 \frac{1}{4\pi g} (\partial_{\mu}\theta_j)^2. \quad (4.2)$$

The precise definition of the dual field θ_j and the derivation of the action (4.2) is discussed in Sections VII and VIII. Here we just note that, while φ_j represents the quantum mechanical phase of the electron, θ_j represents the phase of the charge-density wave. In the bulk, both phases φ_j and θ_j are not fixed to a particular value, reflecting the strong fluctuation in one dimension.

Of course, the effective action (4.1) by itself does not give an answer to the problem of our interest. In fact, the theory defined on the half-line is not completely well defined without specifying the *boundary condition* at $x = 0$. In the present formalism, it is the boundary condition that represents the physics of the junction. In particular, the renormalization-group (RG) fixed points of the problem correspond to conformally invariant boundary

conditions. It turns out that there is a rich variety of RG fixed points (conformally invariant boundary conditions) for the present problem, as we presented in Sec. II and will discuss in detail in Sec. X.

In this Section, we begin our analysis starting from the simplest RG fixed point of the problem: the limit of three disconnected wires without any transfer of electrons between different wires. It is clear that this limit should exist as a RG fixed point. The corresponding boundary condition is known from the previous studies on the open end of a single quantum wire: each boson field ϕ_j obeys the Neumann boundary condition, $\partial\phi_j/\partial x = 0$ at the boundary $x = 0$. In terms of the dual field θ_j , it is equivalent to the Dirichlet boundary condition $\theta_j = \text{const.}$ at $x = 0$. Thus, the disconnected limit can be described by the effective action (4.1) with the Neumann boundary condition on φ_j imposed.

We defer the technical discussion of the boundary condition to Sections VII and VIII. Instead, now we introduce the electron hopping term (3.3) as a perturbation. In the low-energy effective theory, the perturbation should also be bosonized.

The electron annihilation operators *at the open ends* ($x = 0$) of the three 1D wires can be written in terms of bosonic fields φ_j , $j = 1, 2, 3$ [5, 22, 34]:

$$\psi_j \sim \eta_j e^{i\varphi_j/\sqrt{2}}, \quad (4.3)$$

where the η_j are the so-called Klein factors satisfying $\{\eta_j, \eta_k\} = 2\delta_{jk}$, which are necessary to ensure the anticommutation relations of the fermion operators in different wires. Notice that for electron operators on the same wire j , the correct anticommutation relations follow, via the bosonization scheme, from the commutation relations of the boson field φ_j , and the Klein factor η_j plays no role. However, for $i \neq j$, $[\varphi_i, \varphi_j] = 0$; hence, for electron operators on different leads, it is only the Klein factors that are responsible for the correct anticommutation relations. The Klein factors may be represented by the Pauli matrices. An alternative representation using the boson zero modes is described in Appendix E when we discuss tunneling in junctions of fractional quantum Hall liquids.

The boundary action Eq. (3.3), when rewritten in terms of the boson fields, is thus equivalent to

$$H_{\mathcal{B}} = - \sum_{j=1}^3 \left[\left(\Gamma e^{i\phi/3} \eta_j \eta_{j-1} e^{-\frac{i}{\sqrt{2}}(\varphi_j - \varphi_{j-1})} + \text{h.c.} \right) + r \partial_x \varphi_j \right] \Big|_{x=0}. \quad (4.4)$$

It is useful to define the rotated basis

$$\begin{aligned} \Phi_0 &= \frac{1}{\sqrt{3}}(\varphi_1 + \varphi_2 + \varphi_3) \\ \Phi_1 &= \frac{1}{\sqrt{2}}(\varphi_1 - \varphi_2) \\ \Phi_2 &= \frac{1}{\sqrt{6}}(\varphi_1 + \varphi_2 - 2\varphi_3) \end{aligned} \quad (4.5)$$

and similarly

$$\begin{aligned} \Theta_0 &= \frac{1}{\sqrt{3}}(\theta_1 + \theta_2 + \theta_3) \\ \Theta_1 &= \frac{1}{\sqrt{2}}(\theta_1 - \theta_2) \\ \Theta_2 &= \frac{1}{\sqrt{6}}(\theta_1 + \theta_2 - 2\theta_3). \end{aligned} \quad (4.6)$$

The $x = 0$ tunneling operators between the three wires are more easily expressible in terms of these rotated fields. Also, the product of two Klein factors is simplified by using $\eta_j \eta_{j-1} = -i\eta_{j+1}$ (recall that lead $0 \equiv 3$), we can write

$$H_B = \sum_{a=1}^3 \left(i\Gamma e^{i\phi/3} \eta_a e^{i\vec{K}_a \cdot \vec{\Phi}} + \text{h.c.} \right) + r\sqrt{3} \partial_x \Phi_0 \Big|_{x=0}, \quad (4.7)$$

where

$$\vec{\Phi} = (\Phi_1, \Phi_2), \quad (4.8)$$

and

$$\begin{aligned} \vec{K}_1 &= (-1/2, \sqrt{3}/2) \\ \vec{K}_2 &= (-1/2, -\sqrt{3}/2) \\ \vec{K}_3 &= (1, 0). \end{aligned} \quad (4.9)$$

The boundary interactions lead to renormalization to an infrared fixed point with a different boundary condition from Neumann on the two fields $\Phi_{1,2}$. However, current conservation at the junction requires the ‘‘center of mass’’ field Φ_0 to always obey Neumann boundary conditions. Thus the remaining degrees of freedom at the boundary comprise the two component boson field $\vec{\Phi} = (\Phi_1, \Phi_2)$. Notice that the term proportional to r in Eq. (4.7) is a constant due to the boundary condition on Φ_0 , and hence it can be dropped. Hence, the boundary action can finally be expressed as

$$S_B = i\Gamma e^{i\phi/3} \int d\tau \sum_{a=1}^3 \eta_a e^{i\vec{K}_a \cdot \vec{\Phi}} + \text{h.c.} \quad (4.10)$$

The scaling dimension of the hopping term in the disconnected limit ($\Gamma = 0$) is calculated by standard methods [1] as $1/g$, which is not affected by the Klein factors nor the magnetic flux. The hopping term is thus irrelevant for $g < 1$, and the N fixed point corresponding to disconnected wires is stable.

When $g > 1$, the hopping term is relevant and the N fixed point is unstable. The system is renormalized into an infrared fixed point different from the N fixed point. The infrared fixed point should correspond to some conformally invariant boundary condition. Identification of such a fixed point in general is a rather difficult problem, even in the pure bosonic problem without the Klein factors as discussed in Refs. [1, 15, 16, 33].

In the present case, moreover, additional complicity arises from the Klein factors, namely due to the Fermi statistics of the electrons. In the following Sections, using various approaches, we study possible infrared fixed points that are reached when the effect of the Klein factors is included.

V. STRONG HOPPING LIMIT

As we have discussed in the previous section, for $g > 1$ the hopping term is a relevant perturbation to the N

(disconnected) fixed point. We would like to know where the system flows into, once the relevant hopping term is added to the N fixed point. Tracing the RG flow exactly, starting from the N fixed point down to the infrared fixed point is generally difficult, except in fortunate cases where the flow is integrable. Even when we do not have the exact solution of the integrable RG flow, it often happens that some of the fixed points can be given exactly. Lacking the solution of the RG flow itself, we generally resort to conjecturing the RG flow, based on the known fixed points.

Thus the first step to construct the phase diagram is to construct the candidates for the infrared fixed points. Since the small hopping is relevant and grows under the RG transformation, a naive guess is that the hopping strength ‘‘goes to infinity’’ in the infrared limit. This simple guess turns out to be rather useful in many cases. However, as it will become clear later in this paper, the limit of the ‘‘infinite hopping strength’’ actually depends on the representation of the given problem.

A natural idea may be to take the hopping amplitude $\tilde{\Gamma}$ to infinity in the original electron representation Eq. (3.1). However, in the presence of interaction, it is difficult to know what happens in the $\tilde{\Gamma} \rightarrow \infty$. Instead, we could discuss the strong tunneling limit by taking the hopping strength Γ to infinity, *in the bosonized representation* Eq. (4.10). This is generally *different* from taking the hopping amplitude to infinity in the original electron models.

This approach was taken in Ref. [5] for the resonant dot model of the junction. Here we apply a similar argument to our model, namely the junction with direct hoppings between the wires, or equivalently the ‘‘ring’’ junction. The hopping term in the bosonized representation corresponds to the boundary potential for $\vec{\Phi}$. Thus, the field $\vec{\Phi}$ would be pinned to the potential minimum at the boundary in the limit $\Gamma \rightarrow \infty$. Namely, the strong hopping limit corresponds to the Dirichlet boundary condition on $\vec{\Phi}$. However, in fact, there are different types of Dirichlet boundary conditions (or more precisely, boundary states) with different stability. All the Dirichlet boundary conditions, on the other hand, give rise to the same conductance tensor. As was discussed by Nayak et al. [5], the Dirichlet boundary conditions exhibits an enhanced conductivity which may be understood as a result of Andreev reflection (see Ref. [25]).

In order to analyze the stability of the Dirichlet boundary condition, we have to identify the potential minima of the hopping action Eq. (4.10) at the boundary. As was emphasized by Nayak et al. [5], the stability of the Dirichlet boundary condition is indeed affected by the presence of the Klein factors.

To demonstrate the importance of the Klein factors, let us first consider the fictitious problem without them. If there were no Klein factors in Eq. (4.4) to begin with,

the boundary action would read

$$S_B = -2\Gamma \int d\tau \sum_{a=1}^3 \cos(\vec{K}_a \cdot \vec{\Phi} + \phi/3). \quad (5.1)$$

This is equivalent to the model studied by Yi and Kane [16] (see also Ref. [33]) in the context of the quantum Brownian motion on a triangular/honeycomb lattice. The minima of this boundary potential is given by a honeycomb lattice with lattice constant (distance between nearest neighbors) $4\pi/3$ if $\phi/3 \equiv \pi(\text{mod } 2\pi)$, and a triangular lattice with lattice constant $4\pi/\sqrt{3}$ otherwise.

The stability of the $\Gamma \rightarrow \infty$ fixed point is conveniently studied after integrating out the fields $\vec{\Phi}(\tau, x)$ for $x > 0$, thus deriving an effective boundary action. [A more detailed discussion in a related context is given in Subsubsection (XC2).] Consider a general boundary field $\vec{\Phi}(\tau)$, in the imaginary time formalism at temperature $1 = 1/\beta$, with Fourier expansion:

$$\vec{\Phi}_b(\tau) = \frac{1}{\beta} \sum_n \vec{\Phi}(\omega_n) e^{i\omega_n \tau}. \quad (5.2)$$

(Here $\omega_n \equiv 2\pi n/\beta$.) The solution of the classical equations of motion, $\partial^2 \vec{\Phi}(\tau, x) = 0$ with boundary condition $\vec{\Phi}(\tau, 0) = \vec{\Phi}_b(\tau)$, (defined for $x > 0$ only) is

$$\vec{\Phi}^{\text{cl}}(\tau, x) = \frac{1}{\beta} \sum_n \vec{\Phi}_n e^{i\omega_n \tau - |\omega_n| x}. \quad (5.3)$$

Substituting into Eq. (4.1) gives the non-interaction term in the boundary action (at $\beta \rightarrow \infty$):

$$S_0 = g \int \frac{d\omega}{(2\pi)^2} |\omega| \vec{\Phi}^*(\omega) \cdot \vec{\Phi}(\omega). \quad (5.4)$$

The full boundary action also includes the potential term of Eq. (5.1), which can be written entirely in terms of the boundary field $\vec{\Phi}_b(\tau)$, the Fourier transform of $\vec{\Phi}(\omega)$. When $\Gamma \rightarrow \infty$ the path integral is dominated by configurations where the fields $\vec{\Phi}_b(\tau)$ stay close to one of the minima of the potential. Rare tunneling events (instantons) occur in which $\vec{\Phi}_b(\tau)$ goes from one minimum to a neighboring one. In general, multi-instanton configurations must be considered in the dilute gas approximation. This is reviewed in some detail in a related context in Subsec. (VIC). The conclusion is that, for a multi-instanton configuration in which $\vec{\Phi}$ tunnels between minima of V separated by \vec{M}_i at time τ_i , the instanton interaction term in the action, for large time separations, $|\tau_i - \tau_j|$, takes the form:

$$S_{\text{int}} = -\frac{g}{(2\pi)^2} \sum_{i>j} \vec{M}_i \cdot \vec{M}_j \ln(\tau_i - \tau_j)^2. \quad (5.5)$$

This implies that a single tunneling process corresponds to an operator in the effective Hamiltonian, at the infinite Γ fixed point, with a RG scaling dimension:

$$\Delta = \frac{g}{(2\pi)^2} |\vec{M}_i|^2. \quad (5.6)$$

This is $4g/9$ and $4g/3$ respectively for the honeycomb and triangular cases. Thus these Dirichlet boundary conditions are stable for $g > 9/4$ and $g > 3/4$ respectively. This would be troublesome especially in the noninteracting case $g = 1$, as the “triangular” Dirichlet boundary condition is stable. Because the Dirichlet boundary condition corresponds to the enhanced conductance due to the Andreev reflection, it should not be realized if there is no interaction.

However, the correct bosonized representation for the junction of electron systems should include the Klein factors (as Pauli matrices) as in Eq. (4.10), to reproduce the effect of the Fermi statistics of electrons. Following Ref. [5], the classical value for the boundary field $\vec{\Phi}$ is obtained by diagonalizing the boundary term in the auxiliary two-dimensional Hilbert space on which the Pauli matrices act. The resulting potential is

$$V(\vec{\Phi}) = \pm \sqrt{\sum_a \sin^2(\vec{K}_a \cdot \vec{\Phi} + \phi/3)}, \quad (5.7)$$

with two branches corresponding to \pm for a given boundary value of $\vec{\Phi}$. The potential minima of $\vec{\Phi}$, in the $-$ branch, are those which make the argument of the square-root maximum. As in the case without the Klein factors, the structure of the potential minima depends on the flux ϕ . For the time-reversal symmetric case $\phi = 0, \pi$, the potential minima form a honeycomb lattice with the nearest neighbor distance $2\pi/3$. For other cases ($\phi \neq 0, \pi$) the potential minima is instead a triangular lattice with the nearest neighbor distance $2\pi/\sqrt{3}$. The scaling dimension of the leading perturbation, which is proportional to the nearest neighbor distance squared, is $g/9$ and $g/3$ respectively for the honeycomb and triangular cases.

As was mentioned above, the “strong hopping” limit in the bosonized representation corresponds to Dirichlet boundary condition for the boson field $\vec{\Phi}$ in either case. However, the operator content (and thus the stability) differs in these cases. Thus we distinguish them by referring to the honeycomb ($\phi = 0, \pi$) and the triangular ($\phi \neq 0, \pi$) cases as D_N and D_P fixed points respectively. N of D_N stands for Nayak et al., as it is identical to the one discussed in Ref. [5] for the junction with the quantum dot. P of D_P stands for pair-tunneling; let us now show that the D_P fixed point may be regarded as the limit of strong tunneling of electron pairs.

We emphasize again that the strong hopping limit $\Gamma \rightarrow \infty$ in the bosonized representation is different from the $\tilde{\Gamma} \rightarrow \infty$ limit in the original electron model. This is evident in the non-interacting case $g = 1$, where the original electron model should be always described by a free electron scattering matrix. In this case, the strong hopping limit in the bosonized representation gives the D_P or D_N fixed point, which exhibits the Andreev reflection and thus cannot be described by free electron scattering. For $g = 1$ both D_P and D_N fixed points are unstable. Thus, as far as the infrared stable fixed point is

concerned, the original electron model and the bosonized representation give consistent conclusions.

If we introduce the hopping of electron pairs instead of electrons, the boundary action should be given by

$$S'_{\mathcal{B}} = 2\Gamma_P \int d\tau \sum_{a=1}^3 \cos\left(2\vec{K}_a \cdot \vec{\Phi} + 2\phi/3\right) + \text{h.c.} \quad (5.8)$$

The sign of the pair-tunneling parameter Γ_P , may be deduced from second order perturbation theory in the single-electron tunneling parameter Γ . From the operator product expansion:

$$e^{i\vec{K}_a \cdot \vec{\Phi}(z)} e^{i\vec{K}_a \cdot \vec{\Phi}(0)} \rightarrow C|z|^{2/g} e^{2i\vec{K}_a \cdot \vec{\Phi}(0)}, \quad (5.9)$$

for a positive constant, C , and taking into account that $\eta_i^2 = -1$, we conclude that $\Gamma_P \propto \Gamma^2 > 0$. We note that the Klein factors are absent from the action. This is natural, considering that the electron pair is a bosonic object. For $\phi \neq 0, \pi$, the potential minima form a triangular lattice with the nearest neighbor distance $2\pi/\sqrt{3}$. Thus the boundary condition in the strong pair-tunneling limit $\Gamma_P \rightarrow \infty$ is identified with D_P . For $\phi = 0, \pi$, the potential minima form a honeycomb lattice with the nearest neighbor distance $2\pi/3$. Thus the strong pair-tunneling limit is again identified with the more unstable D_N , in the time-reversal invariant cases $\phi = 0, \pi$.

Therefore, the strong pair-tunneling limit $\Gamma_P \rightarrow \infty$ gives the same boundary conditions as the strong hopping limit $\Gamma \rightarrow \infty$. As the pair-tunneling term would be generated through the RG transformation even if the microscopic model only contains the single electron hopping, this serves as a consistency check.

We note that even though the junction with $\phi \neq 0, \pi$ is not time reversal symmetric, the strong hopping limit for $\phi \neq 0, \pi$ is the D_P fixed point which is time-reversal symmetric in itself. This is of course not a contradiction because the symmetry may be higher at the infrared fixed point than in the original microscopic model. This symmetry restoration may be understood naturally by considering the maximally time-reversal breaking flux $\phi = \pm\pi/2$ for the electron hopping model. At this value of the flux, the pair-tunneling model Eq. (5.8) is actually time-reversal invariant, as the Aharonov-Bohm phase for the electron pair is π instead of $\pm\pi/2$.

What is more surprising is that the model with $\phi = 0, \pi$ apparently cannot reach the D_P fixed point, although there is no symmetry forbidding it. This was deduced from the structure of the potential minima in the $\Gamma_P \rightarrow \infty$ limit, as discussed above. We note that this result relies on the assumption that the sign of the coefficient Γ_P of the potential does not change under the RG flow. A similar assumption was used in Ref. [16] for the related model of the quantum Brownian motion. Of course, if Γ_P is the only coupling constant in the theory, it should not change sign because the RG flow cannot cross the fixed point corresponding to the Neumann boundary condition. However, in the present problem, the validity of

the assumption is subtle. This is because one should, in principle, consider both the single-electron hopping Γ and the pair hopping Γ_P simultaneously in discussing the RG flow.

While we have not yet resolved this question, the above arguments lead to the following result on the phase diagram of the system.

A. time-reversal symmetric $\phi = 0, \pi$ case

The N fixed point (decoupled wire) is stable for $g < 1$ and unstable for $g > 1$. The D_N fixed point is unstable for $g < 9$ and stable for $g > 9$. Therefore, the system should flow to some ‘‘intermediate’’ stable fixed point for $1 < g < 9$. The intermediate fixed point corresponds to neither Dirichlet nor Neumann boundary conditions.

This conclusion is similar to that in Ref. [5] for a different setup of the junction. The only difference is that the N fixed point in their model is unstable for $g > 1/2$ because of the resonant transmission through the dot.

B. time-reversal breaking $\phi \neq 0, \pi$ case

In our model, we have the flux ϕ as a new parameter which breaks the time-reversal symmetry, and can lead to new physics.

In fact, as it is seen above, the new Dirichlet fixed point D_P can be realized for $\phi \neq 0, \pi$. It is stable for $g > 3$, so we expect a generic junction without time-reversal symmetry to flow to D_P for $g > 3$. We note that although the D_P fixed point itself is time-reversal invariant, it seems that the time-reversal symmetry in the original junction model must be broken to reach D_P .

For $1 < g < 3$, as both the N and D_P fixed points are unstable, there must be an intermediate stable fixed point to which the generic system flows. However, the present argument does not shed light on the nature of the stable fixed point. In the following sections, we will argue that the stable fixed point for $1 < g < 3$ is solvable with different techniques that we present in this paper.

VI. CONNECTION WITH THE DISSIPATIVE HOFSTADTER MODEL

As we have seen in the last section, there are infrared stable fixed points that cannot be identified with either weak- or strong- hopping limit in the bosonized representation Eq. (4.10) with the Klein factors.

The presence of the phase factors due to the fermionic statistics, encoded in the Klein factors, makes the analysis more difficult than that for the standard problems with only bosonic terms in the boundary action. The extra phases due to the fermionic statistics appear, for example, if one attempts a perturbative expansion in the

hopping amplitude Γ . The coefficients appearing in each order in perturbation theory are different than those obtained without the phase factors, and hence they alter the nature of the strong hopping limit.

In this section, we develop an alternative representation, in which the fermionic statistics of electrons are encoded without using the Klein factors. Namely, we will show that the perturbative series in the hopping amplitude Γ for the Y-junction problem is identical to the series obtained for the dissipative Hofstadter model (quantum motion of a single particle under a magnetic field and a periodic potential, subject to dissipation) studied by Callan and Freed in Ref. [23]. In the dissipative Hofstadter action, phase factors arise from the motion in

a magnetic field, but the action contains solely bosonic terms, and hence it is amenable to standard methods for determining the strong coupling behavior, such as instanton expansions.

A. Generalized Coulomb gas from the Y-junction

We consider the perturbation theory in the hopping parameter Γ , starting from the bosonized representation Eq. (4.10) with the Klein factor. The partition function Z_Y of the system can be expanded as

$$Z_Y = \sum_n \Gamma^n \int_{\tau_{n-1}}^{\infty} d\tau_n \int_{\tau_{n-2}}^{\tau_n} d\tau_{n-1} \cdots \int_{-\infty}^{\tau_2} d\tau_1 \sum_{\{\vec{L}_j\}} \left[\zeta_{\vec{L}_n} \cdots \zeta_{\vec{L}_2} \zeta_{\vec{L}_1} \right] \langle e^{i\vec{L}_n \cdot \vec{\Phi}(\tau_n)} \cdots e^{i\vec{L}_2 \cdot \vec{\Phi}(\tau_2)} e^{i\vec{L}_1 \cdot \vec{\Phi}(\tau_1)} \rangle_0, \quad (6.1)$$

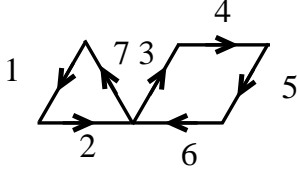


FIG. 14: A typical closed path occurring in perturbative expansion of partition function

where $\vec{L}_j = q_j \vec{K}_{a_j}$ is one of the six vectors $\pm \vec{K}_{1,2,3}$ ($q_j = \pm 1$ and $a_j = 1, 2, 3$), and $\langle \rangle_0$ denotes the expectation value with the Neumann boundary condition on $\vec{\Phi}$. The $\zeta_{\vec{L}_j} = (-i)^{q_j} e^{iq_j \phi/3} \eta_{a_j}$ in the [...] term in Eq. (6.1) keep track of the phase factors.

Now, each term in the expansion Eq. (6.1) corresponds to a closed directed path formed by the vectors $\vec{L}_1, \vec{L}_2, \dots, \vec{L}_n$, on the triangular lattice spanned by the primitive vectors \vec{K}_1 and \vec{K}_2 . An example of a closed path is shown in Fig. 14. A charge vector \vec{L}_j is associated to each vertex operator $e^{i\vec{L}_j \cdot \vec{\Phi}}$, and the condition that the sequence of vectors must form a closed path is a consequence of the charge neutrality condition of the Coulomb gas expansion.

Let us now argue that the total phase factor for a given path $\mathcal{L} = (\vec{L}_1, \vec{L}_2, \dots, \vec{L}_n)$,

$$e^{i\Upsilon_{\mathcal{L}}} = \left[\zeta_{\vec{L}_n} \cdots \zeta_{\vec{L}_2} \zeta_{\vec{L}_1} \right], \quad (6.2)$$

is the sum of the phase contributions from all the elementary triangles enclosed by the loop. The phase contributions from “up” and “down” triangles, however, are different. The phase factor for a counterclockwise loop

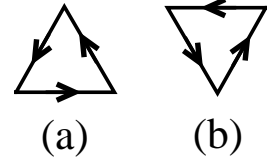


FIG. 15: (a) a counter-clockwise loop around an “up triangle”. (b) A counter-clockwise loop around a “down triangle”.

on the up triangle [see part (a) of Fig. 15] is determined to be

$$e^{iv_{\Delta}} = (-i\eta_3)e^{i\phi/3}(-i\eta_2)e^{i\phi/3}(-i\eta_1)e^{i\phi/3} = e^{i\phi} \quad (6.3)$$

while that for the counterclockwise loop on the down triangle [see part (b) of Fig. 15] is

$$e^{iv_{\nabla}} = (i\eta_3)e^{-i\phi/3}(i\eta_2)e^{-i\phi/3}(i\eta_1)e^{-i\phi/3} = e^{i(\pi-\phi)}. \quad (6.4)$$

Namely, loops on the triangular lattice pick up a phase as if there is a staggered magnetic flux of ϕ and $\pi - \phi$ in each elementary triangle. The total phase accumulated due to the loop \mathcal{L} is thus

$$\Upsilon_{\mathcal{L}} = N_{\Delta}(\mathcal{L}) v_{\Delta} + N_{\nabla}(\mathcal{L}) v_{\nabla}, \quad (6.5)$$

where $N_{\Delta}(\mathcal{L})$ and $N_{\nabla}(\mathcal{L})$ are the *net* numbers of up and down triangles enclosed by the path (a triangle contributes ± 1 to N_{Δ} and N_{∇} depending on whether it is traversed clockwise or counter-clockwise).

The argument why the phase for a given path \mathcal{L} is the sum of the phases due to the enclosed elementary triangles is constructed inductively. First consider the special case where the closed path consists of a single non-intersecting closed loop. This implies that each vertex on

the loop is visited a single time except for the first vertex which is visited twice, at the beginning and end of the loop. The phase from this loop is equal to the sum of phases of elementary triangular loops into which it can be decomposed. Say it is so for all paths enclosing up to m triangles, and then consider a loop enclosing $m + 1$ triangles; we must argue that the phase accumulated around the loop enclosing $m + 1$ triangles is equal to the sum of the phases enclosed by two smaller area paths with m_1 and m_2 triangles ($m_1 + m_2 = m + 1, m_{1,2} \leq m$).

Consider then an arbitrary non-intersecting loop $\mathcal{L} = (\vec{L}_1, \vec{L}_2, \dots, \vec{L}_n)$, which we break into two loops by adding an internal segment that splits the loop into two loops. Let the segment be the sequence of vectors $\vec{L}'_1, \vec{L}'_2, \dots, \vec{L}'_p$. It is easy to show that

$$\left[\zeta_{-\vec{L}'_1} \zeta_{-\vec{L}'_2} \cdots \zeta_{-\vec{L}'_p} \right] \left[\zeta_{\vec{L}'_p} \cdots \zeta_{\vec{L}'_2} \zeta_{\vec{L}'_1} \right] = \mathbb{1}, \quad (6.6)$$

so that

$$e^{i\Upsilon_{\mathcal{L}}} = \left[\zeta_{\vec{L}_n} \cdots \zeta_{\vec{L}_{j+2}} \zeta_{\vec{L}_{j+1}} \zeta_{-\vec{L}'_1} \zeta_{-\vec{L}'_2} \cdots \zeta_{-\vec{L}'_p} \right] \left[\zeta_{\vec{L}'_p} \cdots \zeta_{\vec{L}'_2} \zeta_{\vec{L}'_1} \zeta_{\vec{L}_j} \cdots \zeta_{\vec{L}_2} \zeta_{\vec{L}_1} \right] = e^{i\Upsilon_{\mathcal{L}_1}} e^{i\Upsilon_{\mathcal{L}_2}}, \quad (6.7)$$

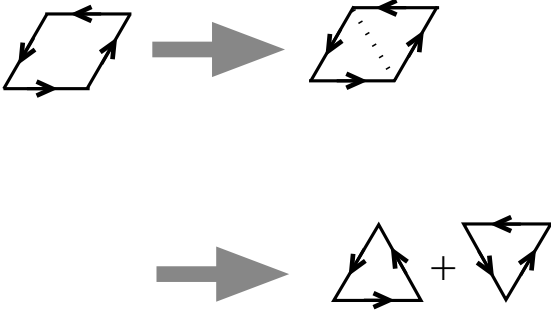


FIG. 16: Decomposition of a non-crossing loop into elementary triangles

for two loops $\mathcal{L}_{1,2}$ that encircle areas smaller than the original loop \mathcal{L} , *i.e.*, $l_{1,2} \leq m$ and with $l_1 + l_2 = m + 1$, as required by the induction argument. An example of a decomposition of a non-crossing loop into elementary triangles is given in Fig. 16.

Finally we must argue that an arbitrary closed path can be decomposed into a set of non-intersecting loops such that the total phase of the path is the sum of phases for each non-intersecting loop. This can be seen as follows. Consider following an arbitrary oriented path. Consider the first time that any vertex on the path is visited for a second time. Label this vertex V_1 . The sequence of edges between the first and second visit to V_1 defines a non-intersecting closed loop, L_1 . (This follows since the first intersection on the path occurs at V_1 at the instant of the second visit.) The phase due to this closed non-intersecting loop may be calculated unambiguously and makes an additive contribution to the total phase of the path. This follows since the product of the Klein factors around a closed loop is always proportional to the identity matrix. Now excise the closed loop, L_1 , from the path. The remaining path remains closed. Consider the first time that any vertex on this excised path is visited twice, at some other vertex, V_2 . This de-

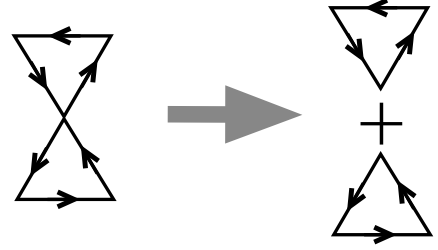


FIG. 17: Decomposition of a path into non-crossing loops

fines another closed loop L_2 which we again excise. We continue in this way until we finally revisit the first point on the path. This final revisitation defines a final closed loop L_n . An example of the decomposition of a path into non-crossing loops is given in Fig. 17. Note that when a path (or an excised path) makes a U-turn and retraces a link this counts as a closed loop of length 2 and zero area. The total phase associated with the path is the sum of phases of each non-intersecting closed loop. These phases can each be expressed as a sum of phases of elementary triangles into which they can be decomposed. Adding up the net number of up triangles and down triangles in all the non-intersecting loops gives us Eq. (6.5) for the total phase.

Let us now turn to the correlation function entering in Eq. (6.1):

$$\langle e^{i\vec{L}_n \cdot \vec{\Phi}(\tau_n)} \cdots e^{i\vec{L}_2 \cdot \vec{\Phi}(\tau_2)} e^{i\vec{L}_1 \cdot \vec{\Phi}(\tau_1)} \rangle_0 = \delta_K(\sum_j \vec{L}_j) \exp \left[\frac{1}{g} \sum_{j>k} \vec{L}_j \cdot \vec{L}_k \ln |\tau_j - \tau_k|^2 \right], \quad (6.8)$$

where $\delta_K(\vec{L}) = 1$ if $\vec{L} = 0$, and $\delta_K(\vec{L}) = 0$ otherwise. The factor $\delta_K(\sum_j \vec{L}_j)$ enforcing the charge vectors \vec{L}_j must form a closed path, as we mentioned above, explicitly follows from of charge conservation in the Coulomb gas expansion.

Using this expression, in conjunction with the phase factor we discussed above, we can rewrite the partition

function as:

$$Z_Y = \sum_n \Gamma^n \int_{\tau_{n-1}}^{\infty} d\tau_n \int_{\tau_{n-2}}^{\tau_n} d\tau_{n-1} \cdots \int_{-\infty}^{\tau_2} d\tau_1 \sum_{\mathcal{L}=(\vec{L}_1, \dots, \vec{L}_n)} \delta_K(\sum_j \vec{L}_j) e^{i\Upsilon_{\mathcal{L}}} e^{\frac{1}{g} \sum_{j>k} \vec{L}_j \cdot \vec{L}_k \ln |\tau_j - \tau_k|^2}. \quad (6.9)$$

Thus, the partition function Z_Y is written in a similar form to the so-called Coulomb gas (particles interacting with the logarithmic potential) in one dimension. The difference from the standard Coulomb gas is in the phase factor $e^{i\Upsilon_{\mathcal{L}}}$, which is indeed the consequence of the Fermi statistics of the electron and of the Aharonov-Bohm phase. We may call this a “generalized Coulomb gas.” In fact, below we show that this is indeed identical to the generalized Coulomb gas which appeared in a quite different problem – the dissipative Hofstadter model on a triangular lattice.

B. Generalized Coulomb gas from the dissipative Hofstadter model

Dissipative quantum mechanics (also known as quantum Brownian motion) is the problem of the quantum motion of a single particle subject to dissipation (see Ref. [26] for a review). In the presence of any periodic potential, single-particle quantum mechanics implies that the particle never localizes due to the tunneling effect. However, if the dissipation is sufficiently strong, the tunneling can be suppressed and the particle may be localized. When the dissipation is Ohmic, there is a surprising mapping of the problem to the boundary problem of the free boson field theory. Here, the bulk of the free boson is related to the heat bath in the dissipative quantum mechanics, and only the boundary field is related to the original particle. By integrating over the bulk degrees of freedom, the boundary problem can be reduced to the

one-dimensional Coulomb gas.

Dissipative quantum mechanics in the presence of the periodic potential and the magnetic field is known as the dissipative Hofstadter problem. It is again related to the boundary problem of the free boson, or the following one-dimensional generalized Coulomb gas. The “free” action for the dissipative Hofstadter model, namely the effective action in the absence of the potential (but with the magnetic field and the dissipation), is

$$S_0[\vec{X}] = \frac{1}{2} \int \frac{d\omega}{(2\pi)^2} [\alpha|\omega|\delta_{\mu\nu} + \beta\omega\epsilon_{\mu\nu}] X_{\mu}^*(\omega) X_{\nu}(\omega), \quad (6.10)$$

where $\mu, \nu = 1, 2$ and $\epsilon_{12} = -\epsilon_{21} = 1$, $\epsilon_{11} = \epsilon_{22} = 0$. α and β are related to the dissipation and the magnetic field, respectively. This determines the propagator:

$$D_{\mu\nu}(\tau) = \langle X_{\mu}(\tau) X_{\nu}(0) \rangle = -\frac{\alpha}{\alpha^2 + \beta^2} \ln \tau^2 \delta_{\mu\nu} + i\pi \frac{\beta}{\alpha^2 + \beta^2} \text{sgn} \tau \epsilon_{\mu\nu}. \quad (6.11)$$

We now introduce a potential term with the periodicity of the triangular lattice (notice the difference from the “rectangular” one in Ref. [23]), as

$$S_V[\vec{X}] = -V e^{i\delta/3} \int d\tau \sum_{a=1}^3 e^{i\vec{K}_a \cdot \vec{X}} + \text{c.c.}, \quad (6.12)$$

where V and δ are chosen to be real. Expanding the partition function in powers of V , one obtains

$$Z_{\text{DHM}} = \sum_n V^n \int_{\tau_{n-1}}^{\infty} d\tau_n \int_{\tau_{n-2}}^{\tau_n} d\tau_{n-1} \cdots \int_{-\infty}^{\tau_2} d\tau_1 \sum_{\{L_j\}} [\kappa_{\vec{L}_n} \cdots \kappa_{\vec{L}_2} \kappa_{\vec{L}_1}] \langle e^{i\vec{L}_n \cdot \vec{X}(\tau_n)} \cdots e^{i\vec{L}_2 \cdot \vec{X}(\tau_2)} e^{i\vec{L}_1 \cdot \vec{X}(\tau_1)} \rangle_0, \quad (6.13)$$

where again $\vec{L}_j = q_j \vec{K}_{a_j}$ is one of the six vectors $\pm \vec{K}_{1,2,3}$ ($q_j = \pm 1$ and $a_j = 1, 2, 3$), and the $\kappa_{\vec{L}_j} = e^{iq_j \delta/3}$ in the [...] term keep track of phase factors due to δ . The

correlation function is given by

$$\langle e^{i\vec{L}_n \cdot \vec{X}(\tau_n)} \cdots e^{i\vec{L}_2 \cdot \vec{X}(\tau_2)} e^{i\vec{L}_1 \cdot \vec{X}(\tau_1)} \rangle_0 = \delta_K(\sum_j \vec{L}_j) \exp \left[\frac{\alpha}{\alpha^2 + \beta^2} \sum_{j>k} \vec{L}_j \cdot \vec{L}_k \ln |\tau_j - \tau_k|^2 - i\pi \frac{\beta}{\alpha^2 + \beta^2} \sum_{j>k} \vec{L}_j \times \vec{L}_k \text{sgn}(\tau_j - \tau_k) \right]. \quad (6.14)$$

(Because of the time ordering, notice that $\text{sgn}(\tau_j - \tau_k) = 1$ for all terms in the sum.)

Notice that the $\kappa_{\vec{L}_j}$ in the [...] of Eq. (6.13) commute with one another, in contrast to the Klein factors $\zeta_{\vec{L}_j}$ in the [...] of Eq. (6.1). However, the $\langle \cdot \rangle_0$ term in Eq. (6.14) contains phase factors not present in Eq. (6.8). While the phases entering the perturbative expansions for Z_Y and Z_{DHM} are arising from different sources, their net effect turns out to be identical, as we show below.

The phases in the expansion of the dissipative Hofstadter model can also be associated with the closed paths $\mathcal{L} = (\vec{L}_1, \vec{L}_2, \dots, \vec{L}_n)$. The contribution from the $\vec{L}_j \times \vec{L}_k$ terms amounts to a flux through the oriented area $\mathcal{A}_{\mathcal{L}}$ enclosed by \mathcal{L} . To see this we again decompose any closed path into a set of closed non-intersecting loops. The oriented area of such a non-intersecting loop is

$$\mathcal{A}_{\mathcal{L}} = -\frac{1}{2} \sum_{j>k} \vec{L}_j \times \vec{L}_k . \quad (6.15)$$

Thus, the accumulated phase $\Lambda_{\mathcal{L}}$ due to the magnetic flux is

$$\Lambda_{\mathcal{L}} = 2\pi \frac{\beta}{\alpha^2 + \beta^2} \mathcal{A}_{\mathcal{L}} \quad (6.16)$$

$$= 2\pi \frac{\beta}{\alpha^2 + \beta^2} A [N_{\Delta}(\mathcal{L}) + N_{\nabla}(\mathcal{L})] , \quad (6.17)$$

where $A = \frac{\sqrt{3}}{4}$ is the area of an elementary triangle, and $N_{\Delta}(\mathcal{L})$, $N_{\nabla}(\mathcal{L})$ are the *net* numbers of enclosed elementary up and down triangles, as before.

Now we turn to the phase due to the [...] in Eq. (6.13). The total phase factor for a given closed path $\mathcal{L} = (\vec{L}_1, \vec{L}_2, \dots, \vec{L}_n)$,

$$e^{i\Xi_{\mathcal{L}}} = \left[\kappa_{\vec{L}_n} \cdots \kappa_{\vec{L}_2} \kappa_{\vec{L}_1} \right] , \quad (6.18)$$

is the sum of the phase contributions from all the elementary triangles enclosed by the path. The argument

for this is carried out by induction, identically to what we have used for the products of the $\zeta_{\vec{L}_j}$ above.

The phase contributions from “up” and “down” triangles are again different. The phase factor for a counterclockwise loop on the up triangle is determined determined to be

$$e^{i\delta/3} e^{i\delta/3} e^{i\delta/3} = e^{i\delta} \quad (6.19)$$

while that for the counterclockwise loop on the down triangle is

$$e^{-i\delta/3} e^{-i\delta/3} e^{-i\delta/3} = e^{-i\delta} . \quad (6.20)$$

Namely, loops on the triangular lattice pick up a phase as if there is a staggered magnetic flux of δ and $-\delta$ in each elementary triangle. The total phase accumulated due to the loop \mathcal{L} is thus

$$\Xi_{\mathcal{L}} = N_{\Delta}(\mathcal{L}) \delta - N_{\nabla}(\mathcal{L}) \delta , \quad (6.21)$$

where $N_{\Delta}(\mathcal{L})$ and $N_{\nabla}(\mathcal{L})$ are the net numbers of up and down triangles enclosed by the loop.

The total phase factor due to the loop \mathcal{L} is the sum $\tilde{\Upsilon}_{\mathcal{L}} = \Lambda_{\mathcal{L}} + \Xi_{\mathcal{L}}$:

$$\tilde{\Upsilon}_{\mathcal{L}} = N_{\Delta}(\mathcal{L}) \tilde{v}_{\Delta} + N_{\nabla}(\mathcal{L}) \tilde{v}_{\nabla} , \quad (6.22)$$

where

$$\tilde{v}_{\Delta} = 2\pi \frac{\beta}{\alpha^2 + \beta^2} A + \delta \quad (6.23)$$

$$\tilde{v}_{\nabla} = 2\pi \frac{\beta}{\alpha^2 + \beta^2} A - \delta . \quad (6.24)$$

We can now rewrite the partition function for the dissipative Hofstadter model on the triangular lattice as:

$$Z_{\text{DHM}} = \sum_n V^n \int_{\tau_{n-1}}^{\infty} d\tau_n \int_{\tau_{n-2}}^{\tau_{n-1}} d\tau_{n-1} \cdots \int_{-\infty}^{\tau_2} d\tau_1 \sum_{\mathcal{L}=(\vec{L}_1, \dots, \vec{L}_n)} \delta_K(\sum_j \vec{L}_j) e^{i\tilde{\Upsilon}_{\mathcal{L}}} e^{\frac{\alpha}{\alpha^2 + \beta^2} \sum_{j>k} \vec{L}_j \cdot \vec{L}_k \ln |\tau_j - \tau_k|^2} . \quad (6.25)$$

Following Callan and Freed [23], we may regard the DHM partition function as the partition function of a generalized classical 1-dimensional Coulomb gas. τ_j is the position of the j^{th} particle and \vec{L}_j is its generalized “charge”, a vector quantity taking on six possible values.

C. Mapping of the Y-junction to the dissipative Hofstadter model

The expression for Z_{DHM} in Eq. (6.25) is identical to that for Z_Y in Eq. (6.9), provided the following conditions are satisfied. First we need the relation

$$\frac{\alpha}{\alpha^2 + \beta^2} = \frac{1}{g} , \quad (6.26)$$

for the scaling dimension of the leading perturbation to be matched between the two theories. Furthermore, in order to match the phase factor, we require $\tilde{\Upsilon}_{\mathcal{L}} \equiv \Upsilon_{\mathcal{L}} \bmod 2\pi$, or equivalently

$$\tilde{v}_{\Delta} \equiv v_{\Delta} \bmod 2\pi, \quad (6.27)$$

$$\tilde{v}_{\nabla} \equiv v_{\nabla} \bmod 2\pi, \quad (6.28)$$

i.e.

$$\begin{aligned} \frac{\sqrt{3}\pi}{2} \frac{\beta}{\alpha^2 + \beta^2} + \delta &= \phi \bmod 2\pi, \\ \frac{\sqrt{3}\pi}{2} \frac{\beta}{\alpha^2 + \beta^2} - \delta &= \pi - \phi \bmod 2\pi. \end{aligned} \quad (6.29)$$

The above two equations imply:

$$\begin{aligned} \sqrt{3} \frac{\beta}{\alpha^2 + \beta^2} &= (2n - 1) \\ \delta &= \phi + \pi(1/2 - n). \end{aligned} \quad (6.30)$$

for an arbitrary integer, n . Because the phases, ϕ and δ , are only defined modulo 2π , there is actually an infinite

number of different choices of α and β labeled by the integer n . Eqs. (6.26) and (6.30) give:

$$\begin{aligned} \alpha &= \frac{3g}{3 + (2n - 1)^2 g^2} \\ \beta &= \frac{\sqrt{3}(2n - 1)g^2}{3 + (2n - 1)^2 g^2}. \end{aligned} \quad (6.31)$$

To understand the ambiguity in the integer n , let us define the Coulomb gas charge density

$$\tilde{\rho}(\tau) \equiv \sum_{j=1}^N \vec{L}_j \delta(\tau - \tau_j). \quad (6.32)$$

The generalized ‘‘energy’’, E , of an arbitrary classical gas configuration is determined by the N positions, τ_j and charges, L_j . This generalized ‘‘energy’’ is now a complex quantity and $\exp(-E/T)$ (where T is the classical temperature) is given by Eq. (6.13). i.e.

$$-\frac{E}{T} = \sum_{j=1}^n [\ln V + i\delta q_j/3] + \frac{\alpha}{\alpha^2 + \beta^2} \sum_{j>k} \vec{L}_j \cdot \vec{L}_k \ln |\tau_j - \tau_k|^2 - i\pi \frac{\beta}{\alpha^2 + \beta^2} \sum_{j>k} \vec{L}_j \times \vec{L}_k \operatorname{sgn}(\tau_j - \tau_k), \quad (6.33)$$

where q_j is defined by $\vec{L}_j \equiv q_j \vec{K}_{a_j}$ as before. Since $\vec{L}_j \times \vec{L}_k$ is always 0 or $\pm\sqrt{3}/2$, $\exp[-E/T]$ is invariant under a shift:

$$\frac{\pi\sqrt{3}}{2} \frac{\beta}{\alpha^2 + \beta^2} \rightarrow \frac{\pi\sqrt{3}}{2} \frac{\beta}{\alpha^2 + \beta^2} + 2\pi. \quad (6.34)$$

Eqs. (6.23), (6.24) imply that there is also a symmetry under:

$$\begin{aligned} \frac{\pi\sqrt{3}}{2} \frac{\beta}{\alpha^2 + \beta^2} &\rightarrow \frac{\pi\sqrt{3}}{2} \frac{\beta}{\alpha^2 + \beta^2} + \pi \\ \delta &\rightarrow \delta - \pi, \end{aligned} \quad (6.35)$$

which corresponds to shifting the integer n in Eq. (6.31) by 1. Since the energy of any configuration is independent of n , it follows that the Coulomb gas charge density correlation function, $\langle \rho_{\mu}(\tau) \rho_{\nu}(\tau') \rangle$, is also n -independent.

On the other hand, the correlation function $\langle X^{\mu}(\tau) X^{\nu}(\tau') \rangle$, does depend on n . These two correlation functions can be simply related to each other by adding an external source, $\vec{a}(\tau)$, to the action, coupling to the Coulomb gas charge density. That is, we modify the energy of the Coulomb gas by:

$$-E/T \rightarrow -E/T - i \int d\tau \vec{a}(\tau) \cdot \tilde{\rho}(\tau). \quad (6.36)$$

The Coulomb gas correlation function is given by the

functional derivative of the partition function with respect to the source term:

$$\frac{\partial^2 \ln Z}{\partial a^{\mu}(\omega_n) \partial a^{\nu}(\omega'_n)} = -\frac{1}{(2\pi)^2} \langle \rho_{\mu}(-\omega_n) \rho_{\nu}(-\omega'_n) \rangle. \quad (6.37)$$

Note that the Coulomb gas energy arises from the functional integral over \vec{X} :

$$e^{-E/T} = \frac{1}{Z_0} V^n e^{i(\delta/3) \sum_j q_j} \int [d\vec{X}(\tau)] e^{-S_q(\vec{X})}, \quad (6.38)$$

where:

$$S_q \equiv S_0(\vec{X}) - i \int d\tau \vec{X}(\tau) \cdot \tilde{\rho}(\tau). \quad (6.39)$$

Here Z_0 is the functional integral with S_q replaced by S_0 , which is given by Eq. (6.10). Thus, adding a source term to the Coulomb gas corresponds to a modification of the potential term in the DHM action:

$$S_V[\vec{X}] \rightarrow -V e^{i\delta/3} \int d\tau \sum_{a=1}^3 e^{i\vec{K}_a \cdot [\vec{X}(\tau) + \vec{a}(\tau)]} + \text{c.c.}, \quad (6.40)$$

Alternatively, we may shift $\vec{X}(\tau) \rightarrow \vec{X}(\tau) - \vec{a}(\tau)$, removing the source term from the potential term in the DHM action but inserting it into the non-interaction term, S_0 :

$$S_0 \rightarrow \frac{1}{2} \int \frac{d\omega_n}{(2\pi)^2} [X^\mu(\omega_n) - a^\mu]^*(\omega_n) (D^{-1})_{\mu\nu}(\omega_n) [X^\nu(\omega_n) - a^\nu](\omega_n). \quad (6.41)$$

Here we have introduced the inverse of the DHM propagator, defined in Eq. (6.11), which is simply the matrix appearing in S_0 , in Eq. (6.10):

$$(D^{-1})_{\mu\nu} \equiv \alpha \delta_{\mu\nu} |\omega| + \beta \epsilon_{\mu\nu} \omega. \quad (6.42)$$

Taking a second derivative with respect to a^μ we see that:

$$\langle \rho_\mu(-\omega) \rho_\nu(-\omega') \rangle = \delta(\omega + \omega') (D)_{\mu\nu}^{-1}(-\omega) - \frac{1}{(2\pi)^2} (D^{-1})_{\mu\sigma}(-\omega) \langle X^\sigma(-\omega) X^\lambda(-\omega') \rangle (D)_{\lambda\nu}^{-1}(\omega'), \quad (6.43)$$

or, equivalently:

$$\langle X^\mu(-\omega_n) X^\nu(-\omega'_n) \rangle = (2\pi)^2 \delta(\omega_n + \omega'_n) D^{\mu\sigma}(-\omega_n) - (2\pi)^2 D^{\mu\sigma}(-\omega_n) \langle \rho_\sigma(-\omega_n) \rho_\lambda(-\omega'_n) \rangle D^{\lambda\nu}(\omega'_n) \quad (6.44)$$

Due to the complicated dependence of α and β on n , given by Eq. (6.31), and hence the complicated dependence of $D^{\mu\nu}$ on n , we see that $\langle X^\mu X^\nu \rangle$ is n -dependent.

However, what we are interested in here, for obtaining properties of the Y-junction, is only the Coulomb gas correlation functions, which are n -independent. Hence we may choose any value of n that we find convenient. It will sometimes be useful to deduce the long time behavior of $\langle X^\mu X^\nu \rangle$ by RG and physical arguments and then use Eq. (6.43) to deduce the Coulomb gas correlation function. In so doing we may choose any value of n . In general, the behavior of $\langle X^\mu X^\nu \rangle$ will depend strongly on n but this n -dependence will cancel when we compute $\langle \rho_\mu \rho_\nu \rangle$ using Eq. (6.43).

Let us now use this mapping between the Y-junction problem and the dissipative Hofstadter model and consider the case of $g > 1$. Then, as we have already discussed, the electron hopping is a relevant perturbation in the disconnected limit. In the DHM, for any choice of n , V is a relevant perturbation for $g > 1$. We would like to find the infrared stable fixed point reached in the low energy limit. A simple guess is that it occurs at $V \rightarrow \infty$. The stability of the $V \rightarrow \infty$ fixed point can be determined using the instanton method [23]. Namely, in the strong potential limit, the \vec{X} field is pinned at one of the minima of the potential (6.12). The leading perturbation to this limit is given by a tunneling process between the neighboring minima, represented by an ‘‘instanton.’’ This is a classical solution, $\vec{X}_{cl}(\tau)$ which interpolates between two adjacent minima of the potential as τ goes from $-\infty$ to ∞ . The nature of these solutions is discussed in Callan and Fried and, in more detail, in Ref. [27]. To determine the scaling dimension of the tunneling operator we must consider the classical action of

a dilute multi-instanton configuration which tunnels successively from minimum to minimum with each tunneling event well separated in time from the rest. This instanton gas is dilute because, in the limit of large V , the action of an instanton goes to infinity, so the density of instantons goes to zero. In the dilute limit, we can approximate such a multi-instanton by a sum of the form:

$$\vec{X}(\tau) \approx \vec{X}_0 + \sum_{j=1}^n \vec{X}_j(\tau - \tau_j), \quad (6.45)$$

where

$$\begin{aligned} \vec{X}_j(\tau) &\rightarrow 0, & (\tau \rightarrow -\infty) \\ &\rightarrow \vec{M}_j, & (\tau \rightarrow \infty). \end{aligned} \quad (6.46)$$

Here the j^{th} tunneling event takes place at time τ_j and involves the particle tunneling between two adjacent minima of $V(\vec{X})$, displaced by \vec{M}_j . In the dilute limit each function $\vec{X}_j(\tau)$ is a single instanton solution. In the long time low energy limit of interest to us, we may regard the single instanton solutions as having the form:

$$\vec{X}_{a_j}(\tau) \approx \vec{M}_j f(\tau), \quad (6.47)$$

for a real function, $f(\tau)$ which interpolates between 0 and 1. The Fourier transform of the multi-instanton solution can then be approximated as:

$$\vec{X}(\omega) \approx \sum_j \vec{M}_j e^{i\omega\tau_j} f(\omega). \quad (6.48)$$

The low frequency behavior of $f(\omega)$, which follows from the long time asymptotic behavior of the interpolating

function $f(\tau)$, is given by:

$$f(\omega) \rightarrow \frac{1}{i\omega}. \quad (6.49)$$

The important interaction term in the instanton action

$$S_{\text{int}} \approx \sum_{i>j} M_{i,\mu} M_{j,\nu} \int \frac{d\omega}{(2\pi)^2} e^{i\omega(\tau_j - \tau_i)} [\alpha|\omega|\delta_{\mu\nu} + \beta\epsilon_{\mu\nu}\omega] |f(\omega)|^2. \quad (6.50)$$

In the dilute limit, where the time separations are large, we may use the asymptotic form of $f(\omega)$ in Eq. (6.49).

$$S_{\text{int}} \approx -\frac{\alpha}{(2\pi)^2} \sum_{i>j} \vec{M}_i \cdot \vec{M}_j \ln |\tau_i - \tau_j|^2 + \frac{i\pi\beta}{(2\pi)^2} \sum_{i>j} \vec{M}_i \times \vec{M}_j \text{sgn}(\tau_i - \tau_j). \quad (6.51)$$

We see that this expansion is equivalent to the weak V expansion and therefore that the tunneling events are relevant only if

$$|\vec{M}_i|^2 \alpha^2 / (2\pi)^2 < 1. \quad (6.52)$$

Thus we see that the separation of the minima of the potential, $|\vec{M}_i|$ is a crucial quantity in determining the stability of the localized fixed point. This separation is determined by a simple classical analysis of the potential, $V(\vec{X})$ in Eq. (6.12). The stationary points of $V(\vec{X})$ occur at the points:

$$\vec{X} = \frac{4\pi}{3} \sum_{i=1}^2 n_i \vec{K}_i, \quad (6.53)$$

independent of δ and forming a triangular lattice. However, the energies (values of V) at these stationary points depend on δ . For general values of δ , these energies are different at the 3 sub-lattices into which the triangular lattice can be partitioned:

$$\begin{aligned} V(\vec{0}) &= -6V \cos(\delta/3) \\ V\left(4\pi \frac{\vec{K}_1}{3}\right) &= -6V \cos[(2\pi - \delta)/3] \\ V\left(-4\pi \frac{\vec{K}_2}{3}\right) &= -6V \cos[(2\pi + \delta)/3]. \end{aligned} \quad (6.54)$$

The sub-lattice containing $\vec{0}$, is a triangular lattice with basis vectors, $2\pi\vec{R}_i$ ($i = 1, 2$) with

$$\vec{R}_i \equiv (2/\sqrt{3}) \vec{K}_i \times \hat{z}. \quad (6.55)$$

comes simply from S_0 and is obtained by substituting Eq. (6.45) into S_0 in Eq. (6.10). This gives the instanton interaction term in the action:

In this we recover the Coulomb gas energy:

Of course, the other sub-lattices are simply displaced from this one by the fixed vectors, $(4\pi/3)\vec{K}_1$ and $(4\pi/3)\vec{K}_2$. Therefore, the vectors \vec{M}_i occurring in the instanton solutions are $\pm 2\pi\vec{R}_1$, $\pm 2\pi\vec{R}_2$ and $\pm 2\pi(\vec{R}_1 + \vec{R}_2)$ with length $4\pi/\sqrt{3}$. As we vary δ the relative energies on the three sub-lattices change. For $\delta = 0$, the potential minima occur on the $\vec{X} = 0$ sublattice. As we increase δ from zero, the minima remains on the $\vec{X} = 0$ sublattice until we reach $\delta = \pi$. For $\pi < \delta < 2\pi$, the minima are rather on the $\vec{X} = (4\pi/3)\vec{K}_1$ sub-lattice. Right at $\delta = \pi$, there are degenerate minima on both $\vec{X} = 0$ and $\vec{X} = (4\pi/3)\vec{K}_1$ sub-lattices. These two sub-lattices define a honeycomb lattice with lattice spacing $4\pi/3$, smaller by a factor of $1/\sqrt{3}$ compared to that of the triangular lattices.

Thus, from the dilute instanton analysis, we conclude that, for general δ , the localized phase is stable when

$$\Delta \equiv \frac{\alpha|2\pi R_i|^2}{(2\pi)^2} = \frac{4\alpha}{3} = \frac{4g}{3 + (2n - 1)^2 g^2} > 1. \quad (6.56)$$

While this does not prove rigorously that the DHM is in a localized phase for small V when this inequality is satisfied, it is reasonable to believe that the system is in a localized phase for large enough V , in this region of α .

For $n \neq 0$ or 1, the localized phase is never stable, for any value of g . This follows since the maximum value of Δ , with respect to g , for fixed n is $2/[\sqrt{3}|2n - 1|]$, which is < 1 for $n \neq 0$ or 1. On the other hand, for $n = 0$ or 1, $\Delta < 1$, for $1 < g < 3$. Thus it is reasonable to assume that the behavior of the Y-junction, at least for large Γ , corresponds to the localized phase of the DHM

in the $n = 0$, or 1 representation. This result appears at first peculiar because we might just as well have chosen a different value of n , in which case we would conclude that the DHM is *not* in the localized phase. For $g > 1$, the DHM is not in the freely diffusing phase either, since V is relevant. It therefore must be in some intermediate phase which is neither freely diffusing nor localized. Remarkably, Eq. (6.44) allows us to determine $\langle XX \rangle$ in these intermediate phases by determining $\langle \rho\rho \rangle$ using $n = 0$ or 1 [23].

However, an ambiguity still remains because both $n = 0$ and 1 give stable localized fixed points. However, the localized fixed points for these two values of n predict different $\langle \rho\rho \rangle$. Consistency requires that, while both of these fixed points is stable at large V , the RG flow goes all the way to the localized fixed point, starting from a small V , for only one of these two values of n . For the other value of n the RG flow should go to an intermediate V fixed point, which must give the same $\langle \rho\rho \rangle$.

The particular cases $\phi = \pm\pi/2$, which maximally break time-reversal, are instructive in understanding the resolution of this ambiguity. From Eq. (6.30), for $\phi = \pi/2$, the choice $n = 1$ (β positive) gives $\delta = 0$, and the potential minima forms a triangular lattice as usual. However the other choice $n = 0$ (β negative) gives $\delta = \pi$, for which the potential minima form a honeycomb lattice with spacing $4\pi/3$, making the strong potential limit unstable for all g . Similarly, for $\phi = -\pi/2$, $n = 0$ (β negative) is the unique choice that gives a stable fixed point. This suggests that these localized fixed points χ_{\pm} reflect the breaking of time reversal symmetry due to the magnetic flux ϕ . Indeed, the conductance at these fixed points exhibits a chiral behavior breaking the time reversal invariance, as we show below.

Let us next consider the case when ϕ is very close to, but not exactly equal to, $\pi/2$. If one chooses $n = 1$, δ will be close to zero, and the potential minima forms a triangular lattice with a large separation between the true minima and secondary minima. However, if one chooses $n = 0$ instead of $n = 1$, the minima of the potential $V(\vec{X})$ will form a triangular lattice with spacing $4\pi/\sqrt{3}$, but there are local minima with only slightly larger energy such that the distance between a true minimum and the nearest local minima is $4\pi/3$. We could then envision another type of approximate instanton solution where the particle tunnels from a true minimum to a local minimum where it lingers for a long but finite time but must eventually tunnel to a true minimum. The typical time that the particle spends at a minimum is determined by the instanton fugacity, and grows exponentially as $V \rightarrow \infty$. Thus this other type of instanton might never be important for sufficiently large V . However, for intermediate values of V , these instantons could play an important role, effectively preventing the RG flow to go to infinite V for the $n = 0$ choice. This argument suggests that the choice of $n = 1$ should represent the stable fixed point around a vicinity of $\phi = \pi/2$. Of course, similar statements hold regarding the case ϕ very close to $-\pi/2$, for

which $n = 0$ should represent the stable fixed point.

We are thus led to conjecture that the localized fixed point for $n = 1$ ($n = 0$) corresponds to the stable fixed point of the Y-junction, for $1 < g < 3$, even for small bare V , for a range of ϕ around $\pi/2$ ($-\pi/2$). While none of our arguments have proven rigorously that the RG flow really goes all the way from $V = 0$ to $V = \infty$ (i.e. to the localized phase) for any values of g and ϕ , this seems like the most “economical” assumption since otherwise there would necessarily be intermediate V fixed points for all values of n . On the other hand, for $\phi = 0$ or π , the $n = 0$ and $n = 1$ fixed points appear equally stable. Since, as we show in the next sub-section, the conductance exhibits broken time-reversal symmetry for these localized fixed points, we expect that neither of them is stable at $\phi = 0$. There must be some other stable fixed point, corresponding to intermediate V , in this case. We refer to this fixed point as M (for mysterious).

It is convenient to now think about the RG flow in the space of the physical parameters of the Y-junction, Γ and ϕ . We have proposed (unique) stable fixed points for ϕ near $\pi/2$ (χ_+) or $-\pi/2$ (χ_-) and another fixed point, M, stable for $\phi = 0$. While the χ_{\pm} fixed points are stable against a small change in the flux, we do not know whether the M fixed point has such a stability. The simplest assumption is that it is does not. In this case the RG flows might go to the χ_{\pm} fixed points for any non-zero ϕ , starting from arbitrarily small V . Alternatively, it is possible that the M fixed point is stable against adding a small flux. In that case, there would have to be additional unstable fixed points defining the boundaries between the basins of attraction of the M, χ_+ and χ_- fixed points. So again, an “economy” principle, suggests the simple picture with only 3 stable fixed points, for $1 < g < 3$, as sketched in Fig. 9.

D. Calculation of the conductance tensor

Let us calculate the conductance tensor G_{jk} as defined in Eq. (2.2) at the chiral fixed points χ_{\pm} . There are two convenient ways of introducing the voltages drops. They can either occur right at the junction, or else can be spread over finite regions of the wires which are long compared to microscopic length scales like k_F^{-1} but could still be short compared to the length of the wires and other long length scales such as an inelastic scattering length. Both lead to the same results. The former approach has the advantage that it allows the conductance tensor to be expressed in terms of the Coulomb gas correlation function. The latter approach is useful when the BCFT formalism is used and is the only method at our disposal in the case of the Dirichlet fixed point. We discuss each in turn, one in this section and the other in the next. For convenience, we set the electron charge, e , to -1 . (In our convention the actual electron charge $e < 0$.) We also set $\hbar = 1$.

We first consider the case where the voltage drop oc-

curs right at the junction. We then modify the tunneling Hamiltonian by time-dependent phases, $A_j(t)$:

$$H_T \rightarrow -\Gamma e^{i\phi/3} \sum_j \psi_j^\dagger \psi_{j-1} e^{i(A_j - A_{j-1})} + h.c. \quad (6.57)$$

Note that, in the case where $A_j(t) = -V_j t$, that this corresponds to the replacement:

$$\psi_j^\dagger(t) \rightarrow e^{-iV_j t} \psi_j^\dagger(t). \quad (6.58)$$

This corresponds to a potential V_j on wire j , so we see

that:

$$dA_j/dt = -V_j. \quad (6.59)$$

It is convenient to define I_j as the current on wire i , headed towards the junction:

$$I_j = -dN_j/dt = i[N_j, H]. \quad (6.60)$$

Here N_j is the total number of particles on wire j . Since only the tunneling terms destroy conservation of particle number on each wire separately, we readily obtain:

$$I_j = -i\Gamma \left[e^{i\phi/3} e^{i(A_j - A_{j-1})} \psi_j^\dagger \psi_{j-1} + e^{-i\phi/3} e^{i(A_j - A_{j+1})} \psi_j^\dagger \psi_{j+1} \right] + h.c. \quad (6.61)$$

Expanding to first order in the A_j 's gives:

$$\langle I_j \rangle = \langle I_j^0 \rangle - [(A_j - A_{j-1}) + (A_j - A_{j+1})] E_T/3. \quad (6.62)$$

Here E_T is the tunneling energy:

$$E_T = -\Gamma e^{i\phi/3} \sum_j \langle \psi_j^\dagger \psi_{j-1} \rangle + c.c. = -3\Gamma e^{i\phi/3} \langle \psi_j^\dagger \psi_{j-1} \rangle + c.c. \quad (6.63)$$

where the Z_3 symmetry was used in the last step. I_j^0 is the current operator to zeroth order in the A_k :

$$I_j^0 \equiv -i\Gamma \left[e^{i\phi/3} \psi_j^\dagger \psi_{j-1} + e^{-i\phi/3} \psi_j^\dagger \psi_{j+1} \right] + h.c. \quad (6.64)$$

$\langle I_j^0 \rangle$ is calculated to first order in $A_j(t)$ using:

$$H \approx H_0 + H' = H_0 + \sum_j I_j^0 A_j. \quad (6.65)$$

$$\langle I_j^0(t) \rangle = -i \int_{-\infty}^t dt' \langle [I_j^0(t), H'(t')] \rangle = -i \sum_k \int_{-\infty}^t dt' \langle [I_j^0(t), I_k^0(t')] \rangle A_k(t') = \sum_k \int_{-\infty}^{\infty} dt' K_{jk}^{\text{ret}}(t - t') A_k(t'). \quad (6.66)$$

Here K_{ij}^{ret} is the retarded Green's function of the I_j^0 operators. Fourier transforming,

$$A_j(\omega) \equiv \int dt e^{i\omega t} A_j(t), \quad (6.67)$$

and including the ‘‘diamagnetic term’’ in Eq. (6.62), we obtain the Kubo formula in the form:

$$\langle I_j \rangle(\omega) = \sum_k G_{jk}(\omega) V_k(\omega). \quad (6.68)$$

where the conductance matrix is given by:

$$G_{jk}(\omega) = \frac{1}{i\omega} [K_{jk}^{\text{ret}}(\omega) - C_{jk}], \quad (6.69)$$

and the ω -independent symmetric matrix, C_{jk} is given by:

$$\begin{aligned} C_{jj} &= 2E_T/3, \\ C_{jk} &= -E_T/3 \quad (j \neq k). \end{aligned} \quad (6.70)$$

Note that

$$\sum_j C_{jk} = \sum_k C_{jk} = 0, \quad (6.71)$$

which combined with Eqs. (2.4) and (6.69) implies

$$\sum_j K_{jk}^{\text{ret}} = \sum_k K_{jk}^{\text{ret}} = 0. \quad (6.72)$$

The retarded Green's function may be obtained by analytic continuation from the Matsubara Green's function:

$$K_{jk}^M(\omega_n) \equiv - \int d\tau e^{i\omega_n\tau} \langle \mathcal{T} I_j^0(\tau) I_k^0(0) \rangle. \quad (6.73)$$

Here $\omega_n = 2\pi nT$ for integer n , at temperature T , τ is imaginary time and \mathcal{T} represents time ordering. The retarded Green's function is obtained, as usual, by:

$$K_{jk}^{\text{ret}}(\omega) = \lim_{\delta \rightarrow 0^+} K_{jk}^M(\delta - i\omega). \quad (6.74)$$

The conductivity can be conveniently derived from the imaginary time path integral, with a vector potential, $A_j(\tau)$, defined as in Eq. (6.57) which depends on imaginary time. The imaginary time partition function, $Z_I[A_j(\tau)]$, is obtained from the path integral of $\exp[-S_0 - \int d\tau H_T(\tau)]$, where S_0 is the imaginary time action for the three independent leads. We see that:

$$\frac{\delta \ln Z_I}{\delta A_j(\tau)} = -\langle I_j(\tau) \rangle \quad (6.75)$$

and, at $A_j \rightarrow 0$,

$$\frac{\delta^2 \ln Z_I}{\delta A_j(\tau) \delta A_k(\tau')} = -K_{jk}^M(\tau - \tau') + \delta(\tau - \tau') C_{jk}. \quad (6.76)$$

Fourier transforming:

$$\frac{\delta^2 \ln Z_I}{\delta A_j(\omega_n) \delta A_k(\omega'_n)} = \frac{\delta(\omega_n + \omega'_n)}{2\pi} [-K_{jk}^M(\omega_n) + C_{jk}]. \quad (6.77)$$

The conductivity can be obtained from this by analytic continuation. Explicitly, writing:

$$\frac{\delta^2 \ln Z_I}{\delta A_j(\omega_n) \delta A_k(\omega'_n)} = \frac{1}{(2\pi)^2} \delta(\omega_n + \omega'_n) Z_{jk}(\omega_n), \quad (6.78)$$

the dc conductance is given by:

$$G_{jk} = \lim_{\omega_n \rightarrow 0} \frac{1}{2\pi\omega_n} Z_{jk}(\omega_n). \quad (6.79)$$

Here the limit $\omega_n \rightarrow 0$ must be taken by first continuing ω_n into the complex plane and then taking $\omega_n \rightarrow 0$ along the imaginary axis with a small positive real part. This version of the Kubo formula is convenient because this second derivative of $\ln Z_I$ is proportional to the Coulomb

gas density correlation function in the DHM. To make this connection it is convenient to rewrite the three vector potentials, $A_j(\tau)$ in terms of a pair of vector potentials, $a^\mu(\tau)$ such that:

$$A_j - A_k = \sum_l \epsilon_{jkl} \vec{K}_l \cdot \vec{a}. \quad (6.80)$$

Here ϵ_{jkl} is the antisymmetric unit tensor ($\epsilon_{123} = 1$ etc.) and the Greek indices run over 1 and 2 only. Then the tunneling term is modified to:

$$H_T \rightarrow i\Gamma e^{i\phi/3} \sum_{j=1}^3 \eta_j e^{i\vec{K}_j \cdot (\vec{\Phi} + \vec{a})} + h.c. \quad (6.81)$$

The corresponding modification of the DHM action is the shift:

$$\vec{X} \rightarrow \vec{X} + \vec{a}. \quad (6.82)$$

This is precisely the source term coupled to the Coulomb gas density discussed above, which appeared in Eq. (6.40).

We now see that the Y-junction conductivity is directly related to the Coulomb gas correlation function. To make the connection we use:

$$\sum_j K_j^\mu K_j^\mu = (3/2)\delta^{\mu\nu} \quad (6.83)$$

to invert (6.80):

$$\vec{a} = \sum_{j,k,l} \vec{K}_j \epsilon_{jkl} (A_k - A_l)/3. \quad (6.84)$$

This implies:

$$\frac{\partial a^\mu}{\partial A_k} = \frac{2}{3} \sum_{j,l} K_j^\mu \epsilon_{jkl} = \frac{2}{3} \sum_j K_j^\mu \epsilon_{jk}. \quad (6.85)$$

Here we use an anti-symmetric 3×3 tensor, a_{jk} , defined by:

$$\epsilon_{ij} \equiv \sum_k \epsilon_{ijk} \quad (6.86)$$

with $\epsilon_{12} = \epsilon_{23} = \epsilon_{31} = 1$. We may thus write:

$$\frac{\partial^2 \ln Z}{\partial A_j(\omega_n) \partial A_k(\omega'_n)} = \frac{4}{9} \sum_{m,n,\mu,\nu} \epsilon_{jm} \epsilon_{kn} K_m^\mu K_n^\nu \frac{\partial^2 \ln Z}{\partial a^\mu(\omega_n) \partial a^\nu(\omega'_n)}. \quad (6.87)$$

The derivative on the right hand side of Eq. (6.87) is proportional to the Coulomb gas correlation function, $\langle \rho_\mu(\omega_n) \rho_\nu(\omega'_n) \rangle$ as we observed in Eq. (6.37).

There are two simple limits of the DHM. One is the case where the potential, V , is irrelevant. Then the correlators of the X -fields are determined by S_0 :

$$\langle X^\sigma(-\omega_n) X^\lambda(-\omega'_n) \rangle = (2\pi)^2 \delta(\omega_n + \omega'_n) (D^{-1})^{\sigma\lambda}(-\omega_n), \quad (6.88)$$

and so the Coulomb gas correlation function vanishes. This corresponds to the limit of disconnected wires and zero conductance. The other simple limit the corresponds to the potential, V , renormalizing to infinity and pinning the X co-ordinates at one of its minima. The Coulomb gas correlation function is then given by the first term only in Eq. (6.43). Thus,

$$Z_{jk}(\omega_n) = -\frac{4}{9} \sum_{m,n,\mu,\nu} \epsilon_{jm} \epsilon_{kn} K_m^\mu K_n^\nu D_{\mu\nu}(-\omega_n). \quad (6.89)$$

Using this gives:

$$Z_{jk}(\omega_n) = \frac{2}{3}(3\delta_{jk} - 1)\alpha|\omega_n| + \frac{2}{\sqrt{3}}\beta\omega_n\epsilon_{jk}. \quad (6.90)$$

Thus, from Eq. (6.79), the dc conductivity is given by:

$$G_{jk} = \frac{e^2}{h} \left[\frac{2}{3}(3\delta_{jk} - 1)\alpha + \frac{2}{\sqrt{3}}\beta\epsilon_{jk} \right]. \quad (6.91)$$

We have restored the factors of e^2 and \hbar which we had previously set equal to one. The values of α, β for the chiral fixed points are obtained from Eq. (6.31) with $n = 1$ and $n = 0$, and lead to the conductance tensor

$$G_{jk}^\pm = \frac{e^2}{h} \frac{2g}{(3+g^2)} [(3\delta_{jk} - 1) \pm g\epsilon_{jk}], \quad (6.92)$$

with \pm corresponding to the fixed points χ_\pm . It is interesting to check that the same result can be obtained by applying electric fields uniformly to the entire wire j , which we do in the next section, where we address the Y-junction problem using BCFT.

VII. APPROACHES BASED ON BOUNDARY CONDITIONS

After studying the junctions of three quantum wires using the mapping into the dissipative Hofstadter model in the previous section, we now turn to a study based on boundary conditions satisfied by the bosonic fields describing the degrees of freedom of the wires. The boundary condition of the boson fields represents the physics at the junction. In particular, conformally invariant boundary conditions corresponds to RG fixed points of the junction problem. Among them, stable fixed points are of special importance, as they govern the physical properties of the junction at low bias voltages and low temperatures. From these boundary conditions, one can determine the conductance tensor of the junctions as well as the scaling of perturbations to the fixed point, *i.e.*, the perturbing operators and the physical processes that they correspond to. The study of conformally invariant boundary conditions will allow us to identify other fixed points in addition to the ones discussed in section VI.

We carry out the analysis based on boundary conditions in two ways. The first approach is based on the

formalism of boundary conformal field theory (BCFT), which is a systematic treatment of conformally invariant boundary conditions for a given (bulk) CFT. The second way is an approach that we introduce in this paper, which we refer to as the method of delayed evaluation of boundary conditions (DEBC).

A theory with free c -component bosons is a conformal field theory with central charge c . The classification of all possible conformally invariant boundary conditions, even for free bosons, is a rather difficult and rich problem especially for $c \geq 2$. For $c \geq 2$, it is possible to have a ‘‘magnetic flux’’ at the boundary, as was discussed in Refs. [23] in the context of Dissipative Hofstadter Model. Nontrivial boundary conditions, which have no simple description in terms of the original boson field, have been discussed in Refs. [16, 33] for $c = 2$ free boson. As the junction of 3 wires is mapped to the boundary problem of $c = 2$ free bosons, we can expect these features to be relevant in the present problem. App. B, C and D review aspects of BCFT, BCFT for free bosons and the calculation of the conductance using BCFT, respectively.

In the bosonization approach, the Fermi statistics of the electrons may be taken care of by the Klein factors. On the other hand, in the BCFT, conformally invariant boundary conditions, in particular the nontrivial ones, are formulated in terms of *boundary states*. Boundary states belong to the Hilbert space of the theory with the periodic boundary condition in the ‘‘space’’ direction. The implication of the Fermi statistics of electrons on the boundary state formulation is not obvious.

Considering the Fermi statistics of the electrons, we show in section VIII that the structure of the Hilbert space is ‘‘twisted’’ compared to that of the standard free boson. The twisted structure affects the possible boundary states, the scaling dimensions of the boundary operators, and stability. We show that the derived boundary states are indeed consistent with electrons with Fermi statistics. Thus the twisted structure encodes the effect of the Fermi statistics.

The formulation of the problem of tunneling between multiple quantum wires within the DEBC approach, presented in section IX, provides another angle of attack, which gives results consistent with the BCFT approach. The DEBC method allows us to give a simple physical interpretation of the operators that become relevant and enforce the correct boundary conditions, as well as the operators that correspond to perturbations around the fixed point boundary condition.

The DEBC method consists of doubling the number of degrees of freedom in the problem by keeping both the bosonic fields φ_i , $i = 1, 2, 3$ in each lead as well as its conjugate momentum θ_i . Notice that such construction, in terms of both sets of bosonic fields φ_i and θ_i , is the usual one when describing systems on the infinite line, but is unusual if we want to describe the system on the half line $x > 0$, appropriate for describing the quantum wires that meet at a junction. There must be a boundary condition imposed at $x = 0$ which cuts in half the number of degrees

of freedom, when describing the system on the half-line. It is only with this imposed boundary condition that the operators above describe the electronic degrees of freedom on the half-line. The essence of the method is that we delay the choice of boundary condition (hence the name “delayed evaluation”) until after we write the operators corresponding to the physical tunneling of electrons (and pairs or multiplets), working with twice the physical degrees of freedom. With the tunneling operators in hand, we can then study the correct boundary

condition that must be imposed on φ_i and θ_i .

In Sec. X we use both methods to discuss various fixed points of the Y-junction.

VIII. FERMI STATISTICS AND THE TWISTED STRUCTURE IN BOSONIZATION

The BCFT of free bosons can be applied to the system of interacting electrons via bosonization. However, owing to the Fermi statistics of the electron, there are various differences compared to the standard compactified boson field theory, reviewed in App. C. In this section we formulate the effect of the Fermi statistics in terms of a twisted structure in the Hilbert space of the free boson theory. This approach was first developed in Ref. [36]. In this paper, we further propose a simplified treatment of the twisted structure for the junction problem, and apply it to the junction of three wires.

A. Bosonization of a single wire

Let us start from the bosonization of a single wire, carefully taking the effect of the Fermi statistics into account.

1. Derivation of the twisted structure

Since the Matsubara formalism implies *anti-periodic* boundary conditions in imaginary time, anti-periodic boundary conditions in the space direction will also occur after a modular transformation. These must be imposed independently on left and right-movers:

$$\psi_{L/R}(t, x) = -\psi_{L/R}(t, x + \beta). \quad (8.1)$$

It will be important to determine the corresponding b.c.’s on the bosons, using the bosonization formulas reviewed in Sec. IV. Let us first consider the case, $g = 1$, corresponding to free fermions. The b.c.’s are then:

$$\exp[i\sqrt{2}\varphi_{L/R}(t, \beta)] = -\exp[i\sqrt{2}\varphi_{L/R}(t, 0)]. \quad (8.2)$$

Because $[\varphi_{L/R}, \varphi_{L/R}] \neq 0$ it is not so straightforward to deduce the boundary conditions on the boson fields from Eq. (8.2). One way of proceeding is to determine the b.c.’s on the bosons which reproduce the finite-size spectrum implied by anti-periodic b.c.’s on the fermions. The allowed wave-vectors for single-particle fermion states are:

$$k = \frac{2\pi(n + 1/2)}{\beta}, \quad (n \in Z). \quad (8.3)$$

Recognizing that k is measured from $\pm k_F$ for right and left-movers respectively, we see that n may be positive or negative in Eq. (8.3) for both left and right movers. The negative n states correspond to hole states for right-movers and electron states for left-movers. It is straightforward to calculate the energy of an arbitrary multi-particle fermionic state with this linearized dispersion relation. Consider the energy of an arbitrary state of the right-movers. The lowest energy state of charge $Q_R \in Z$, is:

$$E(Q_R) = \frac{2\pi}{\beta} \sum_{n=0}^{|Q_R|-1} (n + 1/2) = \frac{2\pi}{\beta} \frac{Q_R^2}{2}. \quad (8.4)$$

Here Q_R may be positive or negative, corresponding to creating particles or holes. An arbitrary multi particle-hole state can be constructed, on top of the charge Q_R groundstate, by first raising the lowest n_m fermions by m levels, then raising the next n_{m-1} by $m-1$ levels, etc., finally raising n_1 fermions by 1 level. Thus the energy of an arbitrary excited state of the right-movers may be written:

$$E = \frac{2\pi}{\beta} \left[\frac{Q_R^2}{2} + \sum_{m=1}^{\infty} mn_m \right], \quad (8.5)$$

where Q_R is an arbitrary integer and the n_m 's are arbitrary non-negative integers.

Precisely this spectrum arises from right-moving bosons. We assume that the right and left moving boson field, $\phi_{R/L}$ are periodic variables:

$$\varphi_{R/L}(t, x + \beta) \leftrightarrow \varphi_{R/L}(t, x) + \sqrt{2}\pi n, \quad (n \in Z). \quad (8.6)$$

This is reasonable since all physical operators, local in fermion fields, are single-valued with this identification. We then find that the anti-periodic b.c.'s on fermions arise from *periodic* b.c.'s on bosons. To see this, consider the mode expansion for periodic right-movers:

$$\varphi_R(x_-) = \hat{\varphi}_0^R + \frac{\pi}{\beta} \hat{P}_R x_- + \frac{1}{\sqrt{2}} \sum_{n=1}^{\infty} \frac{1}{\sqrt{n}} \left[a_n^R \exp[-in x_- \frac{2\pi}{\beta}] + \text{h.c.} \right]. \quad (8.7)$$

Here \hat{P}_R , the momentum variable conjugate to $\hat{\varphi}_0^R$, has eigenvalues $\sqrt{2}$ times an integer. consistent with the assumed periodic b.c.'s. Substituting this mode expansion into the right-moving Hamiltonian:

$$H_R = \frac{1}{2\pi} \int_0^\beta (\partial_- \varphi_R)^2 dx, \quad (8.8)$$

gives precisely the spectrum of Eq. (8.5), upon the identification, $\hat{P}_R \leftrightarrow \sqrt{2}Q_R$. Thus we see that *anti-periodic* b.c.'s on fermions turn into *periodic* b.c.'s on the *chiral* boson field.

Alternatively, it is also possible to derive the periodic b.c.'s on right-moving bosons from anti-periodic b.c.'s on right-moving fermions from Eq. (8.2), taking into account the boson commutation relations. The equal-time commutator follows from Eq. (8.7):

$$[\varphi_R(x), \varphi_R(0)] = (i\pi/2)\epsilon_P(x), \quad (8.9)$$

where $\epsilon_P(x)$ is the function, anti-symmetric in x , which is constant everywhere except at $x = n\beta$, for $n \in Z$, where it jumps by 2:

$$\epsilon_P(x) = (2n + 1), \quad [n\beta < x < (n + 1)\beta]. \quad (8.10)$$

We multiply both sides of (the "right version") of Eq. (8.2) on the right by $\exp[-i\sqrt{2}\varphi_R(\delta)]$ where δ is a small positive quantity, giving:

$$\exp[i\sqrt{2}\varphi_R(\beta)] \exp[-i\sqrt{2}\varphi_R(\delta)] = -\exp[i\sqrt{2}\varphi_R(0)] \exp[-i\sqrt{2}\varphi_R(\delta)]. \quad (8.11)$$

This can be rewritten:

$$\exp\{i\sqrt{2}[\varphi_R(\beta) - \varphi_R(\delta)]\} \exp\{[\varphi_R(\beta), \varphi_R(\delta)]\} = -\exp\{i\sqrt{2}[\varphi_R(0) - \varphi_R(\delta)]\} \exp\{[\varphi_R(0), \varphi_R(\delta)]\} \quad (8.12)$$

Since $0 < \beta - \delta < \beta$ and $-\beta < 0 - \delta < 0$, using Eq. (8.9) this becomes:

$$i \exp\{i\sqrt{2}[\varphi_R(\beta) - \varphi_R(\delta)]\} = i \exp\{i\sqrt{2}[\varphi_R(0) - \varphi_R(\delta)]\} \quad (8.13)$$

We may finally let $\delta \rightarrow 0^+$, giving:

$$\exp\{i\sqrt{2}[\varphi_R(\beta) - \varphi_R(0)]\} = 1, \quad (8.14)$$

and hence periodic b.c.'s:

$$\varphi_R(\beta) = \varphi_R(0) \pmod{\sqrt{2}\pi n}. \quad (8.15)$$

Note that if we had instead chosen the infinitesimal $\delta < 0$, so that $\beta < \beta - \delta < 2\beta$ and $0 < 0 - \delta < \beta$, the two commutators in Eq. (8.12) would still differ by π from Eq. (8.10) so that we would still obtain Eq. (8.14).

2. *Finite-size spectrum and bulk operators*

The left-moving fermions with anti-periodic b.c.'s have an identical spectrum to the right-movers which again is given by periodic b.c.'s on the left-moving bosons. Adding left and right contributions, we obtain the mode expansions:

$$\begin{aligned}\varphi(t, x) &= \hat{\varphi}_0 + \frac{\sqrt{2}\pi}{\beta} [(\hat{Q}_L + \hat{Q}_R)t + (\hat{Q}_L - \hat{Q}_R)x] \\ &\quad + \frac{1}{\sqrt{2}} \sum_{n=1}^{\infty} \frac{1}{\sqrt{n}} \left[a_n^R \exp(-inx - \frac{2\pi}{\beta}) + a_n^L \exp(-inx + \frac{2\pi}{\beta}) + \text{h.c.} \right], \\ \theta(t, x) &= \hat{\theta}_0 + \frac{\sqrt{2}\pi}{\beta} [(\hat{Q}_L - \hat{Q}_R)t + (\hat{Q}_L + \hat{Q}_R)x] \\ &\quad + \frac{1}{\sqrt{2}} \sum_{n=1}^{\infty} \frac{1}{\sqrt{n}} \left[a_n^R \exp(-inx - \frac{2\pi}{\beta}) - a_n^L \exp(-inx + \frac{2\pi}{\beta}) + \text{h.c.} \right].\end{aligned}\tag{8.16}$$

Here

$$\begin{aligned}\hat{\varphi}_0 &\equiv \hat{\varphi}_0^R + \hat{\varphi}_0^L \\ \hat{\theta}_0 &\equiv \hat{\varphi}_0^R - \hat{\varphi}_0^L.\end{aligned}\tag{8.17}$$

While it is convenient to define a new set of integer quantum numbers:

$$\begin{aligned}Q &\equiv Q_L + Q_R \\ \tilde{Q} &\equiv Q_L - Q_R,\end{aligned}\tag{8.18}$$

it is important to realize that they do not run independently over the integers, but rather obey the ‘‘gluing condition’’ [36]:

$$Q = \tilde{Q} \pmod{2}\tag{8.19}$$

Thus, the periodic identifications of the fields $\varphi(t, x)$ and $\theta(t, x)$ do not simply correspond to them being angular variables. They are of the form:

$$\begin{aligned}\varphi &\sim \varphi + \tilde{Q}\sqrt{2}\pi, \\ \theta &\sim \theta + Q\sqrt{2}\pi,\end{aligned}\tag{8.20}$$

but rather with the gluing condition (8.19). We refer to this as a ‘‘twisted structure’’. It simply reflects the fact that the bosons arise from bosonizing fermions. It can be verified that the finite size energies (with anti-periodic b.c.'s on the fermions) are in one-to-one correspondance with the (bulk) operator content. For example, the right-moving oscillator vacuum with quantum number $Q_R < 0$ corresponds to the lowest dimension (right-moving) operator with charge Q_R . Taking into account Fermi statistics, this operator is:

$$\prod_{j=0}^{Q_R-1} [(\partial_{x_-})^j \psi_R],\tag{8.21}$$

with the (right-moving) conformal dimension

$$\sum_{i=0}^{Q_R-1} \left(\frac{1}{2} + j\right) = \frac{Q_R^2}{2}.\tag{8.22}$$

Comparing with eq. (8.4), we see that the usual relationship between the finite size energy and scaling dimension, Δ , is obeyed: $E = (2\pi/\beta)\Delta$. The corresponding bosonized operator is $\exp[iQ_R\sqrt{2}\varphi_R]$.

We have discussed extensively the case $g = 1$, corresponding to free fermions. However, these results can be seen to carry over to the case of interacting fermions, with general values of g . In general, the mode expansion for φ is:

$$\begin{aligned}\varphi(t, x) &= \hat{\varphi}_0 + \frac{\sqrt{2}\pi}{\beta} \left[\frac{1}{g} \hat{Q}t + \hat{Q}x \right] \\ &\quad + \frac{1}{\sqrt{2g}} \sum_{n=1}^{\infty} \frac{1}{\sqrt{n}} \left[a_n^R \exp(-inx - \frac{2\pi}{\beta}) + a_n^L \exp(-inx + \frac{2\pi}{\beta}) + \text{h.c.} \right]\end{aligned}\tag{8.23}$$

and the corresponding spectrum is:

$$E = \frac{2\pi}{\beta} \left[\frac{Q^2}{4g} + \frac{g\tilde{Q}^2}{4} + \sum_{m=1}^{\infty} m(n_m^L + n_m^R) \right], \quad (8.24)$$

again with the gluing condition (8.19). The corresponding *bulk* primary operators are:

$$\exp[i(Q\varphi + \tilde{Q}\theta)/\sqrt{2}], \quad (8.25)$$

with dimensions:

$$\Delta = \frac{Q^2}{4g} + \frac{g\tilde{Q}^2}{4}. \quad (8.26)$$

When we form boundary states from the Hilbert space with the anti-periodic b.c.'s on the fermions, the condition $[\mathcal{H}_R - \mathcal{H}_L]|A\rangle = 0$ will simplify this twisted structure, as we will see.

3. Boundary states and boundary operators

Let us now consider the boundary operators, finite size spectrum and boundary states. We consider BC's on the fermions either of the free type:

$$\psi_L(t, 0) = \psi_R(t, 0), \quad (8.27)$$

corresponding to $\theta(0) = \theta_0$ (a constant), i.e. N b.c.'s on φ or else of Andreev type:

$$\psi_L(t, 0) = \psi_R^\dagger(t, 0) \quad (8.28)$$

corresponding to D BC's on φ . The N BC turns the operators of Eq. (8.25) into:

$$\exp\left[\frac{i}{\sqrt{2}}(Q\varphi(t, 0) + \tilde{Q}\theta(t, 0))\right] \rightarrow \exp\left[-\frac{i}{\sqrt{2}}(Q\varphi(t, 0) + \tilde{Q}\theta_0)\right] \propto \exp[iQ\sqrt{2}\varphi_L(t, 0)], \quad (8.29)$$

of dimension:

$$\Delta_N = \frac{Q^2}{2g}. \quad (8.30)$$

We find that the value of \tilde{Q} is now immaterial to the scaling dimension. Consequently, we can allow Q to take any integer value, even or odd, despite the gluing condition (8.19). Also note that, in the free fermion case, $g = 1$, we obtain $\Delta_N = Q^2/2$, corresponding to the operator spectrum of a single left-mover, which we can obtain by regarding the right movers as the continuation of the left-movers to the negative x -axis.

As reviewed in VII, the spectrum of the *boundary* operators is related to the FSS on the finite-width strip with the same boundary condition imposed on the both ends. To find the corresponding FSS, let us consider the strip $0 < x < l$, and impose the N b.c. on φ at the both ends $x = 0, l$. We notice that the N b.c. (on φ) corresponds to the D b.c. on the dual field θ . The mode expansion consistent with the D b.c.'s on θ

$$\begin{aligned} \theta(0) &= 0 \pmod{\sqrt{2}\pi} \\ \theta(l) &= 0 \pmod{\sqrt{2}\pi} \end{aligned} \quad (8.31)$$

reads:

$$\theta = \frac{\sqrt{2}\pi}{l}\hat{Q}x + \frac{1}{\sqrt{2}g} \sum_{n=1}^{\infty} 2 \sin \frac{n\pi x}{l} [a_n^L \exp(-int\frac{\pi}{l}) + \text{h.c.}]. \quad (8.32)$$

This implies the Hamiltonian:

$$H = \frac{\pi}{l} \left[\frac{(\hat{Q})^2}{2g} + \sum_{n=1}^{\infty} na_n^{L\dagger} a_n^L \right]. \quad (8.33)$$

This is indeed consistent with the scaling dimension of the boundary primary operator in Eq. (8.30).

On the other hand, as discussed in Sec. VII, the boundary condition generally can be described in terms of the corresponding boundary state upon modular transformation. Naturally, the N boundary state for the present case is similar to the N boundary state of a standard free boson. However, here the gluing condition (8.19) is important in determining the boundary state. Since the N boundary state (on φ) is Dirichlet boundary state on θ , the winding of θ along the boundary is zero. Consequently, we have the quantum number $Q = 0$. Because of the gluing condition (8.19), the quantum number \tilde{Q} is now restricted to *even* integers. The N boundary state is:

$$|N(\theta_0)\rangle = g^{1/4} \exp \left[\sum_{n=1}^{\infty} a_n^{L\dagger} a_n^{R\dagger} \right] \sum_{\tilde{Q}}' e^{-i\sqrt{2}\tilde{Q}\theta_0} |(\tilde{Q}, 0)\rangle. \quad (8.34)$$

Here the $'$ on the summation indicates that \tilde{Q} is restricted to even integers. Upon performing the modular transformation we obtain:

$$\langle N(\theta_0) | \exp[-lH_\beta^P] | N(\theta_0) \rangle = \frac{1}{\eta(q)} \sum_{m=-\infty}^{\infty} \exp -\frac{\pi\beta}{l} \frac{m^2}{2g}. \quad (8.35)$$

Here m is summed over *all* integers. This corresponds to the finite size spectrum of Eq. (8.33), demonstrating the consistency.

We can repeat the similar analysis for the D b.c. on φ . The primary boundary operators have dimensions:

$$\Delta_D = \frac{g(\tilde{Q})^2}{2}, \quad (8.36)$$

where \tilde{Q} can be even or odd, and the mode expansion becomes:

$$\varphi = \frac{\sqrt{2}\pi}{l} \hat{Q}x + \frac{1}{\sqrt{2}g} \sum_{n=1}^{\infty} 2 \sin \frac{n\pi x}{l} [a_n^L \exp(-int\frac{\pi}{l}) + \text{h.c.}], \quad (8.37)$$

where \tilde{Q} can be even or odd. This implies the Hamiltonian:

$$H = \frac{\pi}{l} \left[\frac{g\hat{Q}^2}{2} + \sum_{n=1}^{\infty} n a_n^{L\dagger} a_n^L \right]. \quad (8.38)$$

The D boundary state is:

$$|D(\varphi_0)\rangle = g^{-1/4} \exp \left[- \sum_{n=1}^{\infty} a_n^{L\dagger} a_n^{R\dagger} \right] \sum_Q' \exp[-i\sqrt{2}Q\varphi_0] |(0, Q)\rangle, \quad (8.39)$$

where the sum is restricted to even Q since \tilde{Q} is now set to zero. We now obtain:

$$\langle D(\varphi_0) | \exp[-lH_\beta^P] | D(\varphi_0) \rangle = \frac{1}{\eta(q)} \sum_{m=-\infty}^{\infty} \exp \left[-\frac{\pi\beta}{l} \frac{gm^2}{2} \right], \quad (8.40)$$

consistent with the FSS of Eq. (8.38).

B. Junction of two wires

Now let us consider the implications of the twisted structure for the junction of two wires.

1. Structure of the boundary states

We introduce 2 fermion fields $\psi_{j,L/R}$ ($j = 1, 2$), corresponding to each wire. In order to apply the boundary state formalism, we define them on a circle of circumference β with the antiperiodic boundary condition. Bosonizing each

fermion fields, we introduce 2 boson fields φ_j and their duals, θ_j . They independently obey the twisted periodic identification of Eq. (8.20):

$$\begin{aligned}\varphi_j &\sim \varphi_j + \tilde{Q}_j \sqrt{2}\pi \\ \theta_j &\sim \theta_j + Q_j \sqrt{2}\pi \\ \tilde{Q}_j &= Q_j \pmod{2}\end{aligned}\tag{8.41}$$

It is convenient to define linear combinations:

$$\Phi_0 = \frac{\varphi_1 + \varphi_2}{\sqrt{2}} \quad \text{and} \quad \Phi = \frac{\varphi_1 - \varphi_2}{\sqrt{2}}\tag{8.42}$$

$$\Theta_0 = \frac{\theta_1 + \theta_2}{\sqrt{2}} \quad \text{and} \quad \Theta = \frac{\theta_1 - \theta_2}{\sqrt{2}}.\tag{8.43}$$

As already discussed in Sec. VII, as long as the charge is conserved at the junction, Φ_0 always obeys the Neumann boundary condition. The Hamiltonian will thus decouple into separate terms for Φ and Φ_0 , with Φ_0 decoupling from the interactions. Namely, only Φ and Θ will appear in the boundary interactions.

However, the periodic identification conditions (referred to as “gluing conditions” in [36]) now link these 2 fields, as well as linking the Φ and Θ fields. Explicitly, defining:

$$\begin{aligned}Q_0 &\equiv Q_1 + Q_2 \\ Q &\equiv Q_1 - Q_2,\end{aligned}\tag{8.44}$$

corresponding to Φ_0 and Φ , and similarly defining \tilde{Q}_0 and \tilde{Q} , we see that these obey the restrictions, which are equivalent to $Q_j = \tilde{Q}_j \pmod{2}$:

$$\begin{aligned}Q_0 = \tilde{Q}_0 = Q = \tilde{Q} &\pmod{2} \\ Q_0 + Q + \tilde{Q}_0 + \tilde{Q} &= 0 \pmod{4}.\end{aligned}\tag{8.45}$$

the mode expansions for the fields Φ_0 and Φ are:

$$\begin{aligned}\Phi_0(t, x) &= \hat{\Phi}_0^0 + \frac{\pi}{\beta} \left[\frac{1}{g} Q_0 t + \tilde{Q}_0 x \right] + \frac{1}{\sqrt{2g}} \sum_{n=1}^{\infty} \frac{1}{\sqrt{n}} \left[a_n^{R0} \exp(-inx - \frac{2\pi}{\beta}) + a_n^{L0} \exp(-inx + \frac{2\pi}{\beta}) + \text{h.c.} \right] \\ \Phi(t, x) &= \hat{\Phi}_0 + \frac{\pi}{\beta} \left[\frac{1}{g} Q t + \tilde{Q} x \right] + \frac{1}{\sqrt{2g}} \sum_{n=1}^{\infty} \frac{1}{\sqrt{n}} \left[a_n^R \exp(-inx - \frac{2\pi}{\beta}) + a_n^L \exp(-inx + \frac{2\pi}{\beta}) + \text{h.c.} \right],\end{aligned}\tag{8.46}$$

and similarly for Θ_0, Θ . The Q, Q_0, \tilde{Q} and \tilde{Q}_0 quantum numbers obey the gluing conditions of Eq. (8.45).

The FSS is given by two copies of Eq. (8.24). This can be written as:

$$E = \frac{2\pi}{\beta} \left[\frac{Q_0^2 + Q^2}{8g} + \frac{g(\tilde{Q}_0^2 + \tilde{Q}^2)}{8} + \sum_{m=1}^{\infty} m(n_m^{L0} + n_m^{R0} + n_m^L + n_m^R) \right],\tag{8.47}$$

where, again the gluing conditions of Eq. (8.45) are obeyed.

Analogous to what was found in Sec. VII in the 3-wire case, Φ_0 always obeys N BC’s at $x = 0$. This is the “bare” BC corresponding to decoupled leads, and it is not changed by the interactions since Φ_0 does not appear in them. On the other hand, Φ can obey N or D BC’s corresponding to perfect reflection or perfect transmission through the junction, respectively.

It is straightforward to determine directly the full boundary operator spectrum with either set of b.c.’s. (Henceforth we will label these two sets of b.c.’s as simply N or D.) In the N case we simply get 2 copies of the operator spectrum of a single wire with N b.c.’s, since φ_j ($j = 1, 2$) independently obey N b.c.’s in this case. As usual, this spectrum of operator dimensions is in one-to-one correspondance with the FSS with N b.c.’s at both ends of a strip of length l . This is, as in Eq. (8.33):

$$E_N = \frac{\pi}{l} \left[\frac{Q_1^2}{2g} + \frac{Q_2^2}{2g} + \sum_{m=1}^{\infty} m(n_m^1 + n_m^2) \right],\tag{8.48}$$

where Q_1 and Q_2 range independently over all integers. Equivalently, we can write this in terms of the charge quantum numbers Q_0 and Q defined in Eq. (8.44) and the new oscillator operators, which are associated with the fields Φ_0 and Φ :

$$E_N = \frac{\pi}{l} \left[\frac{Q_0^2}{4g} + \frac{Q^2}{4g} + \sum_{m=1}^{\infty} m(n_m^0 + n_m) \right], \quad (8.49)$$

where now:

$$Q = Q_0 \pmod{2} \quad (8.50)$$

The N boundary state is just a product of the single fermion N boundary states. Taking the case where both phases Θ_0 and Θ_0^0 are set to zero, this can be written as:

$$|N\rangle = g^{1/2} \exp \left[\sum_{n=1}^{\infty} (a_n^{L0\dagger} a_n^{R0\dagger} + a_n^{L\dagger} a_n^{R\dagger}) \right] \sum'_{\tilde{Q}_0, \tilde{Q}} |(\tilde{Q}_0, 0)\rangle \otimes |(\tilde{Q}, 0)\rangle. \quad (8.51)$$

Here, as follows from Eq. (8.45), with $Q = Q_0 = 0$, \tilde{Q}_0 and \tilde{Q} are even and $\tilde{Q} + \tilde{Q}_0 = 0 \pmod{4}$.

The FSS with the D b.c.'s at both ends of the strip is equivalent to the FSS of a single wire with periodic BC's on an interval of length $2l$, as follows from an unfolding transformation [36]. This is given by Eq. (8.24) with β replaced by $2l$. We may also replace the n_m^L, n_m^R quantum numbers by a new basis, n_m^0 , and n_m , and identify the total charge Q with Q_0 and \tilde{Q} with the same quantity related to the linear combination φ in Eq. (8.42).

$$E_D = \frac{\pi}{l} \left[\frac{Q_0^2}{4g} + \frac{g\tilde{Q}^2}{4} + \sum_{m=1}^{\infty} m(n_m^0 + n_m) \right], \quad (8.52)$$

with

$$Q_0 = \tilde{Q} \pmod{2}. \quad (8.53)$$

The corresponding boundary state is:

$$|D\rangle = \exp \left[\sum_{n=1}^{\infty} (a_n^{L0\dagger} a_n^{R0\dagger} - a_n^{L\dagger} a_n^{R\dagger}) \right] \sum'_{\tilde{Q}_0, Q} |(\tilde{Q}_0, 0)\rangle \otimes |(0, Q)\rangle, \quad (8.54)$$

where the sum is restricted by the gluing conditions of Eq. (8.45), in the case $Q_0 = \tilde{Q} = 0$, to \tilde{Q}_0 and Q even with $\tilde{Q}_0 + Q = 0 \pmod{4}$.

In fact, we are generally only interested in the $Q_0 = 0$ boundary operators since these are the only ones which can appear in the Hamiltonian. Operators with $Q_0 \neq 0$ corresponds to a vertex operator involving Θ_0 and thus are forbidden by charge conservation. Setting $Q_0 = 0$ in Eq. (8.49) or (8.52) we see that Q or \tilde{Q} respectively must be even. The dimensions of the primary operators can thus be written as:

$$\begin{aligned} \Delta_N &= \frac{n^2}{g} \\ \Delta_D &= gm^2, \end{aligned} \quad (8.55)$$

with n and m arbitrary integers. These are precisely the same as the boundary scaling dimensions of primary fields for a single *periodic boson* with N or D BC's [Eq. (C44) or (C23).] These reproduce the known results on the junction of two wires. [1, 36, 39]

We note that, however, in the presence of a resonant level at the junction, the charge-nonconserving boundary operators with $Q_0 \neq 0$ should be also considered. Suppose for example that there is a single resonant level, exactly at the Fermi energy, at the junction. One may imagine the two wires connected to a quantum dot. Let d and d^\dagger be the annihilation/creation operator of an electron in that level. Then the hopping of an electron between a wire and the dot can be written as $\psi_j d^\dagger + \text{h.c.}$. As d and d^\dagger have zero scaling dimension, the scaling dimension of the hopping operator is determined by the electron annihilation operator ψ_j at the end of the wire. Therefore, in the presence of the resonant level, even if the charge is overall conserved, we have to consider the ‘‘charge-nonconserving’’ boundary operators. Indeed, the effect of the resonant tunneling at the junction has been studied in Refs. [1, 39] for the case of two wires and in Ref. [5] for three wires.

Nevertheless, in this paper, we focus on the problem without the resonant levels. We discuss only the charge-conserving boundary operators, for which we develop a simplified treatment in the following. It should be kept in mind, however, that it does not cover the resonant case.

2. Projection to an effective single component boson

While we have succeeded in correctly reproducing known results on the junction of two wires, the gluing conditions obviously complicates the calculation. On the other hand, if we restrict the analysis to the charge-conserving boundary operators, there is a simpler method to find the dimensions of such boundary operators. This will be generalized in the next sub-section to the 3-wire case.

Note that in any boundary state which is N for Φ_0 , only $Q_0 = 0$ states occur. The restrictions of Eq. (8.45) reduce to:

$$\tilde{Q}_0 = Q = \tilde{Q} = 0 \pmod{2} \quad (8.56)$$

$$Q + \tilde{Q} + \tilde{Q}_0 = 0 \pmod{4}. \quad (8.57)$$

Defining:

$$\begin{aligned} \tilde{Q}_0 &\equiv 2\tilde{n}_0 \\ Q &= 2n \\ \tilde{Q} &= 2\tilde{n}, \end{aligned} \quad (8.58)$$

these integers obey the condition:

$$n + \tilde{n} = \tilde{n}_0 \pmod{2}. \quad (8.59)$$

A general boundary state of this type can be written:

$$|B\rangle = |N_0^0\rangle \otimes \sum_{\tilde{m}, m \in \mathbb{Z}} |\psi_{4\tilde{m}, 4m}\rangle + |N_0^1\rangle \otimes \sum_{\tilde{m}, m \in \mathbb{Z}} |\psi_{4\tilde{m}+2, 4m+2}\rangle. \quad (8.60)$$

Here $|\psi_{\tilde{Q}, Q}\rangle$ are states in the Hilbert space of Φ , proportional to $|(\tilde{Q}, Q)\rangle$. Actually only $|\psi_{2\tilde{n}, 0}\rangle$ is non-zero in the N state and only $|\psi_{0, 2n}\rangle$ is non-zero in the D state but we since we wish to consider both cases at once we use this more general notation. $|N_0^0\rangle$ and $|N_0^1\rangle$ are N states in the Hilbert space of Φ_0 , given explicitly by:

$$\begin{aligned} |N_0^0\rangle &= (2g)^{1/4} \exp \left[\sum_{n=1}^{\infty} a_n^{L0\dagger} a_n^{R0\dagger} \right] \sum_{\tilde{m}_0 \in \mathbb{Z}} |(4\tilde{m}_0, 0)\rangle \\ |N_0^1\rangle &= (2g)^{1/4} \exp \left[\sum_{n=1}^{\infty} a_n^{L0\dagger} a_n^{R0\dagger} \right] \sum_{\tilde{m}_0 \in \mathbb{Z}} |(4\tilde{m}_0 + 2, 0)\rangle. \end{aligned} \quad (8.61)$$

Here we have let $\tilde{n}_0 = 2\tilde{m}_0$ in $|N_0^0\rangle$ and $\tilde{n}_0 = 2\tilde{m}_0 + 1$ in $|N_0^1\rangle$. The diagonal partition function is given by:

$$Z_{BB} = Z_{N_0^0} \sum_{\tilde{m}, m} Z_{4\tilde{m}, 4m} + Z_{N_0^1} \sum_{\tilde{m}, m \in \mathbb{Z}} Z_{4\tilde{m}+2, 4m+2}. \quad (8.62)$$

Here $Z_{N_0^i}$ is a diagonal partition function in the Φ_0 Hilbert space and the second factors are diagonal partition functions in the Φ Hilbert space:

$$Z_{2\tilde{n}, 2n} \equiv \langle \psi_{2\tilde{n}, 2n} | \exp[-lH_\beta^P] | \psi_{2\tilde{n}, 2n} \rangle. \quad (8.63)$$

The former are given explicitly by:

$$\begin{aligned} Z_{N_0^0} &= \frac{\sqrt{2g}}{\eta(\tilde{q})} \sum_{\tilde{m}_0 \in \mathbb{Z}} \tilde{q}^{g\tilde{m}_0^2} = \frac{1}{\eta(q)} \sum_{Q_0 \in \mathbb{Z}} q^{Q_0^2/(4g)} \\ Z_{N_0^1} &= \frac{\sqrt{2g}}{\eta(\tilde{q})} \sum_{\tilde{m}_0 \in \mathbb{Z}} \tilde{q}^{g(2\tilde{m}_0+1)^2/4} = \frac{1}{\eta(q)} \sum_{Q_0 \in \mathbb{Z}} e^{i\pi Q_0} q^{Q_0^2/(4g)}. \end{aligned} \quad (8.64)$$

The complete spectrum of boundary operators can be read off from the partition function Z_{BB} . However, the scaling dimension coming from $Z_{N_0^0}$ and $Z_{N_0^1}$ corresponds to a boundary operator involving the center-of-mass field Φ_0 . In particular, those includes a nontrivial dimensions $Q_0^2/(4g)$ comes from the vertex operator $e^{iQ_0\Phi_0/2}$ which

changes the total charge. Thus they do not appear if we consider only the perturbations which respects the charge conservation at the junction. The other operators with integer dimensions corresponding to the expansion of $1/\eta(q)$ comes from derivatives of Φ_0 . They are all irrelevant or marginal.

Thus, in order to identify potentially relevant operators, we can consider the boundary operators which involves the dynamical field Φ only. For this purpose, we may replace both $Z_{N_0^0}$ and $Z_{N_0^1}$ by

$$Z_{N_0^0}, Z_{N_0^1} \rightarrow 1 \quad (8.65)$$

The resultant effective partition function is

$$Z_{BB} \rightarrow \sum_{\tilde{n}, n} Z_{2\tilde{n}, 2n}, \quad (8.66)$$

from which we can read off the spectrum of boundary operators involving Φ only.

This “reduced partition function” can be obtained by simply ignoring the Φ_0 sector and dropping the constraint of Eq. (8.57), thus allowing $n (= Q/2)$ and $\tilde{n} (= \tilde{Q}/2)$ to be arbitrary integers. Namely, Eq. (8.66) is identical to the diagonal partition function arising from a “reduced” boundary state entirely in the Φ sector of the form:

$$|B\rangle_R \propto \sum_{\tilde{n}, n} |\psi_{2\tilde{n}, 2n}\rangle, \quad (8.67)$$

in which the second constraint of Eq. (8.57) has been simply ignored.

Thus, to obtain the dimensions of boundary operators in Φ sector, we may simply forget about the second constraint of Eq. (8.57) and hence replace the entangled boundary state of Eq. (8.60) by the simpler reduced one, written only in the Φ sector, of Eq. (8.67). This corresponds to a boundary state for a single boson obeying standard periodic b.c.’s. In particular it leads to the primary operators spectra of Eq. (8.55). Therefore, as long as we restrict ourselves to $Q_0 = 0$ operators, we may drop the Φ_0 boson entirely and ignore the twisted structure that results from Fermi statistics. This simplicity appears to be related to the fact that the Klein factors are trivial for a 2 wire junction.

In contrast to the above, we will see that a similar reduction leaves a nontrivial effect for the junction of three wires.

C. Three wires

Let us finally turn to the model of interest here: a 3-wire junction. As in Subsection VIII B on the 2-wire junction, we define 3 fermion fields on a circle of circumference β . Upon bosonizing, we introduce 3 fields and their duals, φ_j and θ_j , which obey the fermionic type (twisted) periodic identification of Eq. (8.41) where now $j = 1, 2$ or 3 . We then introduce the 3 linear combinations of fields Φ_j as in Eq. (4.5). We then combine Φ_1 and Φ_2 into a 2-component vector field, $\vec{\Phi}$ and similarly for $\vec{\Theta}$. We now consider the mode expansions for the fields $\vec{\Phi}$, Φ_0 , $\vec{\Theta}$ and $\vec{\Theta}_0$. We introduce charge and dual charge quantum numbers Q_j and \tilde{Q}_j for each of the original boson, φ_j , as in Eq. (8.23), (8.18). We define the total charge and dual charge:

$$\begin{aligned} Q_0 &\equiv Q_1 + Q_2 + Q_3, \\ \tilde{Q}_0 &\equiv \tilde{Q}_1 + \tilde{Q}_2 + \tilde{Q}_3. \end{aligned} \quad (8.68)$$

We are only interested in b.c.’s which are N for Φ_0 , so that the corresponding b. states are constructed from $Q_0 = 0$ states. It is convenient to parameterize the vectors of integers, Q_i satisfying this condition by:

$$(Q_1, Q_2, Q_3) \equiv m_1(0, 1, -1) + m_2(-1, 0, 1). \quad (8.69)$$

Clearly $m_1 = Q_2$, $m_2 = -Q_1$ and letting the m_i run over all integers uniquely parameterizes all Q_i satisfying $Q_0 = 0$. On the other hand, \tilde{Q}_0 need not be zero and it is convenient to parameterize the \tilde{Q}_i in a different way:

$$(\tilde{Q}_1, \tilde{Q}_2, \tilde{Q}_3) = n_0(1, 1, 1) - n_1(0, 1, 1) - n_2(1, 0, 1). \quad (8.70)$$

This can be inverted to give:

$$(n_0, n_1, n_2) = (\tilde{Q}_1 + \tilde{Q}_2 - \tilde{Q}_3, -\tilde{Q}_3 + \tilde{Q}_1, -\tilde{Q}_3 + \tilde{Q}_2). \quad (8.71)$$

Thus any set of integer dual charges, \tilde{Q}_j , can be uniquely expressed in terms of the integers, n_j . The conditions $Q_j = \tilde{Q}_j \pmod{2}$ imply:

$$\begin{aligned} n_0 &= 2p_0 \quad (\text{i.e. } n_0 \text{ is even}) \\ n_j &= m_j \pmod{2}. \end{aligned} \quad (8.72)$$

In this parameterization, the total dual charge is:

$$\tilde{Q}_0 = 2(3p_0 - n_1 - n_2). \quad (8.73)$$

This implies that \tilde{Q}_0 is even and:

$$\tilde{Q}_0/2 = -n_1 - n_2 \pmod{3}. \quad (8.74)$$

Thus we see that a general boundary state which is N with respect to Φ_0 will be of the form:

$$|B\rangle = \sum_{k=-1,0,1} |N_0^k\rangle \otimes \sum'_{n_1+n_2=-j \pmod{3}} |\psi(n_1, n_2, m_1, m_2)\rangle. \quad (8.75)$$

Here the ' over the summation sign indicates that, in addition to the explicitly noted restriction, the conditions:

$$n_k = m_k \pmod{2}, \quad j = 1, 2 \quad (8.76)$$

must also be imposed. The states $|\psi(n_1, n_2, m_1, m_2)\rangle$ are in the sector of the 2-component field $\vec{\Phi}$, with charges and dual charges labelled by the integers m_j and n_j . The states $|N_0^k\rangle$, for $k = -1, 0$ or 1 , are in the Φ_0 sector and are given explicitly by:

$$|N_0^k\rangle \equiv \left(\frac{3g}{2}\right)^{1/4} \exp\left[\sum_{n=1}^{\infty} a_n^{L0\dagger} a_n^{R0\dagger}\right] \sum_{\tilde{r}_0} |(2(3\tilde{r}_0 + k), 0)\rangle. \quad (8.77)$$

The corresponding ‘‘partial Neumann’’ partition functions in the Φ_0 sector may be readily calculated.

$$Z_{N_0^k} = \sqrt{3g} \frac{1}{\eta(\tilde{q})} \sum_{\tilde{r}_0 \in \mathbb{Z}} \tilde{q}^{g(3\tilde{r}_0+k)^2/6} = \frac{1}{\eta(q)} \sum_{Q_0 \in \mathbb{Z}} e^{-2\pi i Q_0 k/3} q^{Q_0^2/(6g)}. \quad (8.78)$$

As in Subsection VIII B, we are only interested in the boundary operators in the $\vec{\Phi}$ sector, and replace $Z_{N_0^k}$ by unity.

We may equivalently get the dimensions of all such primary boundary operators by using a reduced boundary state, which exists in the reduced Hilbert space of the 2 component boson field, $\vec{\Phi}$. That is:

$$|B\rangle \rightarrow \sum' |\psi(n_1, n_2, m_1, m_2)\rangle. \quad (8.79)$$

The restrictions of Eq. (8.76) remain, but the other conditions, that entangle the $\vec{\Phi}$ sector with the Φ_0 sector disappear upon restricting to boundary states with $Q_0 = 0$ and boundary operators with $Q_0 = 0$.

The windings $\Delta\vec{\Phi} \equiv \vec{\Phi}(\beta) - \vec{\Phi}(0)$ and $\Delta\vec{\Theta} \equiv \vec{\Theta}(\beta) - \vec{\Theta}(0)$ along the boundary follow from the integers (n_1, n_2, m_1, m_2) . $\Delta\vec{\Phi}$ and $\Delta\vec{\Theta}$ can be obtained from the windings of the three pairs of boson fields, $\Delta\varphi_i = \tilde{Q}_i \sqrt{2}\pi$ and $\Delta\theta_i = Q_i \sqrt{2}\pi$, using the rotations in Eqs.(4.5,4.6) and the vectors \vec{K}_j and \vec{R}_j defined, respectively, in Eqs.(4.9) and (6.55). One obtains

$$\vec{\Phi}(\beta) - \vec{\Phi}(0) = 2\pi(n_1 \frac{\vec{R}_1}{2} + n_2 \frac{\vec{R}_2}{2}) \quad (8.80)$$

$$\vec{\Theta}(\beta) - \vec{\Theta}(0) = 2\pi(m_1 \vec{K}_1 + m_2 \vec{K}_2). \quad (8.81)$$

Thus the ‘‘reduced boundary state’’ (8.79) would arise from a 2-component boson field with the mode expansion:

$$\vec{\Phi}(t, x) = \frac{2\pi}{\beta} \left[\frac{1}{g} \sum_{j=1,2} m_j \vec{K}_j t + \frac{1}{2} \sum_{j=1,2} n_j \vec{R}_j x \right] + \frac{1}{\sqrt{2g}} \sum_{n=1}^{\infty} \frac{1}{\sqrt{n}} \left[\vec{a}_n^L \exp[-inx + \frac{2\pi}{\beta}] + \vec{a}_n^R \exp[-inx - \frac{2\pi}{\beta}] + h.c. \right], \quad (8.82)$$

where the integers n_j and m_j are restricted by Eq. (8.76). The corresponding energies are:

$$E = \frac{2\pi}{\beta} \left[\frac{1}{2g} \left(\sum_j m_j \vec{K}_j \right)^2 + \frac{g}{2} \left(\frac{\sum_j n_j \vec{R}_j}{2} \right)^2 + \dots \right], \quad (8.83)$$

where the ... represents the oscillator mode terms. Of course the restriction of Eq. (8.76) must be applied.

Let us compare the mode expansion (8.82) to the corresponding Eq. (C53) for the standard compactified boson, with Λ being the triangular lattice spanned by \vec{R}_1 and \vec{R}_2 . While they are similar, we find that they are in fact different and cannot be identical with any choice of the compactification lattice Λ for the standard free boson. Namely, the fermionic nature of the problem has modified the mode expansion, via the factor of 1/2 multiplying the second term inside the first square bracket in Eq. (8.82) and the restriction of Eq. (8.76) on the quantum numbers n_i and m_i . In contrast to the two wire case, the fermionic nature of the problem survives and makes important changes to the boundary states and the corresponding “reduced mode expansion” of Eq. (8.82). This may be related to the fact that the Klein factors cannot be eliminated for the 3-wire junction whereas they can be eliminated in the 2-wire case.

IX. THE METHOD OF DELAYED EVALUATION OF BOUNDARY CONDITION (DEBC)

In this section we introduce the DEBC method. The method consists of doubling the number of degrees of freedom in the problem by keeping both the bosonic fields ϕ_i and its conjugate momentum θ_i , for each semi-infinite lead i . The redundancy is eliminated by imposing the boundary condition at $x = 0$, which cuts in half the number of degrees of freedom, down to the correct number for the semi-infinite wires. The basic idea behind the method is that we delay the choice of boundary condition until after we write the operators corresponding to the (multi)particle tunneling processes at the junction. The correct (or stable) boundary condition that must be imposed on ϕ_i and θ_i is determined *a posteriori*, taking into account the scaling dimensions of the tunneling operators given the different choices of boundary conditions.

Explicitly, we write the electron operators, both right and left movers (or incoming to and outgoing from the junction at $x = 0$), for each of the semi-infinite leads, labelled by i , defined in the half line $x > 0$:

$$\Psi_i^{L,R} \propto e^{i\frac{1}{\sqrt{2}}(\varphi_i \pm \theta_i)}. \quad (9.1)$$

Klein factors can be absorbed into the zero mode terms of the mode expansion of the φ_i and θ_i bosons. For example, the fermionic commutations between different leads can be taken care of by imposing that $[\varphi_i^{(0)}, \varphi_j^{(0)}] = i2\pi\alpha_{ij}$, with an anti-symmetric $\alpha_{ij} = -\alpha_{ji}$ and unit entries $\alpha_{ij} = \pm 1$. (A different representation of Klein factors using zero modes is introduced in Appendix E when we discuss fractional quantum Hall junctions.) The Θ_i fields can be taken to commute for $i \neq j$.

Notice that the above construction, in terms of both sets of bosonic fields φ_i and θ_i , is the usual one when describing systems on the infinite line, and thus we are working with twice the number of degrees of freedom for the semi-infinite line. What is missing is the boundary condition at the origin $x = 0$ (the choice of which we are delaying) which constraints φ_i and θ_i and thus cuts in half the number of degrees of freedom for systems on the half-line.

The subsequent step is to construct all tunneling operators between the leads using the electron operators in Eq. (9.1), keeping both φ and θ fields, and imposing later the appropriate boundary condition.

For concreteness, let us present below the DEBC method through an example, using the simpler problem of the two-wire junction for this purpose. In the next section, we apply the method to the problem of interest in this paper, the three-wire junction.

For the two-wire problem, the single particle tunneling terms at $x = 0$ can be expressed in terms of the $\Psi_j^{R,L}$ as:

$$T_{21}^{RL} = \Psi_2^{R\dagger} \Psi_1^L|_{x=0} \propto e^{i\frac{\varphi_1 - \varphi_2}{\sqrt{2}}} e^{i\frac{\theta_1 + \theta_2}{\sqrt{2}}} \quad (9.2)$$

$$T_{21}^{LL} = \Psi_2^{L\dagger} \Psi_1^L|_{x=0} \propto e^{i\frac{\varphi_1 - \varphi_2}{\sqrt{2}}} e^{i\frac{\theta_1 - \theta_2}{\sqrt{2}}} \quad (9.3)$$

$$T_{11}^{RL} = \Psi_1^{R\dagger} \Psi_1^L|_{x=0} \propto e^{i\sqrt{2}\theta_1}. \quad (9.4)$$

The fields φ_i and θ_i above are all evaluated at the boundary $x = 0$. Other terms can be obtained by simply taking the Hermitian conjugate or by exchanging RL in these three combinations above. Physically, these terms correspond to tunneling between the leads [terms (9.2) and (9.3)], and backscattering [term (9.4)].

Written in terms of the rotated basis Eqs. (8.42,8.43), we have

$$T_{21}^{RL} \propto e^{i\Phi} e^{i\Theta_0} \propto e^{i\Phi} \quad (9.5)$$

$$T_{21}^{LL} \propto e^{i\Phi} e^{i\Theta} \quad (9.6)$$

$$T_{11}^{RL} \propto e^{i(\Theta + \Theta_0)} \propto e^{i\Theta}, \quad (9.7)$$

where we have used the fact that charge conservation requires that Φ_0 must obey the Neumann boundary condition, or equivalently, Θ_0 must obey the Dirichlet boundary condition (Θ_0 is pinned at the boundary).

The boundary conditions on the other pair of bosons, Φ and Θ , can be expressed in terms of chiral fields as

$$\phi_R = \mathcal{R}\phi_L + C, \quad (9.8)$$

with $\Phi = \frac{1}{\sqrt{g}}(\phi_R + \phi_L)$ and $\Theta = \sqrt{g}(\phi_R - \phi_L)$, where \mathcal{R} is a rotation and C is a constant. Since we just have a single pair of RL fields, the only possibilities are $\mathcal{R} = \pm 1$. We will soon see that in the problem of three leads there will be two pairs of RL boson fields, and more general rotations \mathcal{R}_δ are allowed.

The scaling dimension of a general vertex operator

$$V = e^{ia\sqrt{g}\Phi + ib\frac{1}{\sqrt{g}}\Theta} = e^{i(a+b)\phi_R + i(a-b)\phi_L}, \quad (9.9)$$

is given by

$$\Delta_V = \frac{1}{4}|\mathcal{R}(a+b) + (a-b)|^2. \quad (9.10)$$

For N boundary conditions, Θ is pinned, $\mathcal{R} = 1$ and $\Delta_V = a^2$. For D boundary conditions, Φ is pinned instead, $\mathcal{R} = -1$ and $\Delta_V = b^2$. These results for Δ_V could have been easily guessed, but going through the exercise with the rotation \mathcal{R} is useful as a warm up for the three lead case.

We now analyze the scaling dimensions of the three sets of operators (9.5)-(9.7) for different boundary conditions on Φ .

- *Neumann boundary condition* – In this case

$$\Delta_{T_{21}^{RL}} = g^{-1} \quad , \quad \Delta_{T_{21}^{LL}} = g^{-1} \quad , \quad \Delta_{T_{11}^{RL}} = 0. \quad (9.11)$$

The operator T_{11}^{RL} is proportional to the identity (dimension zero), which is consistent with the fact that it is this backscattering operator that is responsible for pinning the Θ field for N boundary condition (on Φ). This is the perfect backscattering fixed point, stable as long as the other two operators T_{21}^{RL} and T_{21}^{LL} are irrelevant, which is the case for $g < 1$.

- *Dirichlet boundary condition* – In this case

$$\Delta_{T_{21}^{RL}} = 0 \quad , \quad \Delta_{T_{21}^{LL}} = g \quad , \quad \Delta_{T_{11}^{RL}} = g. \quad (9.12)$$

Now it is the operator T_{21}^{RL} which is proportional to the identity (dimension zero), and this transmission operator is responsible for pinning the ϕ field for D boundary condition. This is the perfect transmission fixed point, stable as long as the other two operators T_{21}^{LL} and T_{11}^{RL} are irrelevant, which is the case for $g > 1$.

It is clear from this approach that the two-wire junction can be understood in terms of the boson fields Φ and Θ , which are dual to each other. They can be regarded as subject to the standard compactification $\Phi \sim \Phi + 2\pi$ and $\Theta \sim \Theta + 2\pi$, as can be seen from Eqs. (9.2,9.3,9.4). Also, the DEBC approach reproduces rather simply the results for a junction between two wires as in the Kane-Fisher model [1]. We now apply it to the three-wire junction.

X. FIXED POINTS FOR THE JUNCTION OF THREE WIRES

Now let us discuss the RG fixed points in the junction of three wires. As we have discussed, each fixed point corresponds to a conformally invariant boundary condition of the boson field theory.

In the DEBC approach, we need the $x = 0$ tunneling operators between the three wires. They are easily expressible in terms of the vectors \vec{K}_j defined in Eq. (4.9), with the two-component field $\vec{\Phi}$ defined in Eqs. (4.5,4.6).

The tunneling operators involving the RL combinations can be split into three groups:

- + cycle:

$$T_{21}^{RL} = \Psi_2^{R\dagger} \Psi_1^L \Big|_0 \propto e^{i\vec{K}_3 \cdot \vec{\Phi}} e^{i\frac{1}{\sqrt{3}}\hat{z} \times \vec{K}_3 \cdot \vec{\Theta}} e^{i\sqrt{\frac{2}{3}}\Theta_0} \quad (10.1)$$

$$T_{32}^{RL} = \Psi_3^{R\dagger} \Psi_2^L \Big|_0 \propto e^{i\vec{K}_1 \cdot \vec{\Phi}} e^{i\frac{1}{\sqrt{3}}\hat{z} \times \vec{K}_1 \cdot \vec{\Theta}} e^{i\sqrt{\frac{2}{3}}\Theta_0} \quad (10.2)$$

$$T_{13}^{RL} = \Psi_1^{R\dagger} \Psi_3^L \Big|_0 \propto e^{i\vec{K}_2 \cdot \vec{\Phi}} e^{i\frac{1}{\sqrt{3}}\hat{z} \times \vec{K}_2 \cdot \vec{\Theta}} e^{i\sqrt{\frac{2}{3}}\Theta_0} \quad (10.3)$$

- – cycle:

$$T_{12}^{RL} = \Psi_1^{R\dagger} \Psi_2^L \Big|_0 \propto e^{-i\vec{K}_3 \cdot \vec{\Phi}} e^{i\frac{1}{\sqrt{3}}\hat{z} \times \vec{K}_3 \cdot \vec{\Theta}} e^{i\sqrt{\frac{2}{3}}\Theta_0} \quad (10.4)$$

$$T_{23}^{RL} = \Psi_2^{R\dagger} \Psi_3^L \Big|_0 \propto e^{-i\vec{K}_1 \cdot \vec{\Phi}} e^{i\frac{1}{\sqrt{3}}\hat{z} \times \vec{K}_1 \cdot \vec{\Theta}} e^{i\sqrt{\frac{2}{3}}\Theta_0} \quad (10.5)$$

$$T_{31}^{RL} = \Psi_3^{R\dagger} \Psi_1^L \Big|_0 \propto e^{-i\vec{K}_2 \cdot \vec{\Phi}} e^{i\frac{1}{\sqrt{3}}\hat{z} \times \vec{K}_2 \cdot \vec{\Theta}} e^{i\sqrt{\frac{2}{3}}\Theta_0} \quad (10.6)$$

- backscattering:

$$T_{11}^{RL} = \Psi_1^{R\dagger} \Psi_1^L \Big|_0 \propto e^{-i\frac{2}{\sqrt{3}}\hat{z} \times \vec{K}_1 \cdot \vec{\Theta}} e^{i\sqrt{\frac{2}{3}}\Theta_0} \quad (10.7)$$

$$T_{22}^{RL} = \Psi_2^{R\dagger} \Psi_2^L \Big|_0 \propto e^{-i\frac{2}{\sqrt{3}}\hat{z} \times \vec{K}_2 \cdot \vec{\Theta}} e^{i\sqrt{\frac{2}{3}}\Theta_0} \quad (10.8)$$

$$T_{33}^{RL} = \Psi_3^{R\dagger} \Psi_3^L \Big|_0 \propto e^{-i\frac{2}{\sqrt{3}}\hat{z} \times \vec{K}_3 \cdot \vec{\Theta}} e^{i\sqrt{\frac{2}{3}}\Theta_0} \quad (10.9)$$

The LL and RR combinations lead to another group:

- $LL - RR$:

$$T_{21}^{LL} = \Psi_2^{L\dagger} \Psi_1^L \Big|_0 \propto e^{i\vec{K}_3 \cdot \vec{\Phi}} e^{+i\vec{K}_3 \cdot \vec{\Theta}} \quad (10.10)$$

$$T_{32}^{LL} = \Psi_3^{L\dagger} \Psi_2^L \Big|_0 \propto e^{i\vec{K}_1 \cdot \vec{\Phi}} e^{+i\vec{K}_1 \cdot \vec{\Theta}} \quad (10.11)$$

$$T_{13}^{LL} = \Psi_1^{L\dagger} \Psi_3^L \Big|_0 \propto e^{i\vec{K}_2 \cdot \vec{\Phi}} e^{+i\vec{K}_2 \cdot \vec{\Theta}} \quad (10.12)$$

$$T_{21}^{RR} = \Psi_2^{R\dagger} \Psi_1^R \Big|_0 \propto e^{i\vec{K}_3 \cdot \vec{\Phi}} e^{-i\vec{K}_3 \cdot \vec{\Theta}} \quad (10.13)$$

$$T_{32}^{RR} = \Psi_3^{R\dagger} \Psi_2^R \Big|_0 \propto e^{i\vec{K}_1 \cdot \vec{\Phi}} e^{-i\vec{K}_1 \cdot \vec{\Theta}} \quad (10.14)$$

$$T_{13}^{RR} = \Psi_1^{R\dagger} \Psi_3^R \Big|_0 \propto e^{i\vec{K}_2 \cdot \vec{\Phi}} e^{-i\vec{K}_2 \cdot \vec{\Theta}} \quad (10.15)$$

To these sets of operators we must add their Hermitian conjugates.

In the following, we consider several conformally invariant boundary conditions which can be expressed as

$$\vec{\phi}_R = \mathcal{R}_\xi \vec{\phi}_L + \vec{C}, \quad (10.16)$$

where

$$\mathcal{R}_\xi = \begin{pmatrix} \cos \xi & -\sin \xi \\ \sin \xi & \cos \xi \end{pmatrix}, \quad (10.17)$$

$$\vec{\Phi} = \frac{1}{\sqrt{g}} (\vec{\phi}_R + \vec{\phi}_L) \quad (10.18)$$

$$\vec{\Theta} = \sqrt{g} (\vec{\phi}_L - \vec{\phi}_R) \quad (10.19)$$

and \vec{C} represents a constant vector. Θ_0 is pinned by charge conservation, and can be ignored in all operators above.

Consider a general operator

$$V = e^{i\vec{a}\sqrt{g}\vec{\Phi} + i\vec{b}\frac{1}{\sqrt{g}}\vec{\Theta}} = e^{i(\vec{a}-\vec{b})\cdot\vec{\phi}_R + i(\vec{a}+\vec{b})\cdot\vec{\phi}_L}. \quad (10.20)$$

For the boundary condition (10.16), its boundary scaling dimension is:

$$\Delta_V = \frac{1}{4} |\mathcal{R}_\xi^{-1}(\vec{a} - \vec{b}) + (\vec{a} + \vec{b})|^2 \quad (10.21)$$

$$\begin{aligned} &= \frac{1}{4} |\mathcal{R}_\xi(\vec{a} + \vec{b}) + (\vec{a} - \vec{b})|^2 \quad (10.22) \\ &= \frac{1}{2} [|\vec{a}|^2 + |\vec{b}|^2 + (\mathcal{R}_\xi \vec{a}) \cdot \vec{a} - (\mathcal{R}_\xi \vec{b}) \cdot \vec{b} \\ &\quad - (\mathcal{R}_\xi \vec{a}) \cdot \vec{b} + (\mathcal{R}_\xi \vec{b}) \cdot \vec{a}] \end{aligned}$$

With the scaling dimension of the tunneling operators in hand, we can now analyze the stability of the fixed points that are characterized by a choice of boundary condition. We will carry out this analysis in the following section, where we present, discuss, and parallel the results obtained using both BCFT taking into account the twisted structure of the Hilbert space and the DEBC approach.

A. Disconnected fixed point – Neumann boundary condition on $\vec{\Phi}$

The choice $\xi = 0$ in Eq. (10.16) pins $\vec{\Theta} = \vec{C}$ (back-reflection condition). This amounts to the Dirichlet boundary condition on $\vec{\Theta}$, equivalently the Neumann boundary condition on $\vec{\Phi}$.

Let us calculate the scaling dimensions for the \pm cycle operators. Since $\mathcal{R}_0 = \mathbf{1}$, $\Delta_V = |\vec{a}|^2$. Take T_{21}^{RL} as an example, so $\vec{a} = \frac{1}{\sqrt{g}} \vec{K}_3$ and $\vec{b} = \sqrt{\frac{g}{3}} \hat{z} \times \vec{K}_3$ enter in Eq. (10.21):

$$\Delta_{T_{21}^{RL}} = \frac{1}{g} |\vec{K}_3|^2 = \frac{1}{g} \quad (10.23)$$

The result is the same for all 6 \pm cycle operators, as well as for the 6 $LL - RR$ operators. Upon fixing the boundary condition, many of these operators are redundant; the number of independent operators can be easily accounted for, and we find that there are only 3 independent operators plus their 3 Hermitian conjugates. All these 6 independent operators are irrelevant for $g < 1$, and so the backscattering fixed point is stable for this range of g .

The case just discussed above is the simplest boundary conditions for the problem of the junction of three wires. It corresponds to disconnected wires. Indeed, Neumann boundary condition on $\vec{\Phi}$ (or Dirichlet on $\vec{\Theta}$) is equivalent to Neumann boundary condition on all $\varphi_{1,2,3}$ (or Dirichlet on $\theta_{1,2,3}$).

Let us now connect this to the standard BCFT approach, and construct the boundary state and the cylinder amplitude explicitly. As it is reviewed in App. C for the standard free boson, the Neumann boundary state is given by a superposition of Ishibashi states. Since the boundary condition for $\vec{\Theta}$ is Dirichlet, the boundary state

must have zero winding $\Delta \vec{\Theta} = 0$, namely $m_1 = m_2 = 0$. Let us define the bosonic Ishibashi state

$$|(n_1, n_2, 0, 0)\rangle \equiv \exp \left[\sum_n \vec{a}_n^{L\dagger} \cdot \vec{a}_n^{R\dagger} \right] |(n_1, n_2, 0, 0)\rangle, \quad (10.24)$$

where $|(n_1, n_2, 0, 0)\rangle$ is the oscillator vacuum with the quantum number $(n_1, n_2, m_1 = 0, m_2 = 0)$.

The most stable Neumann-type boundary state would be given by the linear superposition over all the possible Ishibashi states. The important consequence of the twisted structure is that, because of the condition (8.76), n_1 and n_2 cannot run over all integers when $m_1 = m_2 = 0$. Instead, they can only take even integers values. Thus the most stable N boundary is given by

$$|N\rangle = g_N \sum_{n'_1, n'_2 \in \mathbf{Z}} |(2n'_1, 2n'_2, 0, 0)\rangle, \quad (10.25)$$

where the prefactor g_N represents the ground-state degeneracy [41] of the N boundary state. (It is *not* the Tomonaga-Luttinger parameter g introduced in Eq. (4.1).)

The calculation of the cylinder amplitude with the Neumann boundary state at the both ends then follows, exactly as in the case of the standard boson. The diagonal cylinder amplitude is given by

$$\begin{aligned} Z_{NN}(\tilde{q}) &= \langle N | e^{-lH_\beta^P} | N \rangle \\ &= \frac{g_N^2}{\eta(\tilde{q})^2} \sum_{n'_1, n'_2 \in \mathbf{Z}} \tilde{q}^{\frac{g}{4}(n'_1 \vec{R}_1 + n'_2 \vec{R}_2)^2}. \end{aligned} \quad (10.26)$$

This can be identified with the corresponding partition function (C63) of the standard compactified free boson, with Λ being the triangular lattice of lattice constant $2/\sqrt{3}$, spanned by \vec{R}_1 and \vec{R}_2 . Thus we find

$$g_N = \left(\frac{g^2}{3} \right)^{1/4}, \quad (10.27)$$

because $V_0(\Lambda) = 2/\sqrt{3}$. The modular transform of Eq. (C65) should also be given by Eq. (C66), namely

$$Z_{NN}(q) = \frac{1}{\eta(q)^2} \sum_{l_1, l_2 \in \mathbf{Z}} \tilde{q}^{\frac{1}{g}(l_1 \vec{K}_1 + l_2 \vec{K}_2)^2}. \quad (10.28)$$

From Eq. (10.28) we can immediately read off the scaling dimensions of the boundary operators. The leading ones have the smallest scaling dimension $1/g$, and correspond to the \pm cycle operators discussed above based on DEBC. The BCFT analysis confirms that they are indeed the leading operators and the N fixed point is stable for $g < 1$ and is unstable for $g > 1$.

For the Neumann boundary condition on $\vec{\Phi}$, the conductance tensor vanishes: $G_{jk} = 0$. This is most easily seen by observing the Neumann boundary condition $\vec{\Phi}$ is nothing but the Neumann boundary condition on the original fields $\varphi_{1,2,3}$. Alternatively, we find that G_{jk} vanishes by an explicit calculation of Eq. (D23).

B. Andreev reflection fixed point – Dirichlet boundary condition on $\vec{\Phi}$

The other simple boundary condition for the free boson is the Dirichlet boundary condition on $\vec{\Phi}$, which is dual to Neumann. In fact, the Dirichlet boundary condition on $\vec{\Phi}$ is the Neumann boundary condition on $\vec{\Theta}$. The choice of angle $\xi = \pi$ pins $\vec{\Phi} = \vec{C}$. Plugging $\mathcal{R}_\pi = -1$ into Eq. (10.21), we obtain $\Delta_V = |\vec{b}|^2$. Using this, we find, for example, that

$$\Delta_{T_{33}^{RL}} = \frac{4g}{3} |\hat{z} \times \vec{K}_3|^2 = \frac{4g}{3} \quad (10.29)$$

$$\Delta_{T_{21}^{RL}} = \frac{g}{3} |\hat{z} \times \vec{K}_3|^2 = \frac{g}{3} \quad (10.30)$$

$$\Delta_{T_{21}^{LL}} = g |\vec{K}_3|^2 = g. \quad (10.31)$$

There are 3 independent operators with dimension $4g/3$, 3 with dimension $g/3$, and 3 with dimension g , plus their respective Hermitian conjugates. The leading irrelevant terms are the \pm cycle tunneling operators. This fixed point is stable for $g > 3$.

Within the BCFT approach, in the standard compactified boson case, the scaling dimensions of the boundary operators in the Neumann and Dirichlet boundary states are given by the reciprocal lattices as discussed in App. C. If the present problem of the junction were mapped to the standard compactified free bosons, the Dirichlet boundary state would have the leading boundary operator with the scaling dimension $4g/3$, which is irrelevant for $g > 3/4$. Thus, the Dirichlet boundary condition would be stable for $3/4 < g$. In particular, both the Neumann and Dirichlet boundary conditions are then stable for $3/4 < g < 1$. This is discussed by Yi and Kane [16] in the context of the quantum Brownian motion on a triangular lattice. There is a duality $g \leftrightarrow 4/(3g)$ which exchanges the Neumann and Dirichlet boundary conditions.

These considerations for the standard compactified boson exactly matches the potential argument presented in Sec. V. As discussed there, it would not apply to the present problem in which electrons hop between different wires. In Sec. V, the fermi statistics of electrons were taken of care by the Klein factors, to derive sensible results. In the present context, the difference from the standard boundary problem of free boson field theory is given by the twisted structure of the Hilbert space discussed in Section VIII. This affects the stability of the fixed point in an important manner. As it will be shown below, the most stable Dirichlet-type boundary state turns out to be the strong pair-hopping limit, D_P , discussed in Sec. V.

The most stable Dirichlet-type boundary state is given by a superposition of all the Ishibashi states allowed under $\Delta\vec{\Theta} = 0$, namely $n_1 = n_2 = 0$. These Ishibashi states

are given as

$$|(0, 0, m_1, m_2)\rangle\rangle \equiv \exp \left[- \sum_n \vec{a}_n^{L\dagger} \cdot \vec{a}_n^{R\dagger} \right] |(0, 0, m_1, m_2)\rangle, \quad (10.32)$$

As in the construction of the N boundary state, because of the parity condition (8.76), m_1 and m_2 take only even integer values. Thus we have

$$|D_P\rangle = g_{D_P} \sum_{m'_1, m'_2 \in \mathbf{Z}} |(0, 0, 2m'_1, 2m'_2)\rangle\rangle. \quad (10.33)$$

The corresponding diagonal cylinder amplitude is

$$\begin{aligned} Z_{D_P D_P}(\tilde{q}) & \langle D_P | e^{-lH_{\vec{\beta}}} | D_P \rangle \\ & = \frac{g_{D_P}^2}{\eta(\tilde{q})^2} \sum_{m'_1, m'_2 \in \mathbf{Z}} \tilde{q}^{\frac{1}{4g}(2m'_1 \vec{K}_1 + 2m'_2 \vec{K}_2)^2}. \end{aligned} \quad (10.34)$$

Modular transforming using Eq. (C59), now with Λ being the triangular lattice with the lattice constant 2, we obtain

$$Z_{D_P D_P}(q) = \frac{1}{\eta(q)^2} \sum_{l_1, l_2 \in \mathbf{Z}} q^{g(\frac{1}{2}l_1 \vec{R}_1 + \frac{1}{2}l_2 \vec{R}_2)^2}. \quad (10.35)$$

Now the dimension of the leading boundary operator is given by

$$\frac{g}{4} |\vec{R}_j|^2 = \frac{g}{3}. \quad (10.36)$$

Furthermore, the dimensions of the second-leading and third-leading operators are related to the distance between next-nearest and next-next-nearest neighbors on the triangular lattice and given by g and $4g/3$, respectively. These exactly agree with the scaling dimensions of tunneling operators (10.30), (10.31) and (10.29) obtained from the DEBC method. Furthermore, these scaling dimensions coincide with those that can be obtained from the instanton argument for the D_P fixed point, in which $\vec{\Phi}$ is pinned to the triangular lattice with the lattice constant $2\pi/\sqrt{3}$.

The present analysis confirms that $g/3$ is the scaling dimension of the leading boundary operator, and thus the D_P fixed point is stable for $g > 3$ and unstable for $g < 3$. This is quite different from what would obtain for the stability of the Dirichlet boundary state if the problem were mapped to the standard compactified boson. The difference is due to the twisted structure, which originates from the fermionic nature of the electron.

The present result can also be understood from the duality. Eq. (8.82) shows that the twisted boson theory has the duality

$$\vec{\Phi} \rightarrow \vec{\Theta} \quad (10.37)$$

$$g \leftrightarrow \frac{3}{g}, \quad (10.38)$$

instead of $g \leftrightarrow 4/(3g)$ for the standard boson. The duality (10.38) was found in Ref. [5] by a different argument.

Our analysis shows that the duality exists as a structure of the effective Hilbert space, beyond a particular choice of the perturbation.

Let us now discuss the conductance. For the Dirichlet boundary condition, a similar calculation to that in App. D gives

$$\lim_{\omega \rightarrow 0^+} \frac{1}{\pi \omega L} \int_0^L dx \int_{-\infty}^{\infty} d\tau e^{i\omega\tau} \langle J^\mu(y, \tau) J^\nu(x, 0) \rangle = 2g \delta^{\mu\nu} \quad (10.39)$$

We thus find, from Eq. (D23),

$$G_{kl} = 2g \frac{e^2}{h} \sum_{\mu=1,2} v_{k\mu} v_{l\mu} \quad (10.40)$$

The summation $\sum_{\mu=1,2}$ can be interpreted as an inner product of the *two-dimensional* vectors \vec{v}_k and \vec{v}_l . From eq. (D19), we find

$$\vec{v}_k \cdot \vec{v}_l = (\delta_{kl} - \frac{1}{3}) \quad (10.41)$$

Therefore we recover the results in Ref. [5] as

$$G_{kl} = \begin{cases} \frac{4g}{3} \frac{e^2}{h} & (k = l) \\ -\frac{2g}{3} \frac{e^2}{h} & (k \neq l) \end{cases} \quad (10.42)$$

This derivation and the result on the conductance equally apply to D_P and D_N fixed points; they are indistinguishable in terms of the conductance. As pointed out in Ref. [5], the single-terminal conductance in this case is larger than the single ideal wire. This exhibits an enhanced conductance due to the Andreev reflection.

C. Chiral fixed points χ_{\pm}

1. Chiral fixed points from DEBC

In the DHM representation discussed in Section VI, the quantal phases due to the Fermi statistics and the magnetic flux piercing through the junction was accounted by the ‘‘boundary magnetic field’’. In the representation with $n = 0, 1$ the chiral fixed points χ_{\pm} correspond to the localized phase of the DHM, which amounts to the Dirichlet boundary condition on the field \vec{X} . We emphasize that the field \vec{X} is not identical to the fields $\vec{\Theta}$ and $\vec{\Phi}$ we have been using. The χ_{\pm} fixed point corresponds to neither Dirichlet nor Neumann boundary conditions in terms of $\vec{\Theta}$ and $\vec{\Phi}$. As we will see in the following, the field \vec{X} in fact corresponds to a chiral rotation of $\vec{\Theta}$ or $\vec{\Phi}$.

Indeed, by inspecting the operators in the \pm cycles, we would find that if these coupling constants dominate the low-energy physics (flow to strong coupling), then they set boundary conditions that are mixed in the $\vec{\Phi}$ and $\vec{\Theta}$ fields.

For example, pinning the phases in the $+$ cycle corresponds to the boundary condition

$$\chi_+ : \vec{K}_i \cdot \vec{\Phi} + \sqrt{\frac{1}{3}} (\hat{z} \times \vec{K}_i) \cdot \vec{\Theta} = \vec{C}. \quad (10.43)$$

And pinning this combination corresponds to the choice of angle ξ such that

$$\tan \frac{\xi}{2} = \frac{\sqrt{3}}{g}. \quad (10.44)$$

With this choice of boundary condition or angle ξ , the scaling dimension, for example, of a backscattering term such as T_{33}^{RL} is obtained with $\vec{a} = 0$ and $\vec{b} = -2\sqrt{\frac{2}{3}} \hat{z} \times \vec{K}_3$ in Eq. (10.21). Using that $|\hat{z} \times \vec{v}|^2 = |\vec{v}|^2$ and $[\mathcal{R}_\xi(\hat{z}\vec{v}) \cdot (\hat{z} \times \vec{v})] = (\mathcal{R}_\xi \vec{v}) \cdot \vec{v} = |\vec{v}|^2 \cos \xi$ for any vector \vec{v} :

$$\begin{aligned} \Delta_{T_{33}^{RL}} &= 2 \frac{g}{3} \left[|\hat{z} \times \vec{K}_3|^2 - [\mathcal{R}_\xi(\hat{z} \times \vec{K}_3)] \cdot (\hat{z} \times \vec{K}_3) \right] \\ &= 2 \frac{g}{3} |\vec{K}_3|^2 [1 - \cos \xi] = \frac{4g}{3+g^2} \end{aligned} \quad (10.45)$$

after some simple algebra.

Similarly, the scaling dimensions of the $-$ cycle terms (such as T_{12}^{RL}) as well as those of the $LL - RR$ terms (such as T_{12}^{LL}) can be shown to be also $\frac{4g}{3+g^2}$. Again, these operators are not independent after the choice of boundary condition; in total, there are 3 independent operators and their 3 Hermitian conjugates. This agrees with the dimension of the leading operator for the fixed point χ_+ , from the instanton analysis in Sec. VI.

Now, had we chosen to pin the phases in the $-$ cycle set of operators, or select the boundary condition

$$\chi_- : \vec{K}_i \cdot \vec{\Phi} - \sqrt{\frac{1}{3}} (\hat{z} \times \vec{K}_i) \cdot \vec{\Theta} = \vec{C}, \quad (10.46)$$

we would have obtained an analogous case, in which $\tan \frac{\xi}{2} = -\frac{\sqrt{3}}{g}$. The dimensions of the backscattering and $+$ cycle terms, as well as of the $LL - RR$ terms, are again $\frac{4g}{3+g^2}$. This fixed point is stable for $1 < g < 3$. Which of the χ_{\pm} is selected depends on the time-reversal symmetry breaking flux.

2. Relation to the DHM representation

Let us connect the present analysis to the ones based on the dissipative Hofstadter model, more explicitly.

First we formulate the DHM (for $V = 0$) as a boundary problem of a $c = 2$ free boson field theory. This can be done in two different ways. One of them is to begin with the (1+1) dimensional action:

$$S = \int_{-\infty}^{\infty} d\tau \int_0^{\infty} dx \left[\frac{\alpha}{4\pi} (\partial_\mu \vec{X})^2 + \frac{\beta}{4\pi} \epsilon^{\mu\nu} \epsilon_{ab} \partial_\mu X_a \partial_\nu X_b \right]. \quad (10.47)$$

We do not impose any b.c. on \vec{X} at $x = 0$, instead letting the field be dynamical on the boundary. By integrating out the bulk part of the free boson fields, \vec{X} , this is reduced to the (non-interacting part of the) one-dimensional action of Eq. (6.10) introduced in Ref. [23]. To see this explicitly, we may decompose the fields $\vec{X}(\tau, x)$ inside the path integral into a sum of classical and quantum terms:

$$\vec{X}(\tau, x) = \vec{X}^{\text{cl}}(\tau, x) + \vec{X}(\tau, x)'. \quad (10.48)$$

Here \vec{X}^{cl} obeys the classical equations of motion:

$$\partial^2 \vec{X}^{\text{cl}} = 0. \quad (10.49)$$

[Note that the term proportional to β in the action of Eq. (10.47) makes no contribution to the Euler-Lagrange equations because it is a total derivative.] \vec{X}^{cl} is chosen to obey the boundary condition:

$$\vec{X}^{\text{cl}}(\tau, 0) = \vec{X}_b(\tau). \quad (10.50)$$

On the other hand, the quantum part, $\vec{X}'(\tau, x)$ obeys a D b.c., $\vec{X}'(\tau, 0) = 0$. With this choice of b.c. on \vec{X}' , using the fact that \vec{X}^{cl} obeys the Euler-Lagrange equations, we see that:

$$S(\vec{X}^{\text{cl}} + \vec{X}') = S(\vec{X}^{\text{cl}}) + S(\vec{X}'), \quad (10.51)$$

i.e. the cross-term vanishes. Furthermore, in calculating Green's functions of $X(\tau, 0)$, \vec{X}' doesn't appear due to its D b.c. Therefore, the calculation of these boundary Green's functions reduces to a functional integral over the boundary fields, $\vec{X}_b(\tau)$ with a classical action:

$$S_b[\vec{X}_b] = S(\vec{X}^{\text{cl}}) \quad (10.52)$$

where S is the two-dimensional action of Eq. (10.47) and the dependence on the boundary fields, $\vec{X}_b(\tau)$ is induced through the b.c. on \vec{X}^{cl} of Eq. (10.50). Fourier expanding \vec{X}^τ :

$$\vec{X}(\tau) = \sum_n \vec{X}_n e^{i\omega_n \tau}, \quad (10.53)$$

gives the classical solution:

$$\vec{X}^{\text{cl}}(\tau, x) = \sum_n \vec{X}_n e^{i\omega_n \tau - |\omega_n| x}, \quad (10.54)$$

and the boundary action (6.10).

The alternative approach is to take the bulk action with no magnetic field term:

$$S = \int_{-\infty}^{\infty} d\tau \int_0^{\infty} dx \left[\frac{\alpha}{4\pi} (\partial_\mu \vec{X})^2 \right]. \quad (10.55)$$

and impose a chiral boundary condition:

$$\vec{X}_R = \mathcal{R}_{\xi'} \vec{X}_L \quad (10.56)$$

for some rotation angle ξ' .

We wish to show that correlation functions at $x = 0$ for Eq. (10.55) with (10.56) are the same, for an appropriate value of ξ' , as those obtained from the boundary action of Eq. (6.10). This can be shown using a limiting procedure where we first calculate correlation functions for fields $\vec{X}(\tau_i, x_i)$ and then take the limit where $x_i \rightarrow 0^+$. Since we are considering the non-interacting theory at this point, it is sufficient to show this for the 2-point function. Using:

$$\langle X_L^\mu(\tau + ix) X_L^\nu(\tau' + ix') \rangle = \frac{-1}{2\alpha} \ln[(\tau - \tau') + i(x - x')] \quad (10.57)$$

and the fact that the boundary condition of Eq. (10.56) implies:

$$\vec{X}_R(\tau, x) = \mathcal{R}_{\xi'} \vec{X}_L(\tau, -x), \quad (10.58)$$

for $x > 0$, we obtain:

$$\begin{aligned} \langle X^a(\tau, x) X^b(0, x') \rangle &= \langle [X_L^a(\tau + ix) + \mathcal{R}_{\xi'}^{ac} X_L^c(\tau - ix)] [X_L^b(ix') + \mathcal{R}_{\xi'}^{bd} X_L^d(-ix')] \rangle \\ &= -\frac{1}{2\alpha} \{ \delta^{ab} \ln[\tau + i(x - x')] + \delta^{ab} \ln[\tau - i(x - x')] + \mathcal{R}_{\xi'}^{ab} \ln[\tau + i(x + x')] + \mathcal{R}_{\xi'}^{ba} \ln[\tau - i(x + x')] \}. \end{aligned} \quad (10.59)$$

Using the explicit form of $\mathcal{R}_{\xi'}$ given in Eq. (10.17) this can be written:

$$\langle X^a(\tau, x) X^b(0, x') \rangle = -\frac{1}{2\alpha} \{ [1 + \cos \xi'] \delta^{ab} \ln[\tau^2 + (x - x')^2] - \epsilon^{ab} \sin \xi' (\ln[\tau - i(x + x')] - \ln[\tau + i(x + x')]) \}. \quad (10.60)$$

Now letting $x, x' \rightarrow 0^+$, we obtain:

$$\langle X^a(\tau, +0) X^b(0, +0) \rangle \rightarrow -\frac{1 + \cos \xi'}{2\alpha} \delta^{ab} \ln \tau^2 + i\pi \frac{\sin \xi'}{2\alpha} \epsilon^{ab} [\text{sgn}(\tau) - 1]. \quad (10.61)$$

Choosing:

$$\tan \frac{\xi'}{2} = \frac{\beta}{\alpha}, \quad (10.62)$$

this reduces to the correlation function of the DHM model, Eq. (6.11), apart from a constant term:

$$\delta \langle X^a(\tau, +0) X^b(0, +0) \rangle = -i\pi \frac{\beta}{\alpha^2 + \beta^2} \epsilon^{ab}. \quad (10.63)$$

This constant term has no effect on the perturbative expansion discussed in Sec. VI and used to connect the DHM with the Y-junction model. This follows since the extra contribution to Eq. (6.14) is proportional to

$$e^{\sum_{j=1}^n \sum_{k=1}^n \vec{L}_j \times \vec{L}_k} = 1. \quad (10.64)$$

Thus it is shown [24] that imposing the chiral b.c. of Eq. (10.56) on 2-component bosons with the standard action of Eq. (10.55) with the rotation angle, ξ' of Eq. (10.62) gives the DHM model.

In fact, it is possible to derive a general connection between the fields $\vec{X}(\tau, x)$ introduced here and the original fields $\vec{\Phi}(\tau, x)$ introduced in Sec. IV. Naively, by comparing the actions, we might expect that:

$$\vec{X} = \sqrt{g/\alpha} \vec{\Phi} \quad ? \quad (10.65)$$

However, this does not take into account the b.c. correctly. Recall that the disconnected wire fixed point corresponded to N b.c. on $\vec{\Phi}$,

$$\vec{\Phi}_L = \vec{\Phi}_R. \quad (10.66)$$

However, the above discussion establishes that this N. $V = 0$, fixed point corresponds to the chiral b.c. of Eq. (10.56) on \vec{X} . Thus we tentatively identify:

$$\begin{aligned} \vec{X}_R &= \sqrt{g/\alpha} \mathcal{R}_{\xi'} \vec{\Phi}_R \\ \vec{X}_L &= \sqrt{g/\alpha} \vec{\Phi}_L. \end{aligned} \quad (10.67)$$

To check the consistency of this identification, consider the chiral b.c. on $\vec{\Phi}$, given by Eq. (10.16) with the rotation angle of Eq. (10.44). As we argued in Sec. VI, this fixed point corresponds to the localized phase of the DHM which in turn corresponds to a simple D b.c. on \vec{X} :

$$\vec{X}_L = -\vec{X}_R. \quad (10.68)$$

Consistency of Eq. (10.67) [with ξ' given by Eq. (10.62)], which maps \vec{X} into $\vec{\Phi}$, with the b.c. on $\vec{\Phi}$ of Eq. (10.16), (10.44) and the b.c. on \vec{X} of Eq. (10.68) requires:

$$\mathcal{R}_{\xi'} = -\mathcal{R}_{\xi}^{-1}, \quad (10.69)$$

or

$$\xi' = \pi - \xi. \quad (10.70)$$

This implies $\tan(\xi'/2) = \cot(\xi/2)$ and hence is consistent with Eqs. (10.62) and (10.44) for ξ' and ξ together with the value of β/α determined in Eq. (6.30) for the case $n = 1$, corresponding to the stable chiral fixed point.

3. Boundary states and the generalized chiral fixed points

We have now established that the chiral fixed points χ_{\pm} corresponds to the chiral boundary condition (10.16) on the field $\vec{\Phi}$. Let us construct the corresponding boundary state explicitly, taking the twisted structure discussed in Sec. VIII into account.

The winding number along the boundary can be written as

$$\Delta \vec{\phi}_L = \frac{1}{2} \left(\sqrt{g} \Delta \vec{\Phi} + \frac{1}{\sqrt{g}} \Delta \vec{\Theta} \right) \quad (10.71)$$

$$\Delta \vec{\phi}_R = \frac{1}{2} \left(\sqrt{g} \Delta \vec{\Phi} - \frac{1}{\sqrt{g}} \Delta \vec{\Theta} \right). \quad (10.72)$$

For the chiral boundary condition (10.16), we have

$$\sqrt{g} \Delta \vec{\Phi} - \frac{1}{\sqrt{g}} \Delta \vec{\Theta} = \mathcal{R}_{\xi} (\sqrt{g} \Delta \vec{\Phi} + \frac{1}{\sqrt{g}} \Delta \vec{\Theta}) \quad (10.73)$$

For $\xi \neq 0, \pi$, it is clear that we need both $\Delta \vec{\Phi}$ and $\Delta \vec{\Theta}$ nonvanishing. Moreover, \mathcal{R}_{ξ} is a rotation matrix and thus preserves the length of the vector. This requires $\Delta \vec{\Phi}$ and $\Delta \vec{\Theta}$ to be mutually orthogonal.

Thus the only oscillator vacua which can appear in the chiral boundary state is

$$|(rl_1, rl_2, sl_1, sl_2)\rangle, \quad (10.74)$$

for arbitrary integers l_1 and l_2 . Here (r, s) is a fixed set of integers. In order to satisfy the parity condition (8.76) for arbitrary integers $l_{1,2}$,

$$r = s \pmod{2}, \quad (10.75)$$

is required. The chiral rotation angle is fixed by (r, s) as

$$\tan \frac{\xi}{2} = \frac{s \sqrt{3}}{r g}. \quad (10.76)$$

That is, the chiral rotation angle is ‘‘quantized’’.

For each vacuum (10.74), we can construct a chiral bosonic Ishibashi state

$$|(rl_1, rl_2, sl_1, sl_2)\rangle\rangle = \exp \left(\sum_{n=1}^{\infty} \vec{a}_n^{R\dagger} \cdot \mathcal{R}_{\xi} \vec{a}_n^{L\dagger} \right) |(rl_1, rl_2, sl_1, sl_2)\rangle, \quad (10.77)$$

which is conformally invariant.

A single Ishibashi state does not satisfy Cardy’s consistency condition. Similarly to the case of the standard Neumann/Dirichlet boundary state, the summation over all integers $l_{1,2}$ could give a consistent boundary state. Namely,

$$|\chi\rangle = g_{\chi} \sum_{l_1, l_2 \in \mathbf{Z}} |(rl_1, rl_2, sl_1, sl_2)\rangle\rangle, \quad (10.78)$$

where g_{χ} is again the ground-state degeneracy [41] of the chiral boundary states.

The diagonal cylinder amplitude is given by

$$Z_{\chi\chi} = \frac{g_\chi^2}{\eta(\hat{q})^2} \sum_{l_1, l_2 \in \mathbf{Z}} \tilde{q}^{\frac{1}{4} [l_1(\sqrt{g}r \frac{\bar{R}_1}{2} + \frac{s}{\sqrt{g}} \bar{K}_1) + l_2(\sqrt{g}r \frac{\bar{R}_2}{2} + \frac{s}{\sqrt{g}} \bar{K}_2)]^2}. \quad (10.79)$$

This can be written as

$$Z_{\chi\chi} = \frac{g_\chi^2}{\eta(\hat{q})^2} \sum_{\vec{V} \in \Lambda_\chi^*} q^{\frac{1}{4} \vec{V}^2}, \quad (10.80)$$

where Λ_χ^* is a triangular lattice with lattice constant

$$\sqrt{\frac{r^2 g}{3} + \frac{s^2}{g}}. \quad (10.81)$$

Thus, choosing

$$g_\chi = \sqrt{\frac{\sqrt{3}}{4} \left(\frac{r^2 g}{3} + \frac{s^2}{g} \right)}, \quad (10.82)$$

the same amplitude in the open string channel is given by

$$Z_{\chi\chi} = \frac{1}{\eta(q)^2} \sum_{\vec{W} \in \Lambda_\chi} q^{\vec{W}^2}, \quad (10.83)$$

because of eq. (C60). The lattice Λ_χ is dual to Λ_χ^* , and is the triangular lattice with the lattice constant

$$\sqrt{\frac{4g}{r^2 g^2 + 3s^2}}. \quad (10.84)$$

This formula encodes, as usual in the BCFT approach, the complete list of scaling dimensions of possible boundary perturbations to the chiral fixed point. Namely, the scaling dimensions of all the boundary perturbations are given by $\vec{W}^2 + \text{integer}$. In particular, the scaling dimension of the leading perturbation corresponding to the minimal length basis vector of Λ_χ , is given by

$$\Delta_\chi = \frac{4g}{3r^2 + s^2 g^2}. \quad (10.85)$$

From this spectrum of boundary operators, and the ground-state degeneracy (10.82), we see that the boundary state with larger r and s are unstable. While any given chiral rotation angle ξ may be approximated with arbitrary precision by taking large r and s , such a choice gives a highly unstable fixed point.

As a special series of chiral boundary states, let us take $r = 1$. Then, due to the parity condition (10.75), s must be odd: $s = 2n - 1$ for an integer n . Now the boundary states are characterized by the chiral rotation angle

$$\tan \frac{\xi}{2} = (2n - 1) \frac{g}{\sqrt{3}}. \quad (10.86)$$

This agrees with the chiral rotation angle for the chiral fixed points obtained from the mapping to the DHM.

Indeed, the scaling dimension of the leading perturbation

$$\Delta_\chi = \frac{4g}{3 + (2n - 1)^2 g^2} \quad (10.87)$$

also agrees exactly with the instanton analysis on the chiral fixed points in the DHM approach. In particular, $n = 1, 0$ corresponds to the most stable ones which we denoted as χ_\pm .

We have thus succeeded in explicitly constructing the boundary state for the chiral fixed points. In general, a chiral fixed point is characterized by two non-zero integers (r, s) with $r = s \pmod{2}$. It includes the one-parameter series $r = 1, s = 2n - 1$ which was found in Sec. VI. However, except for $(r, s) = (1, \pm 1)$, the chiral fixed point is always unstable for any given value of g .

The only chiral fixed points that can be stable are $(r, s) = (1, \pm 1)$, that is χ_\pm . The BCFT gives us the complete spectrum of the boundary operator, and thus more convincing evidence of the stability. In particular, for $1 < g < 3$, χ_\pm fixed points should be stable against any boundary perturbation, including the asymmetry and the change of the flux ϕ , but excluding the ‘‘resonant’’ type perturbation as discussed in Sec. VIII B.

4. Conductance

Let us calculate the conductance at the chiral fixed points χ_\pm from the above analysis on the boundary condition. Using $J_R^\mu = \mathcal{R} J_L^\mu$, we find

$$\lim_{\omega \rightarrow 0^+} \frac{1}{\pi \omega L} \int_0^L dx \int_{-\infty}^{\infty} d\tau e^{i\omega\tau} \langle J^\mu(y, \tau) J^\nu(x, 0) \rangle = g [(1 - \cos \xi) \delta^{\mu\nu} + \sin \xi \epsilon_{\mu\nu}]. \quad (10.88)$$

Thus, from Eq. (D23) we have

$$G_{jk} = g \frac{e^2}{h} [(1 - \cos \xi) \vec{v}_j \cdot \vec{v}_k + \sin \xi \vec{v}_j \times \vec{v}_k] \quad (10.89)$$

$$= g \frac{e^2}{h} \left[(1 - \cos \xi) (\delta_{jk} - \frac{1}{3}) + \frac{\sin \xi}{\sqrt{3}} \epsilon_{jk} \right] \quad (10.90)$$

For the chiral rotation angle ξ in Eq. (10.76), this reduces to the Z_3 symmetric form (2.5), with

$$G_S = \frac{e^2}{h} \frac{4gs^2}{g^2 r^2 + 3s^2}, \quad (10.91)$$

$$G_A = \frac{e^2}{h} \frac{4g^2 rs}{g^2 r^2 + 3s^2}. \quad (10.92)$$

In particular, for the most stable chiral fixed points χ_\pm , where $r = 1$ and $s = \pm 1$, we recover the same result (6.92) derived from the mapping to the DHM.

D. Asymmetric fixed point

In this paper, we have mostly discussed the junction with Z_3 symmetry among the wires. However, if the

junction of three wires could be realized, it will inevitably contain some asymmetry between the wires. Therefore, it is important to study the effect of Z_3 asymmetry.

Here we restrict our study to the asymmetry at the junction, assuming the three quantum wires are identical in the bulk. Although there would also be some asymmetry in the bulk in reality, it is outside the scope of the present paper.

There is a natural fixed point corresponding to the limit of the strong anisotropy: two of the wires are strongly coupled to form a single wire with perfect transmission at the junction, and the other is decoupled. Without losing generality, let us assume that the wires 1 and 2 are strongly coupled and the wire 3 is decoupled. Let us discuss the stability of this fixed point, which we call D_A .

1. Heuristic analysis

As perturbations to this asymmetric fixed point, we consider the following three operators:

electron hopping between wires 3 and 1& 2

$$\psi_1^\dagger \psi_3 + \text{h.c.}$$

electron pair hopping between wires 3 and 1& 2

$$\psi_1^\dagger \psi_1^\dagger \psi_3 \psi_3 + \text{h.c.}$$

electron backscattering in the wire 1& 2

$$\psi_1^\dagger \psi_2 + \text{h.c.}$$

It is natural to expect that the leading perturbation with the smallest scaling dimension is given by one of these three. Indeed, we confirm this expectation later with the BCFT analysis.

In the first two cases, the scaling dimension of the operator is given by the sum of the scaling dimensions of the operators on wire 3 and wire 1& 2. The disconnected wire 3 is subject to the Neumann boundary condition on φ_3 (Dirichlet on θ_3) at the junction. Thus, from eq. (4.3), the electron annihilation operator ψ_3 corresponds to the boundary operator $e^{i\varphi_3/\sqrt{2}}$ at the Dirichlet boundary condition on θ_3 . Its scaling dimension turns out to be $1/(2g)$.

On the other hand, for the wire 1& 2, the scaling dimension of the electron creation operator ψ_1^\dagger is given by the bulk scaling dimension of ψ_{1L}^\dagger or ψ_{1R}^\dagger . It turns out to be $(g+g^{-1})/4$. This scaling dimension determines the Local Density Of States for the electron tunneling into the TLL [34].

As a result, the scaling dimension of the electron hopping operator $\psi_1^\dagger \psi_3 + \text{h.c.}$ is

$$\frac{1}{2g} + \frac{g+g^{-1}}{4} = \frac{3+g^2}{4g}. \quad (10.93)$$

This, remarkably, is exactly the inverse of the scaling dimension (10.85) of the leading perturbation at χ_{\pm} fixed

points. As a consequence, it is relevant for $1 < g < 3$ and irrelevant for $g < 1$ or $3 < g$.

Next we consider the electron pair hopping between the wire 3 and 1& 2. The pair annihilation operator in the wire 3 $\psi_3 \psi_3$ is given by the boundary operator $e^{i\sqrt{2}\varphi_3/\sqrt{g}}$ at the Dirichlet boundary condition on θ_3 , with the scaling dimension $2/g$. The leading operator in the pair creation operator $\psi_1^\dagger \psi_1^\dagger$ is given by

$$\psi_{1L}^\dagger \psi_{1R}^\dagger \sim e^{i\sqrt{2}\varphi_2}. \quad (10.94)$$

Although this has the identical form to the above $\psi_3 \psi_3$, its scaling dimension is different since it must be evaluated as a bulk operator. The scaling dimension is given by

$$2 \times \frac{1}{4} \times \frac{2}{g} = \frac{1}{g}. \quad (10.95)$$

Thus, the scaling dimension of the pair hopping operator is

$$\frac{2}{g} + \frac{1}{g} = \frac{3}{g}. \quad (10.96)$$

Finally, the scaling dimension of the backscattering operator in the wire 1& 2 is known to be g from Ref. [1].

2. BCFT analysis

Now let us confirm the boundary operator content with the BCFT. The D_A fixed point corresponds to Dirichlet boundary condition on $\Phi_1 = (\varphi_1 - \varphi_2)/\sqrt{2}$, and Neumann boundary condition on Φ_2 .

Thus, the allowed winding numbers in the oscillator vacua is

$$\Delta \vec{\Phi} = -2\pi n \frac{\vec{R}_3}{2} = 2\pi n \frac{\vec{R}_1 + \vec{R}_2}{2}, \quad (10.97)$$

$$\Delta \vec{\Theta} = -2\pi m \vec{K}_3 = 2\pi m (\vec{K}_1 + \vec{K}_2), \quad (10.98)$$

where n, m are integers satisfying

$$n = m \pmod{2}, \quad (10.99)$$

from Eq. (8.76). The unit vectors \vec{K}_i and \vec{R}_i are defined in Eq. (4.10) and (6.55) respectively.

For each permitted oscillator vacuum $|(n, n, m, m)\rangle$, we can construct the bosonic Ishibashi state

$$|(n, n, m, m)\rangle\rangle = \exp\left(\sum_{k=1}^{\infty} \vec{a}_k^{R\dagger} \cdot \mathcal{R}_\zeta \vec{a}_k^{L\dagger}\right) |(n, n, m, m)\rangle, \quad (10.100)$$

where the rotation angle ζ is given by

$$\tan \frac{\zeta}{2} = \frac{m\sqrt{3}}{n-g}, \quad (10.101)$$

similarly to (10.44).

The boundary state for the D_A fixed point is given by the superposition of these Ishibashi states over all possible n, m :

$$|D_A\rangle = g_{D_A} \sum_{n=m \pmod{2}} |(n, n, m, m)\rangle. \quad (10.102)$$

Although the construction is similar to that of the chiral boundary state (10.78), $|D_A\rangle$ is *not* a chiral boundary state. Since the chiral rotation angle ζ determined by Eq. (10.101) depends on each Ishibashi state, the boundary state as a whole cannot be simply related to a chiral boundary condition as in (10.16). Nevertheless, it can be a legitimate conformally invariant boundary state.

The diagonal cylinder amplitude in the closed string channel is given by

$$\begin{aligned} Z_{D_A D_A} &= \frac{g_{D_A}^2}{\eta(\tilde{q})^2} \sum_{n=m \pmod{2}} \tilde{q}^{\frac{1}{4}(\sqrt{g}n\frac{\tilde{R}_3}{2} + \frac{m}{\sqrt{g}}\tilde{R}_3)^2} \\ &= \frac{g_{D_A}^2}{\eta(\tilde{q})^2} \sum_{\tilde{U} \in \Lambda_A^*} \tilde{q}^{\frac{1}{4}\tilde{U}^2}, \end{aligned} \quad (10.103)$$

where Λ_A^* is the two-dimensional Bravais lattice spanned by $(1/\sqrt{g}, \pm\sqrt{g/3})$. Using Eq. (C60), we fix

$$g_{D_A} = \left(\frac{1}{3}\right)^{1/4}, \quad (10.104)$$

to obtain

$$Z_{D_A D_A} = \frac{1}{\eta(q)^2} \sum_{\tilde{W} \in \Lambda_A} q^{\tilde{W}^2}, \quad (10.105)$$

where Λ_A is the Bravais lattice spanned by $(\sqrt{g}/2, \pm\sqrt{3/(4g)})$ and is dual of Λ_A^* .

The scaling dimensions of the boundary operators can be read off from the amplitude, as \tilde{W}^2 for $\tilde{W} \in \Lambda_A$. These include

$$\left(\frac{\sqrt{g}}{2}, \sqrt{\frac{3}{4g}}\right)^2 = \frac{3+g^2}{4g}, \quad (10.106)$$

$$\left(2\frac{\sqrt{g}}{2}, 0\right)^2 = g, \quad (10.107)$$

$$\left(0, 2\sqrt{\frac{3}{4g}}\right)^2 = \frac{3}{g}, \quad (10.108)$$

which exactly match the three operators considered in the heuristic analysis.

3. Restoration of the Z_3 symmetry

We have shown that the asymmetric fixed point D_A is always unstable except for $g = 1, 3$. At $g = 1$, the fixed point belongs to the continuous manifold of fixed points described by free fermion S -matrices. Thus it is natural to have marginal operators. Presumably it belongs to the

similar manifold corresponding to the S -matrices of the free dual fermion, at $g = 3$. For $g < 1$, the backscattering in the wire 2& 3 is relevant. It is most natural to assume that the system flows into the N fixed point, in which all the three wires are disconnected.

For $1 < g < 3$, the electron hopping is relevant. In the time-reversal non-invariant case $\phi \neq 0, \pi$, it is most natural to assume that the system flows into the χ_{\pm} fixed point depending on the sign of the flux ϕ . When $\phi = 0, \pi$, the system is time-reversal invariant and thus cannot flow into χ_{\pm} . We expect the infrared fixed point to be the nontrivial M(ysterious) fixed point, which is stable for $1 < g < 3$ in the time-reversal invariant models.

For $3 < g$, the electron-pair hopping is dominant. In the time-reversal non-invariant case $\phi \neq 0, \pi$, it is most natural to assume that the system flows into the D_P fixed point, which can be regarded as the limit of strong pair tunneling. In the time-reversal invariant cases $\phi = 0, \pi$, the situation is subtle. As discussed in Sec. V, the simple strong pair hopping limit in the time-reversal invariant case suggests that the potential minima forms a finer lattice. This fixed point would correspond to D_N boundary state and thus is unstable for $g < 9$. If this argument applies to any time-reversal symmetric case, for $3 < g < 9$ we expect the system to flow into a nontrivial fixed point.

In any case, our analyses imply that the system recovers the Z_3 symmetry, even if the microscopic model of the junction is not Z_3 symmetric. This is remarkable compared to many other quantum impurity problems, in which a high symmetry is required to reach a nontrivial fixed point. This feature is favorable in observing the intriguing behavior of the chiral fixed points χ_{\pm} in future experiments.

XI. CONSTRAINTS ON CONDUCTANCE FROM ENERGY CONSERVATION

In this section we will show how energy conservation constraints the conductance tensor. We will also show that the three sets of boundary conditions on the bosonic fields studied above, namely Neumann, chiral, and Dirichlet, correspond to a situation where all the energy exchanged in the scattering processes off the junction is between the zero modes. Drops or increases of voltages across the junction are associated with the zero modes, or current carrying states. The non-zero or oscillator modes are neutral, and can carry energy but no electric current. Therefore, scattering without exciting the oscillator modes is the most efficient way of transmitting current without additional dissipation.

It is simpler to discuss the energy exchanges in the unfolded formalism. Let $\phi_i^R(t, x)$, for $i = 1, 2, 3$, be the bosonic fields in each wire. $\phi_i^R(t, x < 0)$ correspond to the incoming fields into the junction at $x = 0$, and $\phi_i^R(t, x > 0)$ are the outgoing fields after scattering. $\phi_R(x)$ obeys periodic boundary conditions,

$$\phi_R(x + 2l) = \phi_R(x) + 2\pi n. \quad (11.1)$$

Away from the impurity, the dynamics is governed by

$$\mathcal{L} = \sum_{i=1}^3 -\frac{g}{2\pi} \partial_x \phi_i^R (\partial_t + \partial_x) \phi_i^R. \quad (11.2)$$

The mode expansion of the fields $\phi_i^R(t, x)$, in a circle of length $2l$, reads:

$$\begin{aligned} \phi_i^R(t, x) = & \hat{\phi}_{0i}^R + \frac{\pi}{lg} \hat{Q}_i^R (t - x) \\ & + \frac{1}{\sqrt{2g}} \sum_{n=1}^{\infty} \frac{1}{\sqrt{n}} \left[a_{n,i} e^{-in\frac{x}{l}(t-x)} + h.c. \right]. \end{aligned} \quad (11.3)$$

and the Hamiltonian can be written as

$$H = \sum_{i=1}^3 \frac{\pi}{l} \left[\frac{1}{g} \left(\hat{Q}_i^R \right)^2 + \sum_{n=1}^{\infty} n a_{n,i}^\dagger a_{n,i} \right], \quad (11.4)$$

where the operator \hat{Q}_i^R takes integer eigenvalues Q_i^R . (Notice that the Hamiltonian and the mode expansion for each of these three chiral fields are exactly those in Eqs. (8.5) and (8.7), respectively, but with β replaced by l and $g \neq 1$.)

The scattering picture is as follows. If an incident pulse of some size w is prepared and imparted into the scatterer at the origin $x = 0$, it will propagate freely according Eq. (11.2) as long as the pulse does not overlap with the origin, *i.e.*, its amplitude is vanishingly small at $x = 0$. In this case, the energy of this incoming pulse is obtained from the Hamiltonian Eq. (11.4), and it is independent of the boundary interaction at the origin, which is what determines the scattering at the junction. Past the junction, once the outgoing pulse has reached a vanishing overlap with the origin, its energy is again obtained from the Hamiltonian Eq. (11.4).

Now, in the case of no tunneling between wires, the dynamics described in Eq. (11.2) is exact even at $x = 0$, because the no tunneling regime corresponds to free propagation through the junction; this is the case of perfect backscattering, or N BC in the unfolded formalism [in which case the Hamiltonian in the circle of size $2l$ in Eq. (11.4) should coincide with that for a finite segment of size l in Eq. (C46)]. We argue that, once tunneling is turned on, the Lagrangian should change due to the tunneling terms at $x = 0$, but that away from $x = 0$ one can still use the free Lagrangian Eq. (11.2) as long as the scattered pulse goes far enough from $x = 0$ so as to have vanishing overlap with the origin. Finally, we should consider the situation where the scattered pulse does not go all around the circle and scatters again; such scattering picture is possible in the limit of $l \rightarrow \infty$, so that scattered charges do not return to take the place of our prepared initial state.

Let us prepare an incoming state $|\text{IN}\rangle$ consisting of only zero modes being occupied; their occupation is dictated by the voltages V_i applied to the leads. After scattering off the impurity at $x = 0$, the state becomes $|\text{OUT}\rangle$, which in general has excitations created in both the zero

modes and the oscillator modes ($n > 0$). The outgoing currents are solely determined by the excitations of the zero modes.

Let I_i^{in} and I_i^{out} , for $i = 1, 2, 3$, be incoming and outgoing currents in each of the three leads, respectively. The incoming currents are related to the voltages on the three leads through

$$I_i^{\text{in}} = g \frac{e^2}{h} V_i = \sum_j g \frac{e^2}{h} \delta_{ij} V_j, \quad (11.5)$$

whereas the outgoing currents are obtained from the junction conductances G_{ij} as in Eq. (2.2) through

$$I_i^{\text{in}} - I_i^{\text{out}} = I_i = \sum_j G_{ij} V_j, \quad (11.6)$$

where I_i is the *net* current flowing into the junction from lead i .

The Q_i^R quantum number is the total charge of the state, which in the unfolded formalism is proportional to the total current I_i^{in} or I_i^{out} for the $|\text{IN}\rangle$ or $|\text{OUT}\rangle$ states, respectively. (The currents are given by the charges multiplied by the velocity, which we set to unity, divided by a length l). Define

$$\Delta E_0 = \sum_{i=1}^3 \frac{\pi l}{g} \left[(I_i^{\text{out}})^2 - (I_i^{\text{in}})^2 \right]. \quad (11.7)$$

This is the difference between the energy carried by the zero modes of the two quantum states $|\text{IN}\rangle$ and $|\text{OUT}\rangle$. The incoming state has no excited oscillator modes, but the outgoing state may have them. Energy is conserved in the scattering process, so it follows [see Eq. (11.4)] that

$$\Delta E_0 \leq 0, \quad (11.8)$$

with the equality holding when no oscillator modes are excited in $|\text{OUT}\rangle$.

Using the expressions for the conductances Eqs. (11.5,11.6), and substituting in Eq. (11.7), we obtain

$$\begin{aligned} \frac{g\Delta E}{l\pi} &= \sum_{ijk} G_{ij} G_{ik} V_j V_k - 2 \sum_{ij} g \frac{e^2}{h} G_{ij} V_i V_j \\ &= -\frac{1}{2} \sum_{ijk} \left(G_{ij} G_{ik} - 2g \frac{e^2}{h} G_{ij} \delta_{ik} \right) (V_j - V_k)^2, \end{aligned} \quad (11.9)$$

where we have used that $\sum_j G_{ij} = 0$, which follows from current conservation, in order to express the second line in Eq. (11.9) in terms of voltage differences.

Now, the most general conductance tensor that satisfies the \mathbf{Z}_3 symmetry of the three lead problem is given by Eq. (2.5). Recall that a non-zero G_A is allowed if time-reversal symmetry is absent. Defining dimensionless parameters

$$G \equiv G_S \frac{h}{e^2} \quad \text{and} \quad \Delta \equiv \frac{1}{\sqrt{3}} G_A \frac{h}{e^2} \quad (11.10)$$

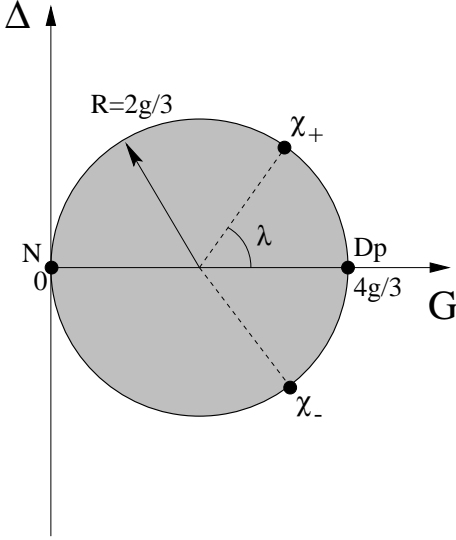


FIG. 18: Physical values of G and Δ , allowed from energy conservation, must lie inside the circle of radius $2g/3$ and origin at $(2g/3, 0)$ in the $G - \Delta$ plane. The boundary of the circle corresponds to the case when no energy is transferred to oscillator modes upon scattering off the junction ($\Delta E = 0$). The points corresponding to boundary conditions N, D_P , and χ_{\pm} lie on this boundary, and are marked on the figure.

for convenience, and inserting the expression for G_{ij} in Eq. (2.5) into the second line of Eq. (11.9), we obtain after some elementary manipulations that

$$\frac{g\Delta E}{l\pi} = \frac{3}{8} \frac{e^4}{h^2} \left[G^2 - \frac{4g}{3} G + \Delta^2 \right] \sum_{jk} (V_j - V_k)^2. \quad (11.11)$$

The last term is always positive, so in order to satisfy $\Delta E \leq 0$ one must have that

$$G^2 - \frac{4g}{3} G + \Delta^2 \leq 0, \quad (11.12)$$

or

$$\left(G - \frac{2g}{3} \right)^2 + \Delta^2 \leq \left(\frac{2g}{3} \right)^2, \quad (11.13)$$

which imposes constraints to the allowed values of G and Δ . The physical values are restricted to inside a circle of radius $2g/3$ and origin at $(2g/3, 0)$ in the $G - \Delta$ plane, as shown in Fig. 18. The boundary of the circle corresponds to the cases where $\Delta E = 0$ when no energy is transferred to oscillator modes.

A. T-invariant case: $\Delta = 0$

If time-reversal is a symmetry in the problem, then Δ must vanish, so that $G_{ij} = G_{ji}$. In this case, the allowed physical values of G lie in the segment that spans the diameter of the circle in the $\Delta = 0$ axis, or

$$0 \leq G_S \leq \frac{4g}{3} \frac{e^2}{h}. \quad (11.14)$$

The equality $\Delta E = 0$ occurs when $G = 0$ and when $G = 4g/3$; these cases correspond, respectively, to N and D_P boundary conditions (for a summary of the conductances for different boundary conditions, see section II). Hence, for these two boundary conditions, no energy is transferred into oscillator modes, and it is simply redistributed among the zero modes of the three boson fields.

B. T-broken case: $\Delta \neq 0$

This is the general case, in which the physical values of G and Δ must lie within the circle, and the boundary corresponds to the cases $\Delta E = 0$. There are two particular cases, as shown in Fig. 18, which correspond to the two chiral fixed points χ_{\pm} , when the angle λ satisfies $\tan \lambda = \pm g/\sqrt{3}$. In this case, the conductances are given by $G_S = \frac{4g}{3+g^2} \frac{e^2}{h}$ and $G_A = \sqrt{3} \Delta \frac{e^2}{h} = \pm g G_S$.

XII. Y-JUNCTIONS ATTACHED TO FERMI LIQUID LEADS

In this Section, we discuss the effective conductance of the junction in the presence of Fermi liquid (FL) leads, as introduced in Fig. 2. The FL leads can be thought of $g_{\text{lead}} = 1$ wires connected at the endpoints of the three Y-junction wires with g parameter. If the leads and the three quantum wires are connected by a point contact, then one can show that only one mode of the FL couples to the wire. This is similar to the case of the Kondo problem, where only the s -channel couples to the point-like impurity. In the case of the FL-quantum wire coupling at a point, it is not the s -channel but instead some other channel that couples. [38].

When we derived the conductance of the junction, we assumed that the wires were subject to voltages V_i , $i = 1, 2, 3$. If we have Fermi liquid leads, what happens is that the reservoirs are at voltages \bar{V}_i , $i = 1, 2, 3$, and one must obtain the relation between the \bar{V}_i and V_i . If that is done, all we have left to do is to re-express the currents I_i in terms of the \bar{V}_i . In other words, we need to calculate the conductance \bar{G}_{ij} from the G_{ij} we already computed:

$$I_j = \sum_k G_{jk} V_k = \sum_k \bar{G}_{jk} \bar{V}_k. \quad (12.1)$$

The question is how to relate the \bar{V}_i to the V_i . The answer is that the voltage difference $\bar{V}_i - V_i$ across the lead/wire contact is related to the current I_i that flows through the contact:

$$I_i = G_c (\bar{V}_i - V_i), \quad (12.2)$$

where the fixed point conductance for $g > 1$ is $G_c = 2g/(g-1) e^2/h$. This can be derived by looking at the problem of a single wire connected to FL leads, or in general for two TLLs with $g_1 > g_2$, as done in Ref. [38],

in which case $G_c^{-1} = (g_2^{-1} - g_1^{-1})/2 e^2/h$. For the case $g < 1$, the fixed point conductance is zero, and there is no transport between the leads and the wires. Notice that if $g \rightarrow 1$ then $G_c \rightarrow \infty$, and hence $\bar{V}_i = V_i$ for any finite current; this makes sense, as for if both sides have $g = 1$, there is no voltage drop across the lead/wire interface.

It is easy to get \bar{G}_{ij} now. We express V_i in terms of \bar{V}_i and I_i :

$$V_i = \bar{V}_i - I_i/G_c, \quad (12.3)$$

and then substitute in the formula for the current in terms of the V_i :

$$I_j = \sum_k G_{jk} V_k = \sum_k G_{jk} (\bar{V}_k - I_k/G_c), \quad (12.4)$$

or in matrix notation

$$I = \mathbf{G} \bar{V} - G_c^{-1} \mathbf{G} I, \quad (12.5)$$

from which we obtain that

$$I = (\mathbb{1} + G_c^{-1} \mathbf{G})^{-1} \mathbf{G} \bar{V} = \bar{\mathbf{G}} \bar{V} \quad (12.6)$$

or, finally,

$$\bar{\mathbf{G}} = (\mathbb{1} + G_c^{-1} \mathbf{G})^{-1} \mathbf{G}, \quad (12.7)$$

and more simply

$$\bar{\mathbf{G}}^{-1} = \mathbf{G}^{-1} + G_c^{-1} \mathbb{1}, \quad (12.8)$$

which can be interpreted physically as saying that the resistance tensors of the Y-junction must be added to the resistances due to the lead/wire interface resistances. [Notice, though, that this is a formal expression since in practice the matrix \mathbf{G} is singular because of the condition $\sum_k G_{jk} = 0$ – hence one must use Eq. (12.7) instead of Eq. (12.8).] We would like to point out that our expressions Eqs. (12.7,12.8) lead to consistent results with those of Refs. [31, 32] when applied to the simpler two-wire problem.

As an example, let us consider the effective conductance at the chiral fixed points χ_{\pm} , in the presence of the FL leads. All we have to do is use the expression for the conductance tensor \mathbf{G} and substitute into Eq. (12.7). For the chiral fixed points χ_{\pm} , recall the conductance Eq. (6.92).

Substitution of Eq. (6.92) into Eq. (12.7) leads to

$$\bar{G}_{jk}^{\pm} = \frac{e^2}{h} [(3\delta_{jk} - 1) \pm 1 \epsilon_{jk}]/2, \quad (12.9)$$

which is simply what one would obtain from the conductance tensor Eq. (6.92) if we set $g = 1$. This result is in agreement with numerical results that find that the current vanishes in one of the leads despite interactions, if the wires are connected to long non-interacting segments [19]. The scaling exponent for the corrections, however, should still depend on g , and is given

by $\Delta = 4g/(3 + g^2)$, which is also consistent with the numerical findings obtained for small attractive interactions. The sensitivity to the flux (and flow to χ_{\pm}) should also be a property of the interacting junction, not the FL leads.

The effective conductance \bar{G}_{jk} at other fixed points can be obtained in similar manner. The results are summarized in Sec. II. We find that the effective conductance tensor at each known fixed points can be identified with a “bare” conductance tensor of the junction of three Fermi liquids ($g = 1$) at an appropriate fixed point. This is rather natural, because the system with finite (interacting) wires and infinite FL leads would eventually be renormalized into a junction of three FL leads in the low-energy limit.

XIII. OPEN PROBLEMS

In this paper we studied the problem of a junction of three quantum wires connected by a ring, through which a magnetic flux can be applied. The electron systems in the three leads were described in terms of a Tomonaga-Luttinger liquid of spinless particles, with dimensionless interaction parameter g . One of the main difficulties in studying the problem with three wires is the necessity to include Klein factors that ensure the proper fermionic statistics for electrons in different leads.

We approached the Y-junction problem using different methods: mapping to the dissipative Hofstadter model, boundary conformal field theory, and delayed evaluation of boundary conditions. These methods gave consistent results and allowed us to calculate the low-voltage and low-temperature fixed point conductance tensor for the junction as a function of the interaction parameter g . (See section II for a summary of the results in the paper.) In this concluding section, we would like to list a few of the open directions that require further investigation.

The first one is the inclusion of electron spin in the problem. Even in the case of tunneling between just two wires, the inclusion of the spin degree of freedom leads to a rather rich phase diagram for the charge and spin conductances as a function of the interaction parameter [1]. For example, one finds situations where the spin conductance can vanish while the charge conductance does not, and vice versa, or systems that conduct both charge and spin, or that conduct neither. In the case of the three-lead junction the situation could, in principle, be much richer. One might wonder, for instance, whether there can be fixed points where the junction can separate the spin and charge of an electron incoming from one lead into different outgoing leads.

It appears that the method of delayed evaluation of boundary conditions may lend itself naturally to the study of the problem with electron spin. The reason is that this approach seems to be generalizable to multiple species. In the case of three leads with spin, one could try to extend the treatment laid down in this paper by

taking six branches altogether.

One of the major open problems concerning the Y-junctions is the nature of the stable fixed point in the range $1 < g < 3$ when time-reversal symmetry is preserved ($\phi = 0, \pi$). So far, we have not been able to identify the correct boundary condition for this “mysterious” (M) fixed point. We can, however, be sure that the nature of this M fixed point is rather different from N, D and χ_{\pm} . For example, using the energy conservation arguments presented in the scattering approach of section XI, we can argue that energy is dissipated into oscillator modes upon scattering off the junctions, which was not the case in the other four fixed points N, D and χ_{\pm} . We expect that the M fixed point should also describe the infrared stable behavior of the resonant tunneling model of Nayak *et al.* [5].

It is also clearly important to test our results by numerical methods, which could also guide analytical work in understanding the M fixed point. One numerical method, used by Barnabe-Therriault *et al.* [19], is an approximation based on the functional renormalization group approach. Within this method, the chiral fixed points we predicted were observed for small attractive interactions, when time-reversal symmetry was broken by an external field. Another fixed point, with maximal symmetric conductance for non-interacting fermions, was found for the case of zero flux. It is not clear whether this maximal conductance value is related to the conductance of the M fixed point once the renormalization effect of Fermi liquid leads is taken into account (the interaction in the wires in the numerical studies was turned off far away from the junction), or whether the approximation scheme can only capture conductance values that are equivalent to those of single particles scattering of a renormalized barrier. It would be interesting to push this approach towards larger values of the attractive potential ($g > 3$), when the D fixed point becomes stable, since the physics in this case will be that of pair tunneling, and hence values for the conductance greater than the maximal one for single particle scattering should be attainable (see II for a discussion).

Finally, the presence of the essential Klein factors in the Y-junction is related to a Fermi minus sign problem which would presumably make Monte Carlo methods difficult. This is to be contrasted with the two wire case where the Klein factors can be trivially eliminated and the resulting Coulomb gas can be very effectively studied by classical Monte Carlo [40]. The Y-junction problem is perhaps the simplest system with a fermion sign problem, which comes only from the junction. (In a lattice formulation, the problem corresponds to three 1D systems connected together by only one rung at one of the end points.) Hence, it seems natural that this system,

together with some of the analytical results that we derive, may be used as a benchmark for approximations that aspire to solve the fermion sign problem.

Acknowledgements

The authors would like to thank V. Meden for useful correspondence and for showing us his numerical results. The work by MO was supported in part by a Grant-in-Aid for scientific research and by the 21st Century COE program at Tokyo Institute of Technology “Nanometer-Scale Quantum Physics”, both from MEXT of Japan. CC was supported in part by the NSF grant DMR-0305482. IA was supported in part by NSERC of Canada, the Canadian Institute for Advanced Research and a JSPS invitation fellowship. The authors would also like to thank the hospitality of the Physics Departments at BU, UBC and Tokyo Tech, and the Aspen Center for Physics, where parts of this work were done.

APPENDIX A: FREE FERMION CASE

In this appendix we calculate the conductivity for the free fermion model ($g = 1$). This is done by first calculating the S -matrix and then using the Landauer formalism. We consider both lattice and continuum free fermion models.

1. Tight binding model

We first consider a tight-binding version of the continuum model that we study using bosonization. $\psi_{n,j}$ annihilates a fermion on site n on wire j . Here $n = 0, 1, 2, \dots, \infty$ and $j = 1, 2, 3$, with the wire index $j = 0$ identified with $j = 3$. The Hamiltonian is (setting the hopping amplitude $t = 1$):

$$H = - \sum_{n=0}^{\infty} \sum_{j=1}^3 (\psi_{n,j}^{\dagger} \psi_{n+1,j} + h.c.) - (\tilde{\Gamma}/2) \sum_{j=1}^3 [e^{i\phi/3} \psi_{0,j}^{\dagger} \psi_{0,j-1} + h.c.]. \quad (\text{A1})$$

Writing a single-electron state as:

$$|\Psi\rangle = \sum_{n,j} \Phi_{n,j} \psi_{n,j}^{\dagger} |0\rangle, \quad (\text{A2})$$

where $\Phi_{n,j}$ is the lattice wave-function, it is seen to obey the lattice Schrödinger equation:

$$\begin{aligned} E\Phi_{n,j} &= -[\Phi_{n+1,j} + \Phi_{n-1,j}] & (n \geq 1) \\ E\Phi_{0,j} &= -\Phi_{1,j} - (\tilde{\Gamma}/2)[e^{i\phi/3}\Phi_{0,j-1} + e^{-i\phi/3}\Phi_{0,j+1}]. \end{aligned} \quad (\text{A3})$$

The scattering solutions of this equation take the form:

$$\Phi_{n,j} = A_{\text{in},j} e^{-ikn} + A_{\text{out},j} e^{ikn}, \quad (\text{A4})$$

for all $n \geq 0$ and $j = 1, 2, 3$. The corresponding energy, which follows from the first line of the Schrödinger equation Eq. (A3) is:

$$E = -2 \cos k. \quad (\text{A5})$$

Noting that Eqs. (A4) and (A5) imply

$$\Phi_{1,j} + E\Phi_{0,j} = -(A_{\text{in},j} e^{ik} + A_{\text{out},j} e^{-ik}), \quad (\text{A6})$$

we see that the second line of the Schroedinger equation Eq. (A3) gives

$$(\tilde{\Gamma}/2) [e^{i\phi/3} (A_{\text{in},j-1} + A_{\text{out},j-1}) + e^{-i\phi/3} (A_{\text{in},j+1} + A_{\text{out},j+1})] = A_{\text{in},j} e^{ik} + A_{\text{out},j} e^{-ik}. \quad (\text{A7})$$

Assembling the three components of the amplitudes, $A_{\text{in},j}$ and $A_{\text{out},j}$ into vectors, \vec{A}_{in} and \vec{A}_{out} , this becomes:

$$[e^{-ik} - (\tilde{\Gamma}/2) M] \vec{A}_{\text{out}} = -[e^{ik} - (\tilde{\Gamma}/2) M] \vec{A}_{\text{in}}, \quad (\text{A8})$$

where

$$M \equiv e^{i\phi/3} B^{-1} + e^{-i\phi/3} B, \quad (\text{A9})$$

and

$$B \equiv \begin{pmatrix} 0 & 1 & 0 \\ 0 & 0 & 1 \\ 1 & 0 & 0 \end{pmatrix}. \quad (\text{A10})$$

Thus, the outgoing and incoming amplitudes are related by a 3-dimensional S-matrix:

$$\vec{A}_{\text{out}} = S \vec{A}_{\text{in}}, \quad (\text{A11})$$

where:

$$S = -[e^{-ik} - (\tilde{\Gamma}/2) M]^{-1} [e^{ik} - (\tilde{\Gamma}/2) M]. \quad (\text{A12})$$

or, equivalently,

$$S = -e^{i2k} [1 - e^{ik} (\tilde{\Gamma}/2) M]^{-1} [1 - e^{-ik} (\tilde{\Gamma}/2) M]. \quad (\text{A13})$$

2. Continuum model

We use the continuum model with the Hamiltonian density:

$$\begin{aligned} \mathcal{H} &= i \sum_j \psi_j^\dagger \frac{d}{dx} \psi_j \\ &\quad - \delta(x) \sum_j \left\{ \Gamma [e^{i\phi/3} \psi_j^\dagger \psi_{j-1} + h.c.] + r \psi_j^\dagger \psi_j \right\}. \end{aligned} \quad (\text{A14})$$

Here we have “unfolded” the system so that all fields are left-movers. We do not explicitly write the subscripts L , and we have set $v_F = 1$. The corresponding Schrödinger equation is:

$$i \frac{d}{dx} \Phi_j - \delta(x) \left\{ \Gamma [e^{i\phi/3} \Phi_{j-1} + e^{-i\phi/3} \Phi_{j+1}] + r \Phi_j \right\} = E \Phi_j. \quad (\text{A15})$$

Writing the scattering states as

$$\Phi_j(x) = \begin{cases} A_{\text{in},j} e^{-ipx} & (x > 0) \\ A_{\text{out},j} e^{-ipx} & (x < 0) \end{cases} \quad (\text{A16})$$

with energy $E = p$, we obtain (for $E \rightarrow 0$):

$$i(A_{\text{in},j} - A_{\text{out},j}) = \frac{1}{2} \left\{ \Gamma [e^{i\phi/3} (A_{\text{in},j-1} + A_{\text{out},j-1}) + e^{-i\phi/3} (A_{\text{in},j+1} + A_{\text{out},j+1})] + r (A_{\text{in},j} + A_{\text{out},j}) \right\}. \quad (\text{A17})$$

Note that we have taken $\Phi_j(0)$ to be the average of its values at 0^+ and 0^- . This can be rewritten:

$$[(r + 2i) + \Gamma M] \vec{A}_{\text{out}} = -[(r - 2i) + \Gamma M] \vec{A}_{\text{in}}, \quad (\text{A18})$$

where M is the same matrix defined in the discussion of the tight-binding model, Eq. (A9). Thus the S-matrix

for the continuum model is:

$$S = -[(r + 2i) + \Gamma M]^{-1}[(r - 2i) + \Gamma M]. \quad (\text{A19})$$

This will be the same S-matrix as in the tight-binding model [Eq. (A12)], for a particular value of k , if we choose r and Γ so that:

$$e^{ik} = -\frac{r - 2i}{|r - 2i|} \quad (\text{A20})$$

and

$$\tilde{\Gamma}/2 = \frac{\Gamma}{|r - 2i|}. \quad (\text{A21})$$

It can be shown that the continuum limit of the tight-binding model, with the spectrum linearized around k_F , gives values of Γ and r satisfying this equation when $k = k_F$. Note, in particular, that for the particle-hole symmetric case, $k_F = \pi/2$, $r = 0$ and $\Gamma = \tilde{\Gamma}$.

3. The S-matrix

An explicit expression for the S-matrix of Eq. (A13) can be found by straightforward algebra (we will drop the overall phase factor e^{i2k} which is of no physical consequence to the conductances). This S-matrix can be parameterized by the most general Z_3 symmetric form:

$$S = S_0 + S_- B + S_+ B^{-1}. \quad (\text{A22})$$

It is convenient to define:

$$z_{\pm} \equiv (\tilde{\Gamma}/2)e^{i(k \pm \phi/3)}. \quad (\text{A23})$$

The coefficients S_i in the S-matrix then are given by:

$$\begin{aligned} S_0 &= (z_+ z_- + |z_+|^2 + |z_-|^2 + z_-^2 z_+^* + z_+^2 z_-^* - 1)/D \\ S_+ &= (z_-^* - z_+ - z_-^2 + z_- z_+^*)/D \\ S_- &= (z_+^* - z_- - z_+^2 + z_+ z_-^*)/D, \end{aligned} \quad (\text{A24})$$

where:

$$D = 1 - 3z_+ z_- - z_-^3 - z_+^3. \quad (\text{A25})$$

It can be readily seen that $S \rightarrow -e^{i2k}I$ at $\tilde{\Gamma} \rightarrow 0$ and $S \rightarrow -I$ at $\tilde{\Gamma} \rightarrow \infty$. For $\tilde{\Gamma}/2 = 1$ a perfectly chiral S-matrix occurs, for some value of ϕ , with S_+ or $S_- = 0$. In this case $|z_{\pm}| = 1$. Thus we see that:

$$z_- z_+ S_+ = (z_+ - z_- z_+^2 - z_-^3 z_+ + z_-^2)/D = (1 - z_+ z_-)(z_+ + z_-^2)/D. \quad (\text{A26})$$

Thus $S_+ = 0$ when $z_-^2 z_+^* = e^{i(k-\phi)} = -1$ or

$$k - \phi = (2n + 1)\pi, \quad (\text{A27})$$

for integer n . At this point,

$$S_0 = (z_+ z_- + 1 + z_-^2 z_+^* + z_+^2 z_-^*)/D = 0, \quad (\text{A28})$$

and therefore only $S_- = -(z_-^*)^2 \neq 0$. This corresponds to an electron incident on wire j being transmitted with probability one to wire $j - 1$. Conversely, $S_- = S_0 = 0$ when $\tilde{\Gamma}/2 = 1$ and

$$k + \phi = (2n + 1)\pi, \quad (\text{A29})$$

so that an electron incident on wire j is transmitted with probability one to wire $j + 1$.

In the time-reversal invariant cases, $\phi = 0$ or π , $S_+ = S_-$; an electron incident on wire j has equal amplitude to be transmitted to wire $j - 1$ or $j + 1$. The maximum possible value of $|S_+| = |S_-|$ consistent with unitarity of the S-matrix is $|S_+| = 2/3$, $|S_0| = 1/3$. For $\phi = 0$, one obtains

$$S_+ = \frac{z^* - z}{(1 + z)(1 - 2z)}, \quad (\text{A30})$$

with $z = (\tilde{\Gamma}/2)e^{ik}$. For any value of k , $|S_+|$ reaches $2/3$ for some value of $\tilde{\Gamma}$ of order one.

4. Conductance

In the free fermion case, we obtain the conductance directly from the S-matrix by the Landauer formalism. We assume a thermal distribution of electrons heading towards the junction from distant reservoirs with different chemical potentials. The total current on wire j is this incoming current minus the reflected current minus the current transmitted from the other 2 wires. Thus:

$$I_j = e \int \frac{dk}{2\pi} v(k) [(1 - |S_{jj}|^2) n_F(\epsilon_k - \mu - eV_j) - |S_{j,j+1}|^2 n_F(\epsilon_k - \mu - eV_{j+1}) - |S_{j,j-1}|^2 n_F(\epsilon_k - \mu - eV_{j-1})] \quad (\text{A31})$$

where $n_F(\epsilon)$ is the Fermi distribution function. Using $v = (d\epsilon/dk)/\hbar$ and expanding to linear order in the V_j 's gives at $T = 0$:

$$I_j = \frac{e^2}{h} \{ [1 - |S_{jj}|^2] V_j - |S_{j,j+1}|^2 V_{j+1} - |S_{j,j-1}|^2 V_{j-1} \}, \quad (\text{A32})$$

where the S-matrix is evaluated at $k = k_F$. Thus the conductance tensor is:

$$G_{jk} = \frac{e^2}{h} \left[(3\delta_{jk} - 1) \frac{|S_+|^2 + |S_-|^2}{2} + \frac{|S_+|^2 - |S_-|^2}{2} \epsilon_{jk} \right], \quad (\text{A33})$$

where S_{\pm} are given by Eq. (A24). In particular, for the perfectly chiral S-matrices discussed above, this reduces to:

$$G_{jk} = \frac{e^2}{2h} [(3\delta_{jk} - 1) \pm \epsilon_{jk}]. \quad (\text{A34})$$

APPENDIX B: REVIEW OF BOUNDARY CONFORMAL FIELD THEORY TECHNIQUES

Here we briefly review the boundary conformal field theory (BCFT) techniques, developed largely by J. Cardy [35], which have been applied to various quantum impurity problems.

We consider a general conformal field theory, such as a collection of free bosons or fermions, defined on the $1/2$ -line, $x \geq 0$, with a conformally invariant boundary condition at $x = 0$. In general two-point correlation functions will be affected by the boundary. While the correlation function of some operator, $\mathcal{O}(x, \tau)$ may behave as:

$$\langle \mathcal{O}(x, \tau) \mathcal{O}(x', \tau') \rangle = \frac{1}{[(x - x')^2 + (\tau - \tau')^2]^{\Delta}}, \quad (\text{B1})$$

in the bulk (i.e. in the absence of a boundary or far from the boundary), in the limit $x, x' \ll |\tau - \tau'|$ it behaves as:

$$\langle \mathcal{O}(x, \tau) \mathcal{O}(x', \tau') \rangle \propto \frac{1}{|\tau - \tau'|^{2\Delta_B}} \quad (\text{B2})$$

Here Δ is the bulk scaling dimension of the operator, \mathcal{O} and Δ_B is its boundary scaling dimension. In general, Δ_B will depend on the boundary conditions. The boundary conditions are always assumed to imply:

$$\mathcal{P}(t, 0) = 0, \quad (\text{B3})$$

where:

$$\mathcal{P}(t, x) \equiv \mathcal{H}_R(t - x) - \mathcal{H}_L(t + x). \quad (\text{B4})$$

\mathcal{P} is the momentum density and $\mathcal{H}_{L/R}$ are the left and right-moving parts of the Hamiltonian density.

We can determine all boundary scaling dimensions for an arbitrary conformally invariant boundary condition, A , denoted Δ_A , from the finite size spectrum of the Hamiltonian on a strip of length l with boundary conditions A at both ends. This is done by the conformal transformation:

$$z = le^{\pi w/l}, \quad (\text{B5})$$

Here

$$z = \tau + ix, \quad (\text{B6})$$

covers the infinite half-plane and $w = u + iv$ the strip with $0 < v < l$. The correlation function for two points at the edge of the strip can be obtained by this conformal transformation:

$$\begin{aligned} \langle \mathcal{O}(u_1) \mathcal{O}(u_2) \rangle &= \left\{ \frac{\frac{\partial z}{\partial w}(u_1) \frac{\partial z}{\partial w}(u_2)}{|z(u_1) - z(u_2)|^2} \right\}^{\Delta_A} \\ &= \left[\frac{2l}{\pi} \sinh \frac{\pi}{2l}(u_1 - u_2) \right]^{-2\Delta_A}. \end{aligned} \quad (\text{B7})$$

As $u_2 - u_1 \rightarrow \infty$, this approaches:

$$\langle \mathcal{O}(u_1) \mathcal{O}(u_2) \rangle \rightarrow \left(\frac{\pi}{l} \right)^{2\Delta_A} \exp \left[-\pi \Delta_A \frac{(u_2 - u_1)}{l} \right]. \quad (\text{B8})$$

On the other hand, since u is imaginary time, we may evaluate the correlation function on the strip by inserting a complete set of states:

$$\langle \mathcal{O}(u_1) \mathcal{O}(u_2) \rangle = \sum_n |\langle 0 | \mathcal{O} | n \rangle_{AA}|^2 \exp[-E_n(u_2 - u_1)]. \quad (\text{B9})$$

Here $|0\rangle$ is the groundstate and $|n\rangle$ an arbitrary excited state for the strip Hamiltonian with b.c.'s A at both ends. (The groundstate occurs here since the strip has infinite length in the imaginary time, u , direction.) E_n is the energy of the n^{th} state (measured from the groundstate energy). As $u_2 - u_1 \rightarrow \infty$, the lowest energy excited state

that can be created from the groundstate by the operator \mathcal{O} dominates so we conclude that this state has energy:

$$E_1 = \pi \frac{\Delta_A}{l}. \quad (\text{B10})$$

There is a one-to-one correspondance between boundary operators and the finite size spectrum with the boundary scaling dimensions and finite size energies related by Eq. (B10).

Another very useful quantity to consider is the partition function Z_{AB} with conformally invariant b.c.'s A and B at the 2 ends of a finite system of length l , at inverse temperature, β . This may be expressed in terms of the finite size spectrum on the strip as:

$$Z_{AB} = \text{tr} \exp[-\beta H_l^{AB}] = \sum_n \exp[-\beta E_n^{AB}], \quad (\text{B11})$$

where the E_n^{AB} are the energies on the strip with b.c.'s A and B at the two ends. This picture is sometimes referred to as ‘‘open string channel’’. On the other hand, we may interchange space and imaginary time and write instead:

$$Z_{AB} = \langle A | \exp[-l H_\beta^P] | B \rangle, \quad (\text{B12})$$

where $|A\rangle$ and $|B\rangle$ are *boundary states* that correspond to the b.c.'s A and B respectively. Here H_β^P denotes the Hamiltonian with periodic b.c.'s on a ring of length β . This point of view is sometimes referred to as ‘‘closed string channel’’. All boundary states obey the condition:

$$\mathcal{P}(x)|A\rangle = 0. \quad (\text{B13})$$

The eigenstates of H_β^P are of the form:

$$E_n^P = \frac{2\pi}{\beta} \Delta_n, \quad (\text{B14})$$

where the Δ_n are bulk scaling dimensions. This follows, similarly to the correspondance between boundary scaling dimensions and boundary energies, from a conformal transformation from the infinite plane to the cylinder of circumference β .

APPENDIX C: REVIEW OF BOUNDARY CONFORMAL FIELD THEORY FOR STANDARD FREE BOSONS

1. One component free boson

A simple example of boundary dimensions and energies is given by the periodic boson. Thus we consider the bulk Lagrangian density:

$$\mathcal{L} = \frac{g}{4\pi} (\partial_\mu \varphi)^2, \quad (\text{C1})$$

and assume that $\varphi(x, t)$ is a periodic variable so that φ is identified as

$$\varphi \leftrightarrow \varphi + 2\pi n \quad (n \in \mathbf{Z}). \quad (\text{C2})$$

These boundary conditions determine the bulk mode expansion for $\varphi(x, t)$ on a circle of circumference β , $0 < x < \beta$:

$$\varphi(t, x) = \hat{\varphi}_0 + \frac{2\pi}{\beta} \left[\hat{P}' x + \frac{1}{g} \hat{P} t \right] + \frac{1}{\sqrt{2g}} \sum_{n=1}^{\infty} \frac{1}{\sqrt{n}} \left\{ a_n^L \exp \left[-inx + \frac{2\pi}{\beta} \right] + a_n^R \exp \left[-inx - \frac{2\pi}{\beta} \right] + h.c. \right\}. \quad (\text{C3})$$

Here: \hat{P} is the momentum operator conjugate to the constant term, $\hat{\varphi}_0$:

$$[\hat{\varphi}_0, \hat{P}] = i, \quad (\text{C4})$$

and \hat{P}' is another momentum operator. They both have integer eigenvalues. The integer eigenvalues of \hat{P}' follow from the periodic b.c.'s and the angular nature of φ :

$$\varphi(\beta) = \varphi(0) + 2\pi n. \quad (\text{C5})$$

The integer eigenvalues of \hat{P} follow from the fact that it is conjugate to an angular variable, $\hat{\varphi}_0$. Explicitly, the wave-function, $\exp[-iP\hat{\varphi}_0]$, with P an eigenvalue of \hat{P} , must be single valued.

$$x_\pm \equiv t \pm x, \quad (\text{C6})$$

and $a_n^{L/R}$ are boson creation operators for the left and right moving finite momentum modes. This mode expansion is consistent with the equal-time commutation relations:

$$\left[\varphi(x), \frac{\partial \varphi(x')}{\partial t} \right] = \frac{2\pi}{g} i \delta(x - x'), \quad (\text{C7})$$

which follow from the normalization of the Lagrangian. We may decompose φ into left and right moving modes:

$$\varphi(t, x) = \varphi_L(x_+) + \varphi_R(x_-), \quad (\text{C8})$$

and then write the dual field:

$$\theta \equiv g(\varphi_L - \varphi_R). \quad (\text{C9})$$

This has the mode expansion:

$$\theta(t, x) = \hat{\theta}_0 + \frac{2\pi}{\beta} [\hat{P}x + g\hat{P}'t] + \sqrt{\frac{g}{2}} \sum_{n=1}^{\infty} \frac{1}{\sqrt{n}} \left\{ a_n^L \exp \left[-inx_+ \frac{2\pi}{\beta} \right] - a_n^R \exp \left[-inx_- \frac{2\pi}{\beta} \right] + h.c. \right\}. \quad (\text{C10})$$

\hat{P}' is the momentum conjugate to $\hat{\theta}_0$:

$$[\hat{\theta}_0, \hat{P}'] = i, \quad (\text{C11})$$

and we see from this mode expansion that $\theta(t, x)$ is also an angular variable:

$$\theta(t, x) \leftrightarrow \theta(t, x) + 2\pi n \quad (n \in \mathbf{Z}). \quad (\text{C12})$$

We may equally well write the Lagrangian density in terms of θ :

$$\mathcal{L} = \frac{1}{4\pi g} (\partial_\mu \theta)^2. \quad (\text{C13})$$

The bulk primary operators are $\exp\{i[n\varphi(t, x) + m\theta(t, x)]\}$ with scaling dimension:

$$\Delta = \frac{n^2}{2g} + \frac{gm^2}{2} \quad (n, m \in \mathbf{Z}). \quad (\text{C14})$$

(All descendent operators are simply primaries multiplied by products of multiple derivatives of φ . These have dimensions equal to that of the corresponding primary plus a positive integer.) Inserting the mode expansion of φ into the Hamiltonian, gives the finite size spectrum with periodic b.c.'s on a circle of circumference β :

$$H = \frac{2\pi}{\beta} \left[\frac{\hat{P}^2}{2g} + \frac{\hat{P}'^2 g}{2} + \sum_{n=1}^{\infty} n(a_n^{L\dagger} a_n^L + a_n^{R\dagger} a_n^R) \right]. \quad (\text{C15})$$

We see that the relationship, Eq. (B14) between the bulk scaling dimensions and finite size energies with periodic b.c.'s is obeyed.

Now consider the Dirichlet (D) b.c. on φ :

$$\varphi(t, 0) = \varphi_0, \quad (\text{a constant, independent of } t), \quad (\text{C16})$$

implying:

$$\frac{\partial \varphi}{\partial t}(t, 0) = 0. \quad (\text{C17})$$

We may calculate the dimensions of all boundary operators directly by recognizing that the D b.c.:

$$\varphi_R(t, 0) = \varphi_0 - \varphi_L(t, 0), \quad (\text{C18})$$

determines $\varphi_R(t, x)$ (for $x > 0$) as the analytic continuation of $\varphi_L(t, x)$ to the negative x -axis:

$$\varphi_R(t, x) = \varphi_0 - \varphi_L(t, -x), \quad (x > 0). \quad (\text{C19})$$

The correlation function for $\varphi_L(t, x)$:

$$\langle \varphi_L(t, x) \varphi_L(0, 0) \rangle = -\frac{1}{2g} \ln x_+ + \text{constant}, \quad (\text{C20})$$

is unaffected by the boundary. Thus we see that the boundary operators can be rewritten by the replacements:

$$\begin{aligned} \varphi(t, 0) &\rightarrow \varphi_0 \\ \theta(t, 0) &\rightarrow 2\varphi_L(t, 0) - \varphi_0. \end{aligned} \quad (\text{C21})$$

Thus the non-trivial operators are:

$$\exp[i m \theta(t, 0)] \rightarrow \exp[2im\varphi_L(t, 0) - im\varphi_0], \quad (\text{C22})$$

of scaling dimension:

$$\Delta_D = gm^2. \quad (\text{C23})$$

Note that this is twice the *bulk* scaling dimension of $\exp[im\theta]$. This factor of 2 arises from the b.c. The bulk scaling dimension of $\exp[im\theta]$ consists of equal contributions of $gm^2/4$ from the left and right factors: $\exp[\pm i\varphi_{L/R}]$. Upon imposing the D b.c. the right factor vanishes and the left factor has an extra factor of 2 in the exponent which quadruples the scaling dimension: $gm^2/4 \rightarrow gm^2$.

We may check the general BCFT results on this simple example. Consider the finite size spectrum with the same D b.c. on both ends of the strip of length l (with the same value of φ_0). The D b.c. essentially sets $\hat{P} = 0$ and $a_n^R = -a_n^L$. The mode expansion of Eq. (C3) becomes:

$$\varphi(t, x) \rightarrow \varphi_0 + \frac{2\pi}{l} \hat{P}' x + \frac{1}{\sqrt{2g}} \sum_{n=1}^{\infty} \frac{1}{\sqrt{n}} 2 \sin\left(\frac{n\pi x}{l}\right) \left[a_n^L \exp\left(-\frac{in\pi t}{l}\right) + h.c. \right]. \quad (\text{C24})$$

\hat{P}' must have integer eigenvalues due to the D b.c. and the periodic nature of φ . Thus the finite size spectrum with D b.c.'s is:

$$H_l^{DD} = \frac{\pi}{l} \left[g \hat{P}'^2 + \sum_{n=1}^{\infty} n a_n^{L\dagger} a_n^L \right]. \quad (\text{C25})$$

We see that the general relation, Eq. (B10) between the dimensions of boundary operators and finite size spectrum on a strip with the corresponding boundary conditions is obeyed.

We may also find the corresponding boundary state. This must obey the operator equation:

$$\varphi(0, x) |D(\varphi_0)\rangle = \varphi_0 |D(\varphi_0)\rangle, \quad (\text{independent of } x). \quad (\text{C26})$$

Note that this implies:

$$\frac{\partial \varphi(0, x)}{\partial x} |D(\varphi_0)\rangle = 0. \quad (\text{C27})$$

Note that, compared to the operator boundary condition of Eq. (C17), t and x have been interchanged. This is a consequence of the interchange of space and time involved in going between the two interpretations of Z_{AB} . In the boundary state representation, the boundary corresponds to the circle $\tau = 0$ and Eq. (C27) is the condition that φ (when acting on the boundary state) be constant along the boundary. The D boundary state is:

$$|D(\varphi_0)\rangle = (2g)^{-1/4} \exp \left[- \sum_{n=1}^{\infty} a_n^{L\dagger} a_n^{R\dagger} \right] \sum_{P=-\infty}^{\infty} \exp[-iP\varphi_0] |(0, P)\rangle. \quad (\text{C28})$$

Here $|(0, P)\rangle$ is the eigenstate of \hat{P}' with eigenvalue 0, the eigenstate of \hat{P} with (integer) eigenvalue P , and the groundstate of all the harmonic oscillators. The condition Eq. (C26) follows using the explicit form of the wavefunction $|(0, P)\rangle$:

$$\langle \varphi_0 | (0, P) \rangle \propto \exp[iP\varphi_0]. \quad (\text{C29})$$

[We apologize for the confusing, but unfortunately standard, notation here. In Eq. (C29), φ_0 is a *co-ordinate* whereas in Eq. (C28), φ_0 is a fixed number, corresponding to an eigenvalue of the co-ordinate.] It is straightforward to calculate Z_{DD} in the boundary state representation:

$$\langle D(\varphi_0) | \exp[-lH_\beta^P] |D(\varphi_0)\rangle = (2g)^{-1/2} \frac{1}{\eta(\tilde{q})} \sum_P \exp \left[-l \frac{2\pi}{\beta} \frac{P^2}{2g} \right]. \quad (\text{C30})$$

Here we have introduced the Dedekind η -function:

$$\eta(\tilde{q}) \equiv \tilde{q}^{1/24} \prod_{n=1}^{\infty} (1 - \tilde{q}^n), \quad (\text{C31})$$

and the convenient notation:

$$\tilde{q} \equiv e^{-\frac{4\pi l}{\beta}}. \quad (\text{C32})$$

The factor of $1/\eta(\tilde{q})$ in Eq. (C30) comes from the oscillator mode factor in the boundary state of Eq. (C28) and

we have included the universal groundstate energy for free bosons (from the zero point motion/ Casimir effect):

$$E_0 = -\frac{\pi}{6\beta}. \quad (\text{C33})$$

The sum in Eq. (C30) can also be written in terms of \tilde{q} :

$$Z_{DD} = (2g)^{-1/2} \frac{1}{\eta(\tilde{q})} \sum_P \tilde{q}^{P^2/4g}. \quad (\text{C34})$$

In order to check that Z_{DD} indeed gives the correct finite size spectrum with D b.c.'s we need to re-express it in terms of:

$$q \equiv e^{-\frac{\pi\beta}{l}}, \quad (\text{C35})$$

i.e. perform a modular transformation. The modular transformation of the Dedekind η -function is:

$$\eta(\tilde{q}) = \sqrt{\frac{\beta}{2l}} \eta(q). \quad (\text{C36})$$

The modular transformation of the sum in Eq. (C30) can be computed using the Poisson summation formula, i.e. the Fourier transform of the periodic $\delta_P(x)$:

$$\begin{aligned} \sum_{P \in \mathbf{Z}} \tilde{q}^{-P^2/(4g)} &= \sum_{P \in \mathbf{Z}} \exp\left[-\frac{\pi l P^2}{g\beta}\right] \\ &= \sqrt{\frac{g\beta}{l}} \sum_{P' \in \mathbf{Z}} \exp\left[-\frac{\pi P'^2 g\beta}{l}\right] \\ &= \sqrt{\frac{g\beta}{l}} \sum_{P' \in \mathbf{Z}} q^{gP'^2}. \end{aligned} \quad (\text{C37})$$

inserting Eqs. (C36) and (C37) into Eq. (C30) gives:

$$Z_{DD} = \frac{1}{\eta(q)} \sum_{P'} q^{gP'^2}. \quad (\text{C38})$$

Using the definition of q in Eq. (C35) and the representation Eq. (B11) for Z_{AB} , we extract the finite size energies with D b.c.'s at both ends of the strip:

$$E^{DD} = \frac{\pi}{l} [gP'^2 + \text{integers}], \quad (\text{C39})$$

in agreement with Eq. (C25).

The Neumann (N) b.c. is:

$$\frac{\partial \varphi}{\partial x}(t, 0) = 0. \quad (\text{C40})$$

This is equivalent to $\partial\theta/\partial t = 0$ or equivalently:

$$\theta(t, 0) = \theta_0. \quad (\text{C41})$$

This implies:

$$\varphi_R(t, x) = -\theta_0/g + \varphi_L(t, -x), \quad (x > 0). \quad (\text{C42})$$

Now the non-trivial primary boundary operators are:

$$\exp[in\varphi(t, 0)] \propto \exp[2in\varphi_L(t, 0) - in\theta_0/g], \quad (\text{C43})$$

of dimension:

$$\Delta_N = n^2/g, \quad (\text{C44})$$

again twice the dimension of the corresponding bulk operator. The mode expansion is:

$$\varphi(t, x) \rightarrow \varphi_0 + \frac{2\pi}{lg} \hat{P}t + \frac{1}{\sqrt{2g}} \sum_{n=1}^{\infty} \frac{1}{\sqrt{n}} 2 \cos\left(\frac{n\pi x}{l}\right) \left[a_n^L \exp\left(-\frac{in\pi t}{l}\right) + h.c. \right], \quad (\text{C45})$$

with \hat{P} having integer eigenvalues. The corresponding spectrum can be read from after rewriting the Hamiltonian as:

$$H_l^{NN} = \frac{\pi}{l} \left[\frac{\hat{P}^2}{g} + \sum_{n=1}^{\infty} n a_n^{L\dagger} a_n^L \right]. \quad (\text{C46})$$

The corresponding boundary state, obeying:

$$\theta(0, x)|N(\theta_0)\rangle = \theta_0|N(\theta_0)\rangle, \quad (\text{C47})$$

is:

$$|N(\theta_0)\rangle = \left(\frac{g}{2}\right)^{1/4} \exp\left[\sum_{n=1}^{\infty} a_n^{L\dagger} a_n^{R\dagger}\right] \sum_{P'=-\infty}^{\infty} \exp[-iP'\theta_0] |(P', 0)\rangle. \quad (\text{C48})$$

2. Multi-component free boson

In some applications, including the subject of the present paper, we need to consider a multi-component free boson field theory. While Ref. [33] also contains a similar review, here we summarize the basics of the multi-component free boson field theory conforming to the normalizations of the present paper. Let

$$\vec{\varphi} = (\varphi_1, \varphi_2, \dots, \varphi_c) \quad (\text{C49})$$

be a c -component free boson field, with the Lagrangian density

$$\mathcal{L} = \frac{g}{4\pi} (\partial_\mu \vec{\varphi})^2. \quad (\text{C50})$$

At this point, the theory is just a collection of c free bosons which are independent of each other. However, we will be interested in various possible boundary interactions which couples different components. In fact, we often introduce a multi-dimensional generalization of the periodicity (C2), which is often called compactifica-

tion. Sometimes the compactification ties different components together, so that they cannot be regarded as completely independent, even before we introduce an interaction at the boundary.

The general form of the compactification would be given as the identification

$$\vec{\varphi} \leftrightarrow \vec{\varphi} + 2\pi\vec{R}, \quad (\text{C51})$$

where $\vec{R} \in \Lambda$ for a Bravais lattice Λ . The different components would be completely independent only if Λ is rectangular. For a given Bravais lattice Λ , we can define a reciprocal lattice Λ^* so that

$$\vec{K} \cdot \vec{R} \in \mathbf{Z} \quad (\text{C52})$$

for any vectors $\vec{K} \in \Lambda^*$ and $\vec{R} \in \Lambda$. [Note that the lattices, $\sum_{i=1}^3 n_i \vec{R}_i$ and $\sum_{i=1}^3 m_i \vec{K}_i$ for arbitrary integers n_i and m_i , where the \vec{K}_i are defined in Eq. (4.10) and the \vec{R}_i in Eq. (6.55), are reciprocal.]

Imposing periodic boundary conditions in the space direction, we can generalize the mode expansion (C3) to the present case as

$$\vec{\varphi}(t, x) = \hat{\varphi}_0 + \frac{2\pi}{\beta} \left[\vec{R}x + \frac{1}{g} \vec{K}t \right] + \frac{1}{\sqrt{2g}} \sum_{n=1}^{\infty} \frac{1}{\sqrt{n}} \left\{ \vec{a}_n^L \exp\left[-inx + \frac{2\pi}{\beta}\right] + \vec{a}_n^R \exp\left[-inx - \frac{2\pi}{\beta}\right] + \text{h.c.} \right\}. \quad (\text{C53})$$

Here we have replaced the zero-mode ‘‘momentum’’ operators with their eigenvalues $\vec{R} \in \Lambda$ and $\vec{K} \in \Lambda^*$. The dual field $\vec{\theta}$ is defined similarly to Eq. (C9). It has a similar mode expansion to the above, generalizing Eq. (C10). As a result, $\vec{\theta}$ can be regarded as compactified as

$$\vec{\theta} \leftrightarrow \vec{\theta} + 2\pi\vec{K}, \quad (\text{C54})$$

where $\vec{K} \in \Lambda^*$.

The vacua of the oscillator modes

$$|(\vec{R}, \vec{K})\rangle \quad (\text{C55})$$

are then labelled by \vec{K} and \vec{R} which are the eigenvalues of \hat{P} and \hat{P}' .

Generalizing (C28), the Dirichlet boundary state corresponding to $\vec{\varphi} = \vec{\varphi}_0$ at the boundary is given as

$$|D(\vec{\varphi}_0)\rangle = (2g)^{-c/4} (V_0(\Lambda))^{-1/2} \sum_{\vec{K} \in \Lambda^*} \exp[-i\vec{K} \cdot \vec{\varphi}_0] |(\vec{0}, \vec{K})\rangle, \quad (\text{C56})$$

where $V_0(\Lambda)$ is the c -dimensional volume of the unit cell of the Bravais lattice Λ , and

$$|(\vec{0}, \vec{K})\rangle \equiv \exp\left[-\sum_{n=1}^{\infty} \vec{a}_n^{L\dagger} \cdot \vec{a}_n^{R\dagger}\right] |(\vec{0}, \vec{K})\rangle, \quad (\text{C57})$$

is the bosonic Ishibashi state. The partition function for the cylinder with the same Dirichlet boundary condition at both ends (diagonal cylinder amplitude) is given, generalizing (C30), as

$$\begin{aligned} Z_{DD}(\tilde{q}) &= \langle D(\vec{\varphi}_0) | \exp[-lH_\beta^P] | D(\vec{\varphi}_0) \rangle \\ &= (2g)^{-c/2} \frac{1}{V_0(\Lambda)} \left(\frac{1}{\eta(\tilde{q})} \right)^c \sum_{\vec{R} \in \Lambda^*} \tilde{q}^{\vec{R}^2/(4g)} \quad (\text{C58}) \end{aligned}$$

In order to find the spectrum of the boundary operators, we must modular transform Eq. (C58). For this purpose, the multi-dimensional generalization of Eq. (C37) is useful:

$$\left(\frac{1}{\eta(\tilde{q})} \right)^c \sum_{\vec{R} \in \Lambda^*} \tilde{q}^{\frac{1}{4g} \vec{R}^2} = (2g)^{c/2} V_0(\Lambda) \left(\frac{1}{\eta(q)} \right)^c \sum_{\vec{R} \in \Lambda} q^{g \vec{R}^2}. \quad (\text{C59})$$

Sometimes it is convenient to renormalize the lattices as $\Lambda^*/\sqrt{g} \rightarrow \Lambda^*$ and $\sqrt{g}\Lambda \rightarrow \Lambda$, to obtain the equivalent expression

$$\left(\frac{1}{\eta(\tilde{q})} \right)^c \sum_{\vec{V} \in \Lambda^*} \tilde{q}^{\frac{1}{4} \vec{V}^2} = 2^{c/2} V_0(\Lambda) \left(\frac{1}{\eta(q)} \right)^c \sum_{\vec{W} \in \Lambda} q^{\vec{W}^2}. \quad (\text{C60})$$

Using eq. (C59), we find

$$Z_{DD}(q) = \left(\frac{1}{\eta(q)} \right)^c \sum_{\vec{R} \in \Lambda} q^{g \vec{R}^2}. \quad (\text{C61})$$

In fact, the prefactor $(2g)^{-c/2} \frac{1}{V_0(\Lambda)}$ in the boundary state (C56), which represents the generally non-integer ‘‘ground-state degeneracy’’ [41], was chosen so that Eq. (C61) satisfies Cardy’s consistency condition. Namely, the coefficient of Eq. (C61) must be unity (or integer) to allow the interpretation as in Eq. (B11). From Eq. (C61) we can read off the scaling dimensions of the boundary operators with Dirichlet boundary condition as

$$\Delta_D = g \vec{R}^2 + \text{integer}, \quad (\text{C62})$$

where $\vec{R} \in \Lambda$ as usual. These are the dimensions of the boundary operators $\exp[i\vec{\Theta} \cdot \vec{R}]$, consistent with the compactification of Eq. (C54).

Likewise, the Neumann boundary state corresponding to $\vec{\theta} = \vec{\theta}_0$ at the boundary is given as

$$|N(\vec{\theta}_0)\rangle = \left(\frac{g}{2} \right)^{c/4} \sqrt{V_0(\Lambda)} \sum_{\vec{R} \in \Lambda} \exp[-i\vec{R} \cdot \vec{\theta}_0] |(\vec{R}, \vec{0})\rangle, \quad (\text{C63})$$

where

$$|(\vec{R}, \vec{0})\rangle \equiv \exp \left[+ \sum_{n=1}^{\infty} \vec{a}_n^{L\dagger} \cdot \vec{a}_n^{R\dagger} \right] |(\vec{R}, \vec{0})\rangle, \quad (\text{C64})$$

is the bosonic Ishibashi state. The cylinder partition function for the Neumann boundary condition at both ends reads

$$Z_{NN}(\tilde{q}) = (g/2)^{c/2} V_0(\Lambda) \left(\frac{1}{\eta(\tilde{q})} \right)^c \sum_{\vec{R} \in \Lambda} \tilde{q}^{g \vec{R}^2/4}, \quad (\text{C65})$$

in the closed string channel. Modular transforming using Eq. (C59) gives the same partition function in the open string channel as

$$Z_{NN}(q) = \left(\frac{1}{\eta(q)} \right)^c \sum_{\vec{K} \in \Lambda^*} q^{\vec{K}^2/g}. \quad (\text{C66})$$

The scaling dimensions of the boundary operators with Neumann boundary conditions are now given by

$$\Delta_N = \frac{\vec{K}^2}{g} + \text{integer}, \quad (\text{C67})$$

where $\vec{K} \in \Lambda^*$. These are the dimensions of the boundary operators $\exp[i\vec{\Phi} \cdot \vec{K}]$, consistent with the compactification of Eq. (C51).

The discussions in this Appendix naturally form a basis for the problem of the junction of three quantum wires, which is mapped to the boundary problem of two-component free boson. However, there is an important modification due to the fermionic nature of the electrons. This is discussed in Sec. VIII, before applying the present formalism to the junction problem in Sec. X.

APPENDIX D: BOUNDARY CONDITIONS AND THE CONDUCTANCE

Physical properties of the multiple wire junctions can be related to the boundary conditions imposed on the bosonic fields describing each wire. In preparation for discussing conformally invariant boundary conditions that correspond to RG fixed points for the 3-wire junction problem, let us show below how the conductivity tensor is extracted from the boundary conditions.

Let us start with a simple example first, that of a single quantum wire, described by fields $\varphi(x, \tau)$ and $\theta(x, \tau)$ with

$$S = \frac{g}{4\pi} \int d\tau dx (\partial_\mu \varphi)^2 \quad (\text{D1})$$

or dual action

$$S = \frac{1}{4\pi g} \int d\tau dx (\partial_\mu \theta)^2. \quad (\text{D2})$$

As in Ref. [1], we calculate the conductance within the linear response theory. Applying an AC electric field in an interval $0 < x < L$ and taking the DC limit, we obtain the Kubo formula for the conductance of the wire as

$$G = \lim_{\omega \rightarrow 0^+} \frac{e^2}{h} \frac{1}{\pi\omega L} \int_{-\infty}^{\infty} d\tau e^{i\omega\tau} \int_0^L dx \langle T_\tau J(y, \tau) J(x, 0) \rangle, \quad (\text{D3})$$

where the current $J(x, \tau) = -i\partial_\tau\theta(x, \tau)$. The current J can be expressed in terms of chiral components as $J = J_R - J_L$, with $J_R = \partial\theta \equiv (\partial_x - i\partial_\tau)\theta/2$ and $J_L = \bar{\partial}\theta \equiv (\partial_x + i\partial_\tau)\theta/2$. In terms of the chiral currents, one has

$$G = \lim_{\omega \rightarrow 0^+} \frac{e^2}{h} \frac{1}{\pi\omega L} \int_{-\infty}^{\infty} d\tau e^{i\omega\tau} \int_0^L dx \left[\langle T_\tau J_R(y, \tau) J_R(x, 0) \rangle + \langle T_\tau J_L(y, \tau) J_L(x, 0) \rangle \right. \quad (\text{D4})$$

$$\left. - \langle T_\tau J_R(y, \tau) J_L(x, 0) \rangle - \langle T_\tau J_L(y, \tau) J_R(x, 0) \rangle \right]. \quad (\text{D5})$$

1. Conductance of an infinite wire

Let us consider first an infinite wire. In this case, the correlation function between the different chiral components of the currents $\langle J_R J_L \rangle$ vanishes. Thus we need only the ‘‘diagonal’’ contributions.

$$\langle J_R(y, \tau) J_R(x, 0) \rangle = \partial^2 \langle \theta(z) \theta(0) \rangle, \quad (\text{D6})$$

where $z \equiv i\tau + (y - x)$. Because

$$\langle \theta(z) \theta(0) \rangle = -\frac{g}{4\pi} \ln |z|^2, \quad (\text{D7})$$

we obtain

$$\langle J_R(y, \tau) J_R(x, 0) \rangle = -\frac{g}{4\pi} \frac{1}{z^2}. \quad (\text{D8})$$

To calculate its contribution to the conductance, we first perform the Fourier transformation. A simple contour integral gives (for $\omega > 0$)

$$\int_{-\infty}^{\infty} d\tau e^{i\omega\tau} \frac{1}{(i\tau + u)^2} = 2\pi\omega H(u) e^{-\omega u}, \quad (\text{D9})$$

where $u = y - x$ and $H(t)$ is the Heaviside step function. Combining with a similar calculation on the $\langle J_L J_L \rangle$ part, the DC conductance for the infinite wire reads

$$G = g \frac{e^2}{h} \frac{1}{L} \int_0^L dx [H(x - y) + H(y - x)] = g \frac{e^2}{h}. \quad (\text{D10})$$

In this calculation, the length L of the section on which the voltage is applied does not affect the final result of the conductance. Moreover, the location y where one measures the current does not matter, and it can even be outside of the region where the voltage is applied. This is natural because in the DC limit, the current would be uniform throughout the wire even if the voltage is applied to a particular section of the wire.

However, the result (D10) should be treated with caution. As it has been discussed by several authors [30, 31, 32], the observed DC conductance per channel in a quantum wire is generally the free electron value $G = e^2/h$ independent of the TL parameter g , rather than the renormalized value eq. (D10). This is related to the fact that

the voltage is applied in a physical setting corresponds to the potential drop between the two reservoirs to which the wire is connected. The assumption of the electric field applied on the finite interval of the wire does not reflect this. Nevertheless, the calculation leading to eq. (D10) is useful as a starting point for various applications. In fact, the physical result $G = e^2/h$ can be recovered within the present approach, by modeling the reservoirs by Fermi liquid leads (TL liquid with $g = 1$).

In this paper, we first ignore the issue of the reservoirs and calculate the conductance simply using the present approach. Later, in Sec. XII we will discuss the physical DC conductance by including the Fermi liquid leads.

2. Conductance of a semi infinite wire

As the simplest example involving a boundary, let us consider a half-infinite wire with an ‘‘open’’ boundary at $x = 0$ (through which no current can flow.) The wire is assumed to extend for $x > 0$. It corresponds to the Dirichlet boundary condition on the field θ or equivalently the Neumann boundary condition on the field φ . The boundary condition $\theta(0, \tau) = 0$ is translated to

$$J_R(0) - J_L(0) = 0. \quad (\text{D11})$$

A convenient trick to respect this condition is to analytically continue the right-mover current to $x < 0$ and identify

$$J_L(x, \tau) \equiv J_R(-x, \tau) \quad (\text{D12})$$

for $x > 0$.

As a general rule, correlation functions of the chiral operators are not affected by the boundary condition. Therefore the contributions from $\langle J_R J_R \rangle$ and $\langle J_L J_L \rangle$ remains the same as in eq. (D10).

Cross correlations between the different chiral components are generally non-vanishing in the presence of the boundary, and are determined by the boundary condition. In the present case, all the left-mover current may be replaced by the right-mover current (in fictitious, neg-

ative x region) according to eq. (D12). As a result,

$$\begin{aligned} \langle J_R(y, \tau) J_L(x, 0) \rangle &= \langle J_R(y, \tau) J_R(-x, 0) \rangle \\ &= -\frac{g}{4\pi} \frac{1}{(i\tau + (x+y))^2} \end{aligned} \quad (\text{D13})$$

Upon Fourier transform, this term contributes to the conductance a term

$$G_{RL} = -g \frac{e^2}{h} \frac{1}{L} \int_0^L dx H(x+y) = -g \frac{e^2}{h} \quad (\text{D14})$$

because $x, y > 0$. On the other hand, the corresponding one from $\langle J_L J_R \rangle$ vanishes because it involves the step function $H(-x-y)$ for $x, y > 0$.

Summing up all the contributions, we obtain the DC conductance

$$G = 0 \quad (\text{D15})$$

for the open wire. This is an intuitively obvious result.

3. Conductance of a half-infinite wire attached to a superconductor

As another simple example, let us consider the half-infinite wire attached to a superconductor at $x = 0$. Again the wire is assumed to extend to $x > 0$. Now the appropriate boundary condition on the boson field is given by the Dirichlet boundary condition on ϕ , since it fixes the phase of a Cooper pair. In terms of current, it is now given as $J_R(0) + J_L(0) = 0$ and it is solved by identifying

$$J_L(x, \tau) \equiv -J_R(-x, \tau) \quad (\text{D16})$$

for $x > 0$. The calculation exactly follows the previous case in Sec. D2, except that the contribution from the cross term $\langle J_R J_L \rangle$ flips the sign. As a result, we find the DC conductance

$$G = 2g \frac{e^2}{h}, \quad (\text{D17})$$

which is doubled from the bulk one. This may be interpreted as a consequence of the (perfect) Andreev reflection.

From Eq. (D18), the conductance in this basis is given by the new basis,

$$G_{jk} = \lim_{\omega \rightarrow 0^+} \frac{e^2}{h} \frac{1}{\pi\omega L} \int_0^L dx \int_{-\infty}^{\infty} d\tau e^{i\omega\tau} v_{j\mu} v_{k\nu} \langle J^\mu(y, \tau) J^\nu(x, 0) \rangle, \quad (\text{D23})$$

where the summation over μ, ν is implicitly assumed.

Conservation of total charge implies that the ‘‘center of

4. Conductance of the Y-junction

Now let us turn to our problem of the Y-junction. We define three half-infinite wires 1, 2 and 3 which extends for $x > 0$, and $x = 0$ is represents the junction. Each wire is bosonized separately and described by the boson fields φ_j and θ_j . Currents are also defined respectively.

We discuss the conductance matrix introduced in Eq. (2.2). In the present approach, the conductance matrix is given as

$$G_{jk} = \lim_{\omega \rightarrow 0^+} \frac{e^2}{h} \frac{1}{\pi\omega L} \int_0^L dx \int_{-\infty}^{\infty} d\tau e^{i\omega\tau} \langle J_j(y, \tau) J_k(x, 0) \rangle, \quad (\text{D18})$$

where $J_j = -i\partial_\tau \theta_j$ is the current operator for wire j .

In analyzing the Y-junction, it is convenient to work on the rotated basis defined in Eqs. (4.5,4.6). We can express the fields φ_j and θ_j in this basis as

$$\varphi_j = \frac{1}{\sqrt{3}} \Phi_0 - \sqrt{\frac{2}{3}} (\hat{z} \times \vec{K}_j) \cdot \vec{\Phi} \quad (\text{D19})$$

$$\theta_j = \frac{1}{\sqrt{3}} \Theta_0 - \sqrt{\frac{2}{3}} (\hat{z} \times \vec{K}_j) \cdot \vec{\Theta}, \quad (\text{D20})$$

where the vectors \vec{K}_j are defined in Eq. (4.9), and recall that $\vec{\Phi} = (\Phi_1, \Phi_2)$ and $\vec{\Theta} = (\Theta_1, \Theta_2)$.

It also defines the transformation of the currents as

$$J_j = v_{j\mu} J_\mu, \quad (\text{D21})$$

where summation over μ is implicitly assumed,

$$J^\mu \equiv -i\partial_\tau \Theta_\mu \quad (\text{D22})$$

and the coefficients $v_{j\mu}$ can be read off from Eqs. (D19,D20):

$$v_{j\mu} = \begin{cases} 1/\sqrt{3} & , \mu = 0 \\ \sqrt{2/3} \epsilon_{\mu\nu} K_j^\nu & , \mu = 1, 2 \end{cases} .$$

mass’’ boson Φ^0 is always subject to the Neumann bound-

ary condition. As a consequence, the cross-terms $\langle J^0 J^\mu \rangle$ vanish for $\mu \neq 0$. Moreover, the contribution from $\langle J^0 J^0 \rangle$ to the conductance also vanishes, because the calculation is identical to that in the open wire. Therefore, the conductance of the Y-junction is given by Eq. (D23) with the μ, ν sum restricted to over just 1, 2.

The boundary conditions will determine the $\langle J^\mu J^\nu \rangle$ correlations. We will use the expression Eq. (D23) explicitly in the calculations carried out for the different boundary conditions we analyze in Sec. X.

APPENDIX E: JUNCTIONS OF THREE FRACTIONAL QUANTUM HALL EDGES

For the case $g = 1$ and for flux $\phi = \pm\pi/2$, we showed that we could understand the scattering in terms of an S -matrix that took incoming/outgoing states cyclically from lead 1 \rightarrow 2, 2 \rightarrow 3, and 3 \rightarrow 1. We can gain a great deal of intuition beyond the $g = 1$ case by studying the case of tunneling in junctions of three edge states of fractional quantum Hall (FQH) liquids, in particular those belonging to the Laughlin sequence (filling fraction $\nu = 1/(2m + 1)$, m odd). In this case, the dynamics of the edge modes is described by chiral bosons, and the fractionally charged edge quasiparticles are constructed from these chiral bosons [37]. We will show here that one can still understand the scattering in junctions of three FQH edges as cycling between the three leads.

One of the results below is that we can construct the Klein factors for the multi-lead problem using the zero-modes of the chiral bosons, instead of the Pauli matrices used by Nayak *et al.* [5].

The geometry we consider is shown in Fig. 19. The shaded areas correspond to Hall liquids, and the white regions to vacuum. Electrons tunnel through the vacuum or the FQH liquid, while quasiparticles tunnel only through the FQH liquid.

In order to understand the quasiparticle tunneling picture for the three leads, we have to ensure that the quasiparticle operators for the three leads respect the appropriate fractional statistics relations: this is the generalization of the Klein factors needed in the fermionic problem of Nayak *et al.*.

1. Klein factors from the boson zero-modes

Consider three right moving boson fields

$$\phi_i(t-x) = X_i + \frac{2\pi}{l} P_i(t-x) + \sum \text{Oscillator modes} \quad (\text{E1})$$

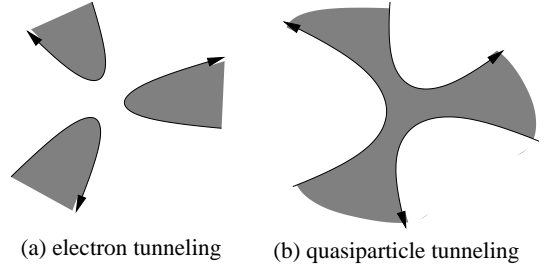


FIG. 19: Two tunneling geometries in a three lead FQH junction. (a) Electron tunneling geometry, where the Hall liquid is separated in three disjoint pieces (dark regions); tunneling occurs through the connected vacuum (white region), so only electrons can tunnel between the tips of the three FQH regions. (b) Quasiparticle tunneling geometry, where there is a single connected FQH liquid (dark region) and so fractionally charged quasiparticles can tunnel between the three closely spaced tips of the liquid.

for $i = 1, 2, 3$ labeling the three leads. The zero-modes satisfy $[X_i, P_j] = i \delta_{ij}$. The Lagrangian is given by

$$\mathcal{L} = - \sum_{i=1}^3 \frac{1}{4\pi} \partial_x \phi_i (\partial_t + \partial_x) \phi_i. \quad (\text{E2})$$

(In this appendix we adopt the standard normalization for edge modes, see Ref. [37]. This normalization is related to our standard normalization throughout the rest of the paper by taking $4\pi \rightarrow 2\pi$ in the Lagrangian Eq. E2.)

The quasiparticle/electron operators are written as

$$\psi_i = e^{i\lambda X_i} e^{i\lambda \frac{2\pi}{l} P_i(t-x)} \tilde{\psi}_i \quad (\text{E3})$$

where $\tilde{\psi}_i$ contains only oscillator modes. ($\lambda = \sqrt{\nu^{-1}}$ for electrons and $\lambda = \sqrt{\nu}$ for quasiparticles within the Laughlin sequence $\nu = \frac{1}{2m+1}$.) These ψ_i have the correct statistics with respect to themselves, but not among each other (they simply commute). To fix this, define the Klein factors

$$\eta_i = e^{i\frac{\theta}{2} \sum_j \alpha_{ij} P_j}, \quad (\text{E4})$$

which satisfy $[\eta_i, \eta_j] = 0$, and

$$\begin{aligned} \eta_i \psi_j &= \psi_j \eta_i \times e^{-[i\frac{\theta}{2} \sum_k \alpha_{ik} P_k, \lambda X_j]} \\ &= \psi_j \eta_i \times e^{i\frac{\theta}{2} \lambda \alpha_{ij}}. \end{aligned} \quad (\text{E5})$$

If we define new edge operators

$$\Psi_i = \eta_i \psi_i, \quad (\text{E6})$$

we do not spoil the statistics between same edge operators as long as we choose $\alpha_{ii} = 0$ for $i = 1, 2, 3$, so that $[\eta_i, \psi_i] = 0$. Now consider the statistical phase when two different edge vertex operators Ψ_i and Ψ_j for $i \neq j$ (so that $[\psi_i, \psi_j] = 0$) are interchanged:

$$\begin{aligned} \Psi_i \Psi_j &= \eta_i \psi_i \eta_j \psi_j \\ &= \Psi_j \Psi_i \times e^{i\frac{\theta}{2} \lambda (\alpha_{ij} - \alpha_{ji})}. \end{aligned} \quad (\text{E7})$$

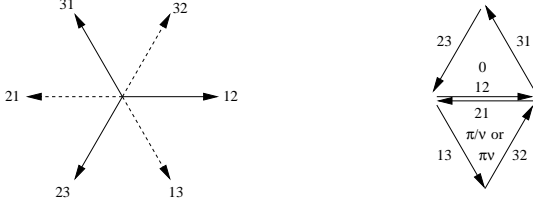


FIG. 20: The six possible tunneling between two edges are depicted on the left, in terms of vectors that span the triangular lattice. On the right, the phases accumulated due to the Klein factors are shown for elementary up and down triangles, according to Eqs. (E9,E10).

It suffices to consider only anti-symmetric matrices so that $\alpha_{ij} = -\alpha_{ji}$, with unit entries $\alpha_{ij} = \pm 1$. The right statistical angle is picked up if we choose $\theta\lambda = \pi\lambda^2$ or $\theta = \pi\lambda$: for electrons $\Psi_i^{el}\Psi_j^{el} = \Psi_j^{el}\Psi_i^{el} \times e^{\pm i\pi\nu^{-1}}$ and for quasiparticles $\Psi_i^{qp}\Psi_j^{qp} = \Psi_j^{qp}\Psi_i^{qp} \times e^{\pm i\pi\nu}$ when $i \neq j$.

Notice that there is still a sign ambiguity in choosing the three $\alpha_{ij} = -\alpha_{ji} = \pm 1$ for $i \neq j$. To consistently fix the correct signs, one must look, for example, at the relative phases as compared to those obtained by closing the system into a single edge, as studied in Ref. [29]. Doing so, we fix $\alpha_{12} = \alpha_{31} = 1$ and $\alpha_{23} = -1$.

2. Tunneling terms and the connection with the Callan-Freed model

Now we turn to the tunneling between the three edges: $T_{ij} = \Psi_i^\dagger \Psi_j$. It is useful to also define

$$t_{ij} = \psi_i^\dagger \psi_j = e^{-i\lambda(\phi_i - \phi_j)}, \quad (\text{E8})$$

which does not contain the Klein factors. In terms of the $\vec{\Phi}$ basis, defined in Eqs. (4.7) and (4.8), we can write six possible operators:

$$t_{12} = e^{-i\lambda\vec{K}_3 \cdot \vec{\Phi}}, \quad t_{23} = e^{-i\lambda\vec{K}_1 \cdot \vec{\Phi}}, \quad t_{31} = e^{-i\lambda\vec{K}_2 \cdot \vec{\Phi}},$$

with $t_{ji} = t_{ij}^*$ where the \vec{K}_i are defined in Eqs. (4.10). The six operators correspond to the six choices of $\pm\vec{K}_a$, $a = 1, 2, 3$.

Now, the Klein factors are responsible for extra phases coming when considering time-ordered products of the T_{ij} operators instead of the t_{ij} 's.

To illustrate this point, let us now calculate the phases obtained when taking products of T_{ij} operators along the elementary up and down triangles in the lattice spanned by the vectors \vec{K}_1 and \vec{K}_2 .

Using the commutation relations of the η and ψ , one can show that

$$T_{12}T_{23}T_{31} = t_{12}t_{23}t_{31}, \quad (\text{E9})$$

so there is no extra phase due to the Klein factors when traversing the elementary up triangles (see Fig. 20). On

the other hand,

$$\begin{aligned} T_{13}T_{21}T_{32} &= t_{13}t_{21}t_{32} \times e^{i\theta\lambda(\alpha_{12} + \alpha_{23} + \alpha_{31})} \\ &= t_{13}t_{21}t_{32} \times e^{i\pi\lambda^2} \end{aligned} \quad (\text{E10})$$

when traversing down triangles.

This is equivalent to a flux flux $\pi\nu^{-1}$ in the electron tunneling problem ($\pi\nu$ in the quasiparticle tunneling problem) for down triangles, and a flux 0 for up triangles (See fig. 20).

Once we have identified the statistical phases for the two elementary triangles in the lattice spanned by the vectors \vec{K}_1 and \vec{K}_2 , we can match order by order a Coulomb gas expansion of electron/quasiparticle tunneling operators with a Coulomb gas expansion in the Callan-Freed model. This procedure is explicitly carried out in Ref. [22] and in full detail in section VI.

3. Callan-Freed applied to the FQH junction

In the case of Fig. 19(a), electron tunneling is irrelevant at low energies, so the configuration is stable. Now, for Fig. 19(b), quasiparticle tunneling is a relevant perturbation, so the question is what is the strong coupling fixed point that is reached. Here we focus on the \mathbf{Z}_3 symmetric case. Since we will concentrate on the quasiparticle tunneling problem, we choose $\lambda = \sqrt{\nu}$.

Following Ref. [22] and section VI, we can match the Coulomb gas expansion of the FQH tunneling problem to that of the Callan-Freed problem model by choosing α, β in the dissipative Hofstadter as follows:

$$\frac{\alpha}{\alpha^2 + \beta^2} = \nu \quad (\text{E11})$$

and

$$4\pi \mathcal{A} \frac{\beta}{\alpha^2 + \beta^2} = 2\pi n + \pi\nu, \quad (\text{E12})$$

where $\mathcal{A} = \sqrt{3}/4$ is the area of the elementary triangle of unit length, and n is an integer. The first condition Eq. (E11) is fixed by the scaling dimension ν of the quasiparticle tunneling operator. The second condition Eq. (E12) is fixed by the statistics originating from the Klein factors explained above.

We can then solve for α, β , and using that the lattice dual to the triangular lattice of unit length has lattice constant $2/\sqrt{3}$ (this dual lattice contains the minima of the periodic potential in the problem, and the distance between the nearby minima are the ‘‘instantons’’), we obtain the scaling dimension $(2/\sqrt{3})^2\alpha$ (of the strong coupling tunneling operators:

$$\Delta_n = \frac{4\nu}{3\nu^2 + (2n - \nu)^2}. \quad (\text{E13})$$

As in Ref. [22], there appears to be a whole family of minima and their associated instanton operators labelled

by different integer n . Notice that the larger $|2n - \nu|$, the more relevant is the operator.

In what follows, let us consider the cases $n = \pm 1, 0$. One can easily show that, for $\nu < 1$, the choices ± 1 lead to relevant operators $\Delta_n < 1$, so the associated strong tunneling fixed points are unstable. Clearly, this will also be the case if $|n| > 1$, since Δ_n decreases as $|n|$ increases. So the only choice for a stable fixed point for $\nu < 1$ is $n = 0$. Notice that when $\nu = 1$, there are two possible choices $n = 0, 1$ (see [22] and section VI for a discussion). In this case, we obtain a simple result,

$$\Delta_0 = \frac{1}{\nu}. \quad (\text{E14})$$

This result has a very simple physical interpretation: that the strong quasiparticle tunneling regime of Fig. 19(b) leads to a dual description similar to that in Fig. 19(a) where the interior of the original single FQH region is pinched, leading to three disconnected FQH leads, between which electrons can tunnel. Indeed, $\Delta_0 = \frac{1}{\nu}$ is the scaling dimension of electron tunneling operators.

-
- [1] C. L. Kane and M. P. A. Fisher, Phys. Rev. Lett. **68**, 1220 (1992); Phys. Rev. **B46**, 15233 (1992).
- [2] S. Eggert and I. Affleck, Phys. Rev. **B46**, 10866 (1992).
- [3] M. Bockrath, D. Coben, R. Lu, A. Rinzler, R. Smalley, L. Balents and P. McEuen, Nature, **397**, 598 (1999).
- [4] Z. Yao, H. Postma, L. Balents and C. Dekker, Nature, **402**, 273 (1999).
- [5] C. Nayak, M.P.A. Fisher, A.W.W. Ludwig, and H.H. Lin, Phys. Rev. B **59**, 15694 (1999).
- [6] S. Lal, S. Rao, and D. Sen, Phys. Rev. B **66** (2002) 165327.
- [7] S. Rao and D. Sen, Phys. Rev. B **70**, 195115 (2004).
- [8] S. Chen, B. Trauzettel, and R. Egger, Phys. Rev. Lett. **89**, 226404 (2002).
- [9] R. Egger, B. Trauzettel, S. Chen, and F. Siano, New Journal of Physics **5** 117.1-117.14 (2003).
- [10] K-V. Pham, F. Piechon, K-I Imura, P. Lederer, Phys. Rev. B **68**, 205110 (2003).
- [11] I. Safi, P. Devillard, and T. Martin Phys. Rev. Lett. **86**, 4628 (2001).
- [12] J.E. Moore and X.-G. Wen, Phys. Rev. B **66**, 115305 (2002).
- [13] Hangmo Yi, Phys. Rev. B **65**, 195101 (2002).
- [14] E. A. Kim, S. Vishveshwara, E. Fradkin, Phys. Rev. Lett. **93**, 266803 (2004).
- [15] A. Furusaki, J. Phys. Soc. Japan **74**, 73 (2005).
- [16] H. Yi and C. L. Kane, Phys. Rev. B **57** R5579 (1998).
- [17] D. Giuliano and P. Sodano, cond-mat/0501378.
- [18] T. Enss, V. Meden, S. Andergassen, X. Barnabe-Theriat, W. Metzner, K. Schoenhammer, cond-mat/0411310.
- [19] X. Barnabe-Theriat, A. Sedeki, V. Meden, K. Schoenhammer, cond-mat/0411612.
- [20] X. Barnabe-Theriat, A. Sedeki, V. Meden, K. Schoenhammer, cond-mat/0501742.
- [21] K. Kazymyrenko and B. Douçot, Phys. Rev. B **71**, 075110 (2005).
- [22] C. Chamon, M. Oshikawa, and I. Affleck, Phys. Rev. Lett. **91**, 206403 (2003).
- [23] C. G. Callan and D. E. Freed, Nucl. Phys. B **374**, 543 (1992)
- [24] C. G. Callan, I. R. Klebanov, J. M. Maldacena, and A. Yegulalp, Nucl. Phys. B **443**, 444 (1995).
- [25] N. P. Sandler, C. de C. Chamon, and E. Fradkin, Phys. Rev. B **57** 12324 (1998).
- [26] A. J. Leggett, S. Chakravarty, A. T. Dorsey, M. P. A. Fisher, A. Garg, and W. Zwerger, Rev. Mod. Phys. **59**, 1 (1987).
- [27] D. Freed and J. A. Harvey Phys. Rev. B **41**, 11328 (1990).
- [28] I. Affleck, J.-S. Caux and A.M. Zagoskin, Phys. Rev. B **62**, 1433 (2000).
- [29] R. Guyon, P. Devillard, T. Martin, and I. Safi, Phys. Rev. B **65**, 153304 (2002).
- [30] S. Tarucha, T. Honda and T. Saku, Solid State Commun. **94**, 413 (1995).
- [31] D. Maslov and M. Stone, Phys. Rev. B **52**, R5539 (1995).
- [32] H. Safi and H. J. Schulz, Phys. Rev. B **52**, R17040 (1995).
- [33] I. Affleck, M. Oshikawa, H. Saleur, Nucl.Phys. B **594**, 535 (2001).
- [34] M. P. A. Fisher, L. I. Glazman, "Transport in one-dimensional Luttinger liquid. In: Mesoscopic Electron Transport", ed. by L.L. Sohn, L.P. Kouwenhoven, and G. Schoen. NATO ASI Series, Vol. 345, Kluwer Academic Publishers, 1997, p. 331.
- [35] J. Cardy, arXiv:hep-th/0411189
- [36] E. Wong and I. Affleck, Nucl. Phys. B **417**, 403 (1994).
- [37] X.-G. Wen, Phys. Rev. B **41**, 12838 (1990).
- [38] C. de C. Chamon and E. Fradkin, Phys. Rev. B **56**, 2012 (1997).
- [39] A. Furusaki and N. Nagaosa, Phys. Rev. B **47**, 4631 (1993).
- [40] K. Moon, H. Yi, C. L. Kane, S. M. Girvin, and M. P. A. Fisher Phys. Rev. Lett. **71**, 4381-4384 (1993).
- [41] I. Affleck and A. W. W. Ludwig, Phys. Rev. Lett. **67**, 161 (1991).